SKB

TECHNICAL REPORT 95-28

DECOVALEX I – Test Case 2:

Calculation of the Fanay-Augères THM Test – Thermomechanical modelling of a fractured rock volume

Lennart Börgesson[1], Jan Hernelind[2]

1 Clay Techonlogy AB, Lund, Sweden
2 Fem-Tech AB, Västerås, Sweden

December 1995

SVENSK KÄRNBRÄNSLEHANTERING AB
SWEDISH NUCLEAR FUEL AND WASTE MANAGEMENT CO

P.O.BOX 5864 S-102 40 STOCKHOLM SWEDEN
PHONE +46 8 665 28 00 TELEX 13108 SKB
FAX +46 8 661 57 19

DECOVALEX I - TEST CASE 2:

CALCULATION OF THE FANAY-AUGÈRES THM TEST - THERMOMECHANICAL MODELLING OF A FRACTURED ROCK VOLUME

Lennart Börgesson[1], Jan Hernelind[2]

1 **Clay Technology AB, Lund, Sweden**
2 **Fem-Tech AB, Västerås, Sweden**

December 1995

DECOVALEX I - TEST CASE 2:

CALCULATION OF THE FANAY-AUGÈRES THM TEST - Thermomechanical modelling of a fractured rock volume

Lennart Börgesson

Clay Technology AB
Lund
Sweden

Jan Hernelind

Fem-Tech AB
Västerås
Sweden

December 1995

PREFACE

This report is an integral part of SKB:s engagement in the first part of the DECOVALEX project (DECOVALEX I). The work is compiled in four reports and two articles.

The following SKB Technical reports have been printed:

Börgesson L. and Hernelind J. (1995) - DECOVALEX I - Test Case 2: Calculation of the Fanay-Augères THM Test - Thermomechanical modelling of a fractured rock volume. SKB Technical Report TR 95-28.

Börgesson L. and Hernelind J. (1995) - DECOVALEX I - Test Case 3: Calculation of the Big Ben Experiment - Coupled modelling of the thermal, mechanical and hydraulic behaviour of water-unsaturated buffer material in a simulated deposition hole. SKB Technical Report TR 95-29.

Israelsson J. (1995) - DECOVALEX I - Bench-Mark Test 3: Thermo-Hydro-Mechanical Modelling. SKB Technical Report TR 95-30.

Rosengren L. and Christianson M. (1995) - DECOVALEX I - Test Case 1: Coupled stress-flow model. SKB Technical Report TR 95-31.

The following articles have been published:

Rehbinder G. (1995) - Analytical Solutions of Stationary Coupled Thermo-Hydro-Mechanical Problems. *Int. J. Rock Mech. Min. Sci. & Geomech. Abstr.* Vol. 32, No 5, pp453-463, 1995.

Claesson J., Follin S., Hellström G., and Wallin N.-O. (1995) - On the use of the diffusion equation in test case 6 of DECOVALEX. *Int. J. Rock Mech. Min. Sci. & Geomech. Abstr.* Vol. 32, No 5, pp525-528, 1995.

ABSTRACT

A large scale thermo-mechanical test in the French uranium mine Fanay Augères at the depth 100 m has been simulated with the finite element code ABAQUS. The calculations have been compared with measurements of rock displacements.

The calculations included excavation of the test room and the heating and cooling periods of the test. The rock has been modelled both as linear elastic and as fractured with elastic-plastic properties of the fractures.

A sensitivity analysis of factors influencing the results were made with elastic calculations. It showed that the boundary conditions and the properties of the surrounding rock had no influence on the effect of the heating but a substantial influence on the effect of the excavation.

Comparisons between calculated and measured results of the heating and cooling test showed that the introduction of fractures did not yield more accurate results than those obtained with the fracture free linear elastic model.

SAMMANFATTNING

Ett termo-mekaniska experimentet i stor skala i den franska urangruvan Fanay Augères som utfördes på 100 m djup har simulerats med finita element programmet ABAQUS. Resultaten från beräkningarna har jämförts med mätta bergförskjutningar.

Beräkningarna omfattade utbrytning av bergrummet och uppvärmnings- och avkylningsfaserna i experimentet. Berget modellerades både som lineär-elastiskt och med sprickor som har elastoplastiska egenskaper.

En känslighetsanalys av olika faktorers inverkan på det beräknade resultatet gjordes med elastiska beräkningar. Den visade att randvillkoren och egenskaperna hos det omgivande berget inte hade något inflytande på den beräknade effekten av uppvärmnings- och avkylningsfaserna men hade en påtaglig inverkan på utbrytningsfasen.

Jämförelser mellan beräknade och uppmätta resultat av de termiska experimentet visade att införande av sprickor inte medförde att de beräknade resultaten blev bättre än resultaten från beräkningarna med den linjärelastiska materialmodellen utan sprickor.

CONTENTS

SUMMARY AND CONCLUSIONS

The thermo-mechanical large scale test in the French uranium mine Fanay Augères at the depth 100 m has been simulated with the finite element code ABAQUS. The calculations have been compared with measurements of rock displacements.

A rock volume of 40x40x40 m^3 was modelled with 7180 three-dimensional elements. Six fractures in the 10x10x5 m^3 test block in the floor of the test room were modelled with measured dip and strike. The fractures were modelled either as elastic-plastic with the properties measured for one of the fractures (fracture model) or as completely linear elastic (elastic model). The rest of the rock was modelled as linear elastic.

The calculations included excavation of the test room and the heating and cooling periods of the TM test. A sensitivity analysis of factors influencing the results were made with elastic calculations.

The sensitivity analysis showed that the boundary conditions and the properties of the surrounding rock had no influence on the effect of the heating but a substantial influence on the effect of the excavation.

Comparison with measured results, which could only be made for the TM test, showed that:

- the expansion of the rock was fairly well modelled with both the elastic and the fracture model
- the strain in the floor was not very well modelled probably because the real floor was more fractured than the simulated floor. A back-calculation showed that the average vertical E-modulus of the floor was only 50% of the one in the model
- the displacements of the two dominating fractures agreed with the calculated one only in about 50% of the floor area
- the introduction of fractures did not yield more accurate results than obtained by assuming the mass to be fracture-free

A general conclusion is that this type of discrete modelling of a few fractures does not seem to be good for accurate predictions of the behaviour of fractured rock.

1 INTRODUCTION

A number of large-scale tests, which have been performed as part of the nuclear waste research program in many countries, are used as examples in the international project DECOVALEX (DEvelopment of COupled models and their VALidation against EXperiments). The test reports are available to project members for mathematical modelling. Phase 3 of the project includes a full scale in situ test of a heated rock block by CEA in the French mine Fanay Augères.

The test is described in detail in the specifications provided by CEA /1-1/ and contains the experimental facility and conditions, fundamental properties and parameters as well as recorded data. The test will be briefly described in this report.

On behalf of SKB, Clay Technology has got the task to model this test and make a complete calculation of the thermo-mechanical response of the rock. This report describes the test, the structural model, the applied properties of the rock and a number of finite element calculations made by use of ABAQUS. Results from hydraulic tests at the test site were intended to be of assistance in the modelling, but they turned out to be useful only for estimating mechanical effects. Thus, the dry conditions that prevailed in the rock during the test made it impossible to measure any hydraulic effects (like pore pressure and flow rates). Hydraulic coupling could therefore not be made in the calculations.

2 FANAY AUGÈRES EXPERIMENT

2.1 GENERAL

The experiment was carried out by IPSN/CEA (Institut de Protection et de Sûreté Nucléaire / Commissariat à l'Energie Atomique) in the Fanay Augères uranium mine at a depth of 100 m during the years 1985 to 1988. The purpose of the test was "to simulate on a reduced scale the thermal, hydraulic and mechanical effects provoked in a granite environment by a heat-producing radwaste repository" /1-1/.

In addition to the test specifications /1-1/ the test is in detail described in a doctor thesis by Amel Rejeb /2-1/. The thesis also includes a result description and some calculations based on non-fractured rock models.

2.2 SITE DESCRIPTION AND TEST ARRANGEMENTS

2.2.1 General

The rock at the site is moderately fractured granite. A test room with the dimensions 12mx13.5m and the height 5m was excavated by blasting. The investigated rock is the mass below the 100 m^2 floor area down to 5 m depth. Fig 2-1 shows a plan of the site /1-1/. The floor, which was heavily instrumented, was produced by blasting using 40 horizontal boreholes. One drift leads into the test room (A-A) and another one was excavated 6 m outside the test room (B-B) with a small inclination downwards to the floor at the end of the drift that was located about 3 meters below the test floor.

5 boreholes were drilled from the outer drift ending 3 meters below the centre of the test floor. These holes were used for installing 5 heaters. Fig 2-2 shows a vertical section through the centre of the test room and the outer drift. The location of the heaters ("radiator") at the end of the bore holes is also shown in the figure.

2.2.2 Fracture description

The fractures in the test floor were carefully mapped and characterized. Fig 2-3 shows all fractures in the 10x10 m^2 test area. All fractures were numbered and a description of each fracture is available on diskette. Only about 10 of them are clearly permeable.

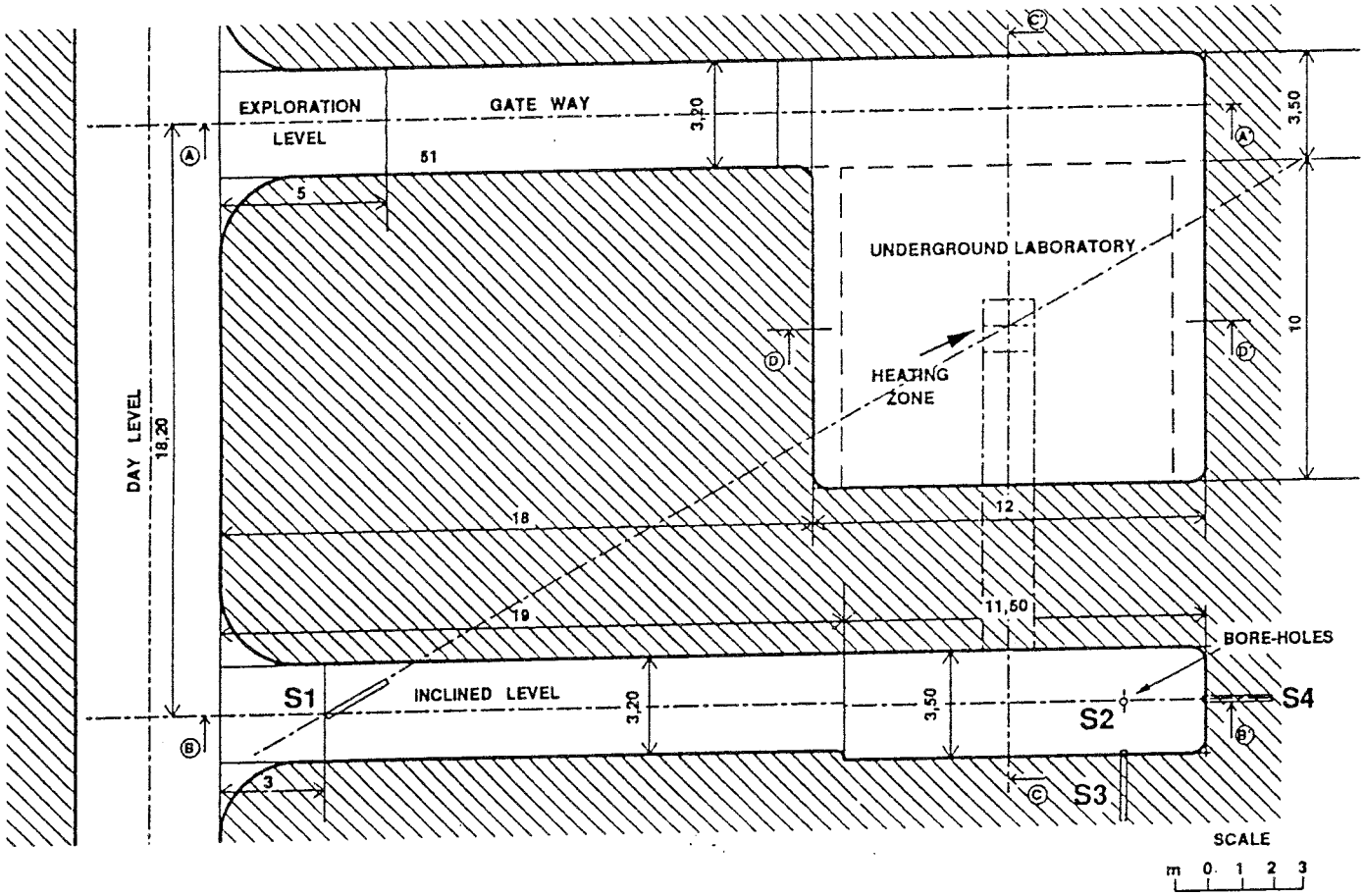

Figure 2-1. Plan of the test site of Fanay Augères.

2.2.3 Instrumentation

Several holes were drilled through the test block for testing and instrumentation. 4 holes were drilled from outside the test room for exploratory purposes (S1-S4). 3 vertical holes were drilled from the test floor for measuring rock displacements with bore-hole extensometers (F1-F3). Another 8 holes were drilled from the test floor for hydraulic measurements (P1-P8). The latter ones have not been used in the present study.

All bore-holes drilled from the test floor were instrumented with temperature gauges.

The test block was defined in a coordinate system with x=y=z=0 in the centre of the test floor. Fig 2-4 shows the coordinate system of the block and the location of the borehole extensometers (and temperature gauges). The displacements were measured in relation to the floor.

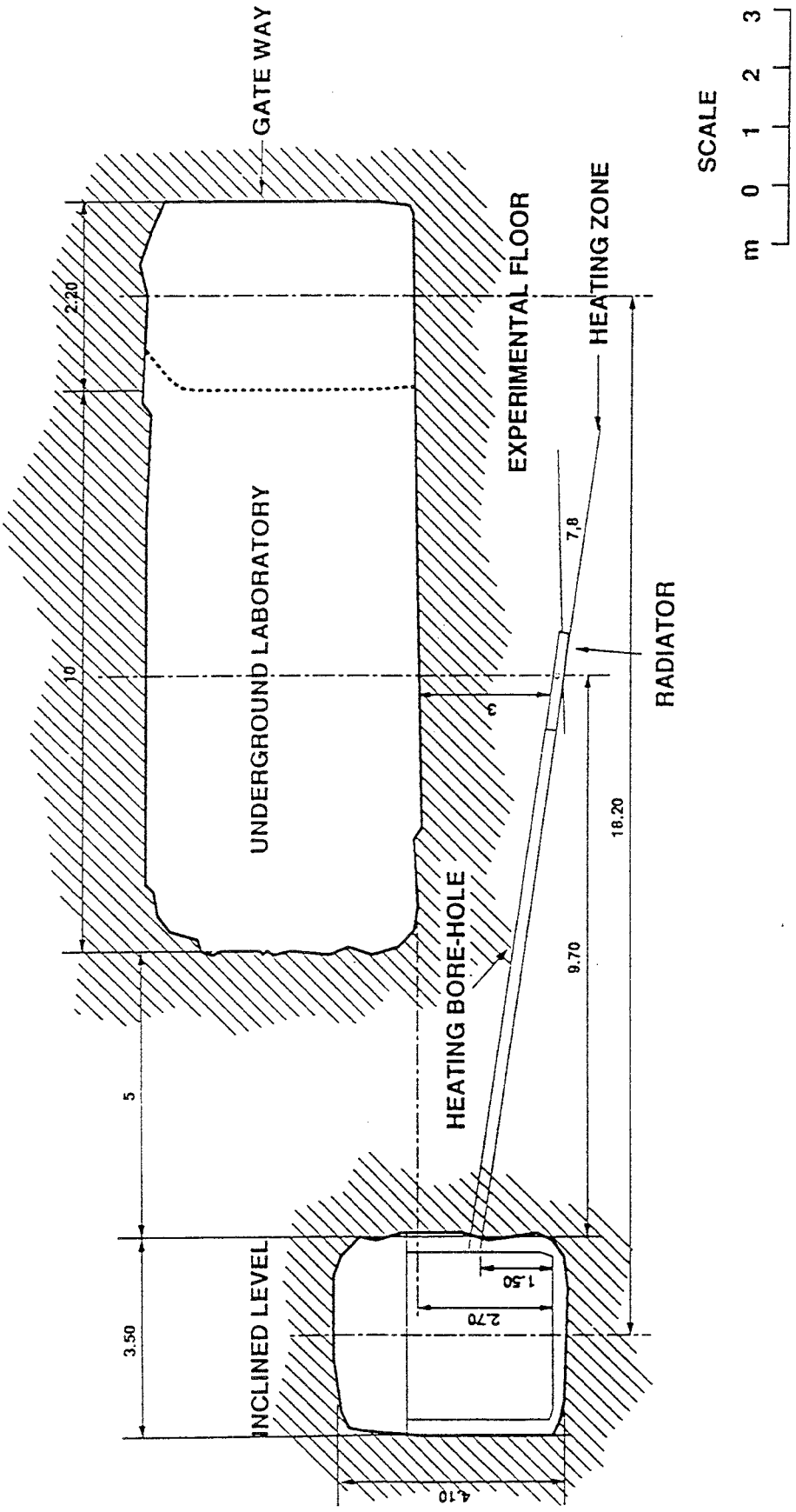

Figure 2-2. Section through the test room at Fanay Augères.

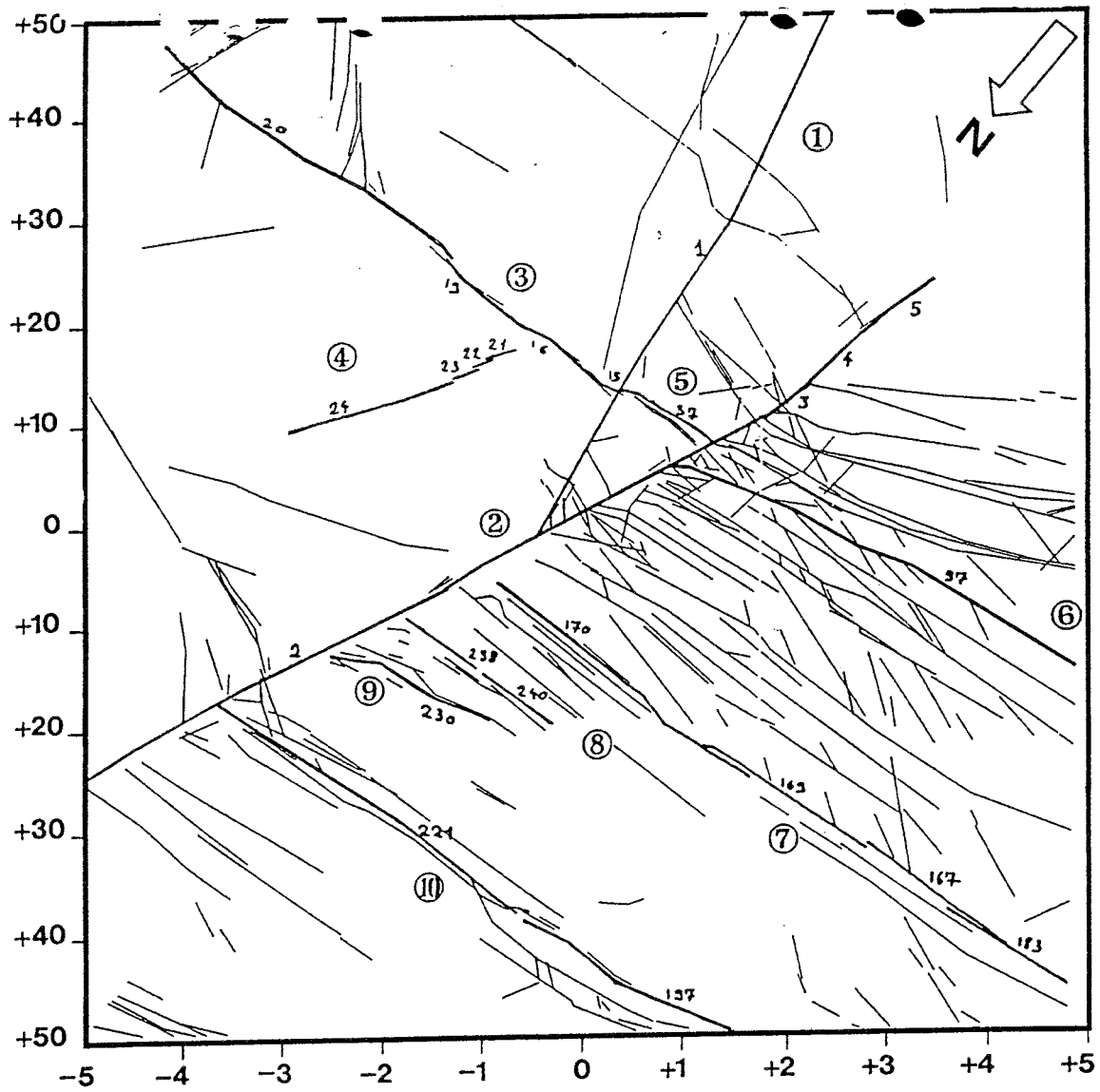

Figure 2-3. Plan of mapped fracture network in the test floor.

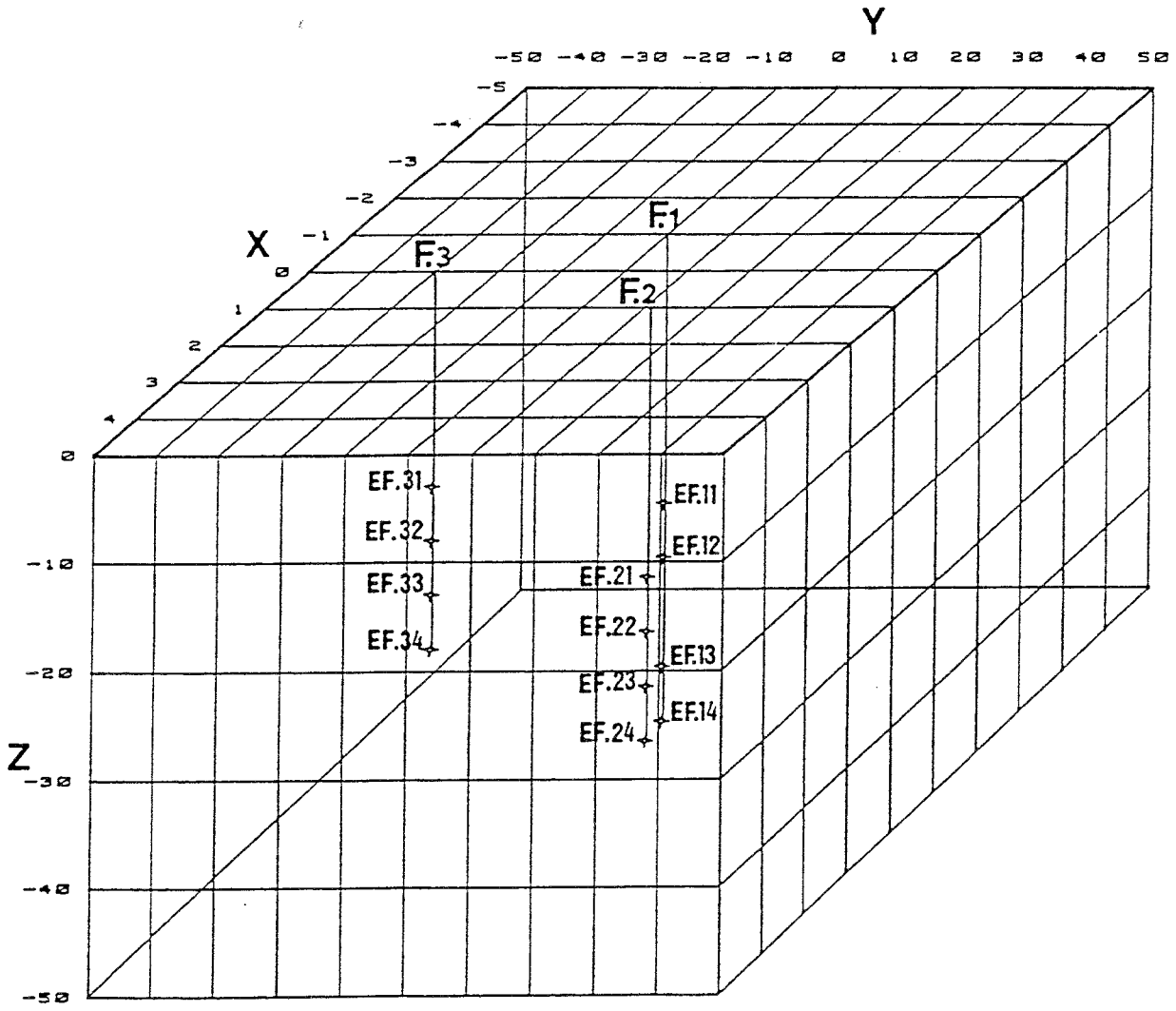

Figure 2-4. *System of coordinates for the test block.*

The instrumentation in the test floor is shown in Fig 2-5. The following measurements were made:

- Vertical displacement of the surface (V1-V8)
- Horizontal displacement of the surface (transformed to strain) in x and y directions (ML/MT1-ML/MT20; EL/ET1-EL/ET18)
- Change in fracture aperture (EF1 and EF2; L11-L13 and L21-L23)
- Vertical fracture shear displacement (EV1-EV4)

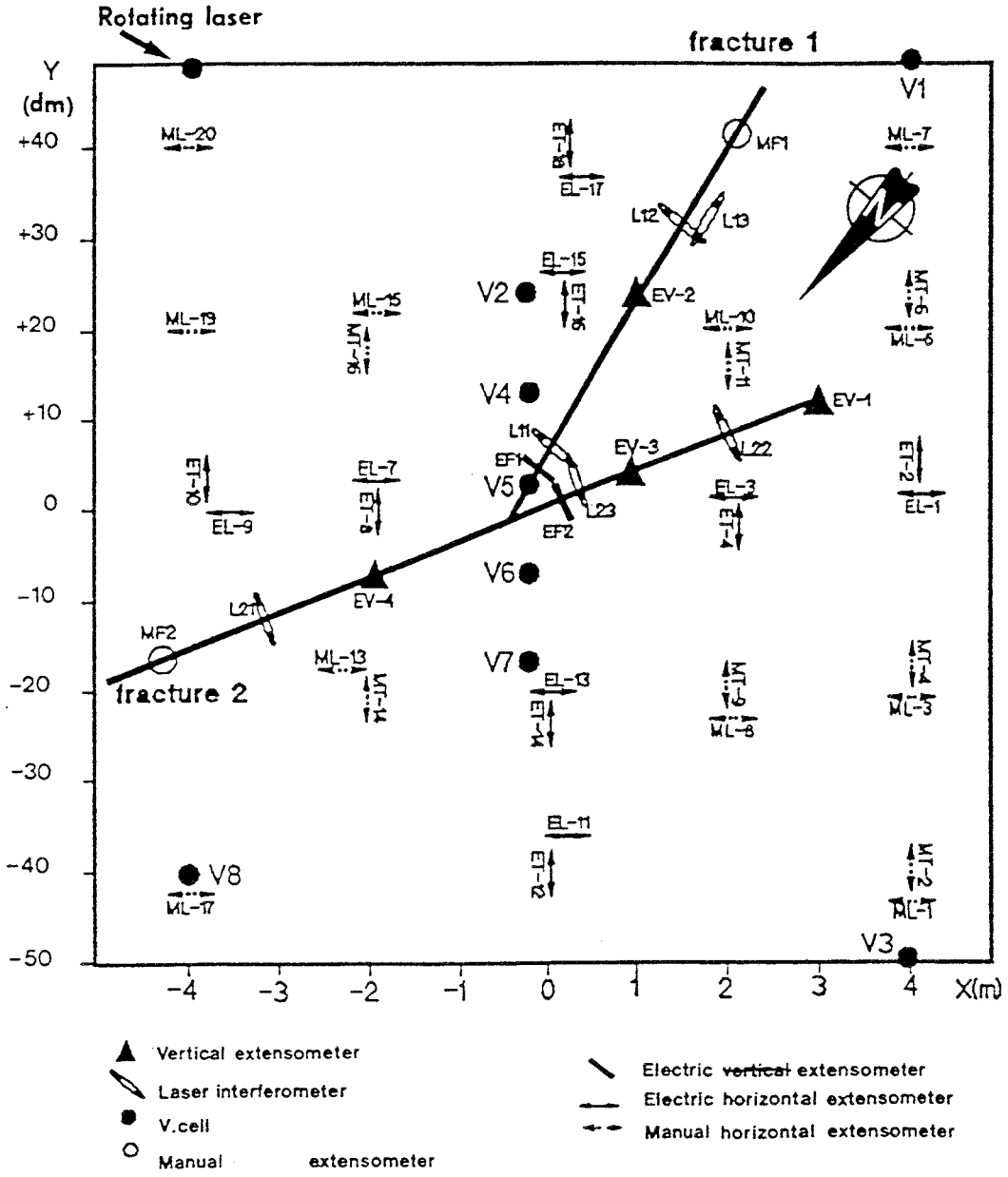

Figure 2-5. Plan of instrumentation of the test floor surface.

2.3 HEATING TEST

Five heater elements 1.5 m long and 11 cm in diameter were emplaced in the five heater holes and a power of 200 W per element was applied, which yielded a total power of 1 kW distributed over a total area of 1.5x1.5 m^2 at 3 meters depth. The power was kept constant during almost 52 days and then turned off. The cooling period was studied during 73 days, which gave a total test time of 125 days.

2.4 RESULTS

All recorded data are collected on diskettes. A few examples will be given in this chapter.

Temperature

The temperature increase in the rock was quite moderate except for very close to the heaters. Outside a radius of 1 m from the centre the temperature was lower than 30 °C and decreased with increasing distance to close to ambient at the block boundary. The temperature measurements have been evaluated with a statistical computer program and transformed to isotherms for the test block /2-1/. Fig 2-6 shows two examples of the maximum temperature representing the end of the heating period. One is a vertical section at x=0 and the other one a horizontal section at z=-3m (cf. Figure 2-4).

Heave of the floor

The heave of the floor, measured at points V1-V8 (Fig 2-5) was quite large. The maximum heave varied between 280 μm and 540 μm in the centre of the floor. However, the measured heave at point V3 close to the rock wall, were it would be expected to be small, was 400 μm, which makes these results questionable.

Strain of the surface of the floor

The displacements of the surface of the test floor were measured in x and y directions at the distance 50 cm by extensometers and then transformed to strain (ML/MT1-ML/MT20; EL/ET1-EL/ET18). See Fig 2-5. The measured strain caused by the heating varied between 0 and 120 μm/m (ε=0-1.2·10^{-4}).

Change in fracture aperture

The recorded change in aperture of the two major fractures 1 and 2 (Fig 2-5), corresponded to an expansion of 4 to 60 μm. No closure was recorded.

Vertical shear displacement of fractures

The vertical shear displacement, also measured at fractures 1 and 2 (Fig 2-5), varied from a few to 10 μm at three measuring points.

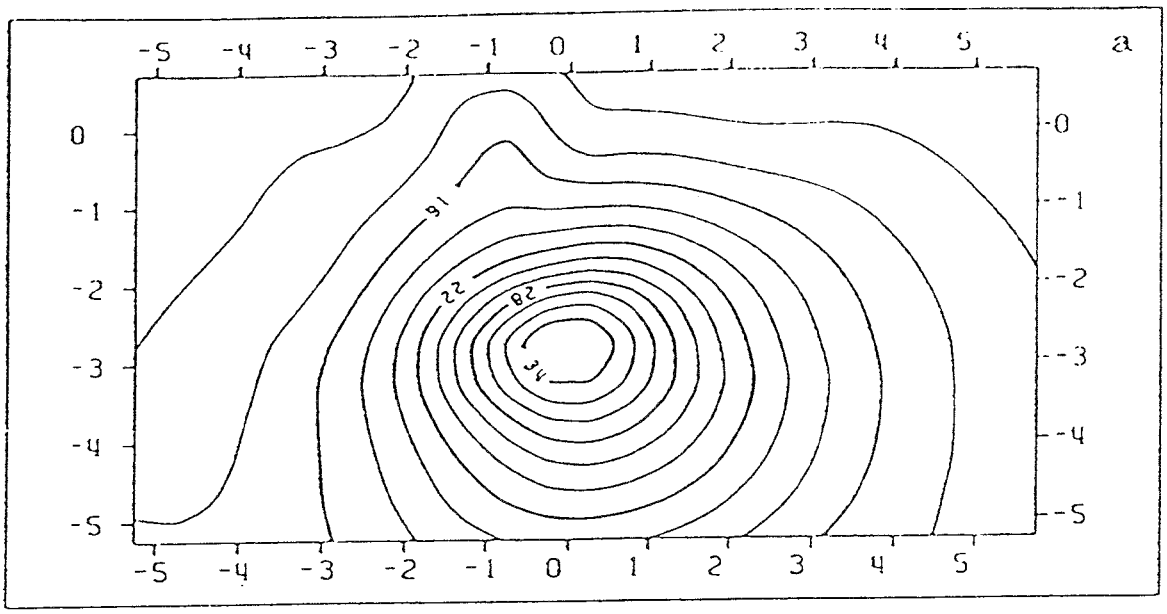

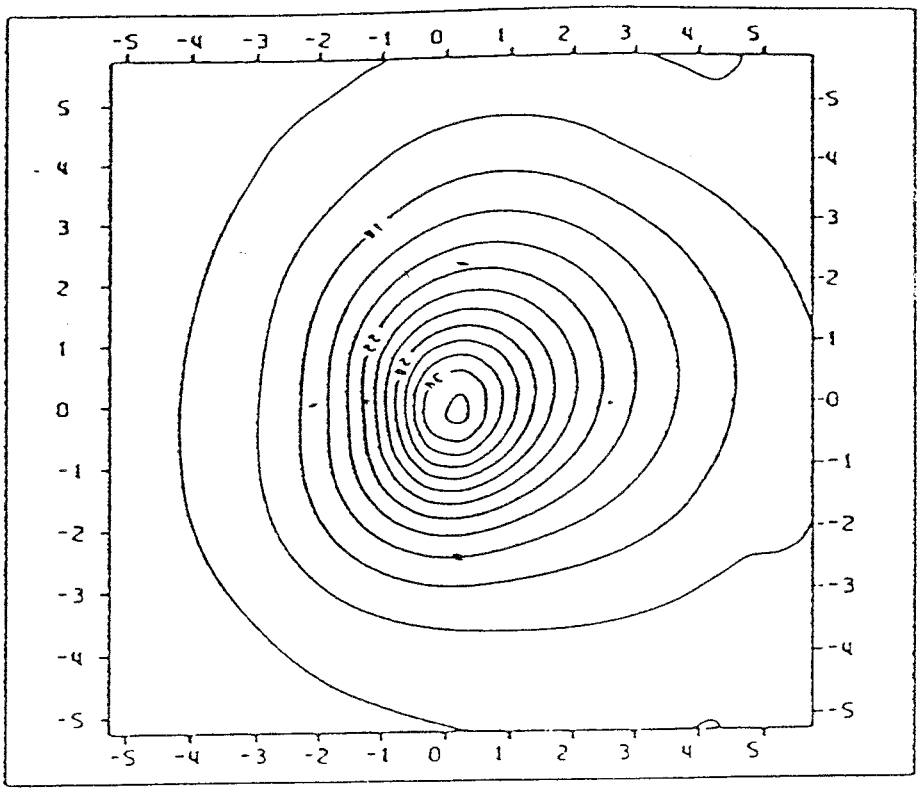

Figure 2-6. *Measured isothermes after 51 days. Upper: Vertical section at x=0. Lower: Horisontal section at z=-3 m.*

Expansion of the heated rock mass

The bore hole extensometers in holes F1 to F3 were used to measure the displacement between the surface of the floor and four points located between 2.0 m and 4.5 m below the floor. The location of the vertical holes are:

F1: x=-1.0 m; y=0.0 m
F2: x=+1.0 m; y=+1.1 m
F3: x=0.0 m; y=-3.0 m

The maximum expansion (measured after 52 days) of the rock between the heater level (z=3.0 m) and the floor (z=0.0 m) varied between 30 μm and 100 μm. The largest measured expansion was 170 μm measured at the depth 4.5 m.

Non-recoverable displacements

Some of the measured displacements seemed to be plastic in the sense that they were not recovered after cooling. These effects were observed at the fracture measurements (opening and shear displacement) and the surface strain measurements but not at the vertical displacement measurements (floor heave and rock expansion).

3 FINITE ELEMENT CODE

The finite element code ABAQUS was used for the calculations. ABAQUS is originally designed for non-linear stress analyses. It has been extended very much in the last 5 years and today contains a capability of modelling a large range of processes in many different materials as well as complicated three-dimensional geometries.

One, two, and three-dimensional elements are available. ABAQUS runs as a batch application. The main input is a file that indicates which options are required and gives the data associated with these options. There may also be many supplementary files, such as restart or result files from previous analyses, or auxiliary data files.

Detailed results from ABAQUS may be obtained via a post-processing code ABAQUS/Post. Detailed information of the available models, application of the code and the theoretical background is given in the ABAQUS Manuals /3-3/.

The code includes special models for rock and soil and ability to model geological formations with infinite boundaries and in situ stresses by e.g. the own weight of the medium.

The calculations in this report were made at FEMTECH in Västerås in close cooperation between the author, Jan Hernelind FEMTECH and Håkan Lind FEMTECH.

4 MATERIAL MODELLING

4.1 GENERAL

The simplest way to model the rock is to assume that it behaves linearly elastic without considering the fractures. Several calculations have been made using such a model. In ABAQUS the fractures can be modelled in several ways, the following being most useful for the calculations.

Joint elements

These elements can simulate fractures with infinitesimal apertures and joint shear/normal stiffnesses. However they cannot simulate dilatancy.

Gap elements

These elements can simulate flow in fractures but are less relevant as concerns the mechanical behavior than the joint elements.

Jointed material

This material model can simulate a jointed material without defining the location of the fracture. Three directions for fracture orientation can be used. The joint will be opened at the most strained location.

Drucker Prager material model

The Drucker-Prager Plasticity model in combination with elastic behaviour at low shear stress can be used if the fractures are modelled with thin elements. This model makes it possible to simulate a defined shear behaviour with dilatancy, as well as water flow in the fractures.

It was concluded that the Drucker-Prager concept was the best one for modelling the given properties of the fractures. The small amount of fractures in the geometrical model also favoured this material model.

4.2 MODELLING OF THE ROCK

The entire rock was mechanically modelled as linearly elastic except for the fractures. Three different E-moduli were given in the specifications. The following parameters were used for the reference calculation:

Rock surrounding the test block:

Mechanical properties

E=55 650 MPa
ν=0.22
ρ=2620 kg/m^3

where E= Modulus of elasticity
ν= Poisson's ratio
ρ= Bulk density

Thermal and thermo-mechanical properties

λ=2.13 W/m,K at T=20 °C
λ=1.95 W/m,K at T=84 °C
(Linear interpolation between these values)
c=890 Ws/kg,K
α=3·10^{-6} 1/K at T=2 °C
α=15·10^{-6} 1/K at T=122 °C
(Linear interpolation between these values)

where λ= heat conductivity
T= temperature
c= heat capacity

The high E-modulus for the surrounding rock was proposed by INERIS and was chosen in order to make the present study compatible with their analysis.

Rock in the test block

All parameters for the rock block were given the same properties as the surrounding rock except for the E-modulus, which was taken to be the average of the values measured in situ.

E=30 000 MPa

4.3 MODELLING OF FRACTURES

4.3.1 General

Six fractures were modelled (the location is shown in chapter 5-2). Since they were defined as ordinary 3D elements with elastic-plastic material properties, the elements must have a thickness that is considerably larger than the aperture of the fracture. In order to adapt the fracture elements to the rock element mesh and to reduce the required total amount of elements, the fracture elements were made with the rather large apparent thickness of d=0.13 m.

The bulk behaviour of these elements must agree with the behaviour of the real fracture with an aperture less than 500 μm. The fracture properties given must thus be transformed to the element thickness. The following properties were measured for one of 5 investigated fractures and proposed by INERIS to be used as fracture input:

K_n=638 000 MPa/m
K_s=577 MPa/m
ϕ_r=34°
ϕ_d=47°
c=0.03 MPa

where K_n= normal stiffness
K_s= shear stiffness
ϕ_r= residual friction angle
ϕ_d= dilatancy angle
c= cohesion

The total friction angle is

$$\tan\phi=\tan\phi_r+\tan\phi_d \qquad (4:1)$$

which yields

ϕ=60°

The Drucker-Prager concept, defined according to Fig 4-1, needs the following input /3-3/:

The plastic part

β="friction angle" in the q-p plane
ψ=dilation angle(=ϕ_d)
K=influence of the intermediate principal stress
Yield function q-ε_v

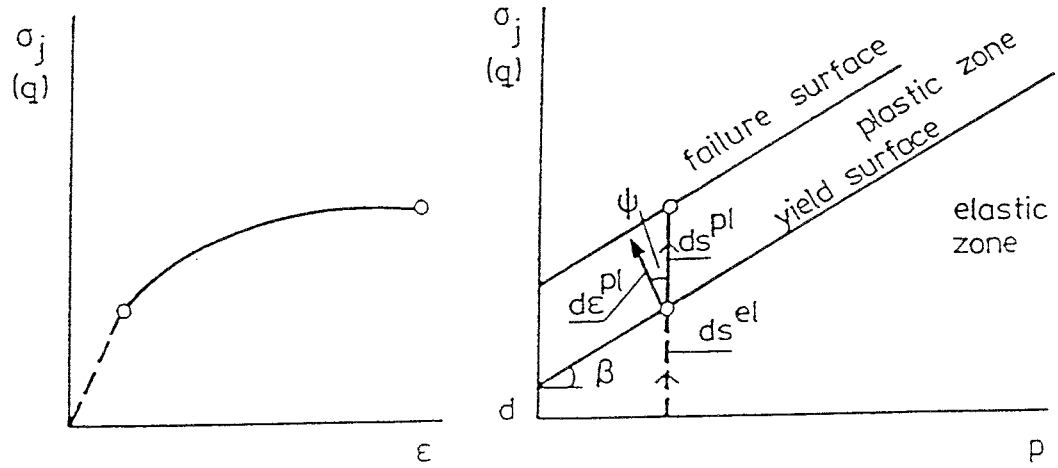

Figure 4-1. *The plasticity model of Drucker-Prager. Ds^{el} and ds^{pl} denote the elastic and plastic stress paths and $d\varepsilon^{pl}$ denotes the plastic flow.*

The yield function, which corresponds to the relation between stress and the plastic strain in the plastic zone, is defined as the plastic strain ε_y for a stress path that corresponds to uniaxial unconfined compression. The total strain is the sum of the elastic and plastic strains.

The elastic part

The elastic parameters E and ν are required.

K_n and K_s must thus be transformed to E and ν. The yield function can be derived from c, K_n, and K_s.

4.3.2 Conversion to the Drucker-Prager concept

Fig 4-2 shows the strain in the fracture element that takes place when a normal stress and a shear stress are applied.

The *shear stiffness* is defined according to Eqn 4:2.

$$K_s=\Delta\tau/\Delta\delta_{//} \qquad (4:2)$$

where τ= shear stress
$\delta_{//}$= shear deformation in the fracture (parallel with the fracture)

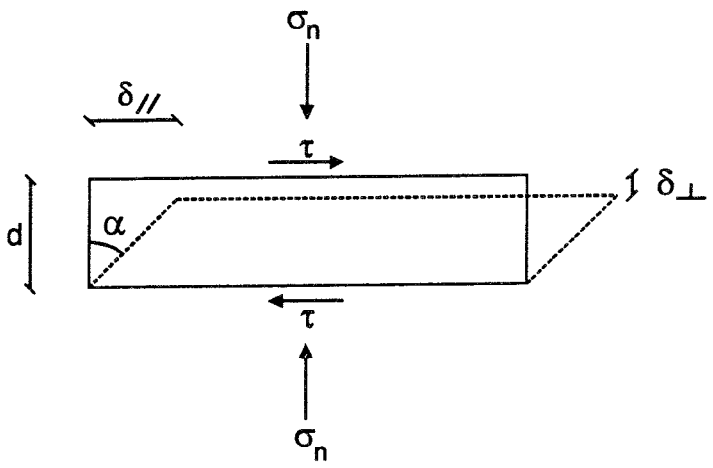

Figure 4-2. *Definition of the strains and stresses in a fracture element.*

The shear modulus G is defined according to Eqn 4:3.

$$G=\Delta\tau/\Delta\gamma \quad (4:3)$$

$$\Delta\gamma=\Delta\delta_{//}/d \quad (4:4)$$

where γ= shear strain in the 13 cm wide fracture in the direction parallel to the fracture
d= width of the fracture element (=0.13 m)

Combining Eqns 4:2 and 4:4 yields Eqn 4:5.

$$G=d\cdot K_s \quad (4:5)$$

Applying d=0.13 m and K_s=577 MPa/m yields

- G = 75 MPa

The *normal stiffness* is defined according to Eqn 4:6.

$$K_n=\Delta\sigma_n/\Delta\delta_\perp \quad (4:6)$$

where σ_n=normal stress
$\delta_\perp$=normal displacement (perpendicular to the fracture)

The one-dimensional compression modulus M is defined according to Eqn 4:7.

$$M=\Delta\sigma_n/\Delta\varepsilon \quad (4:7)$$

$$\Delta\varepsilon=\Delta\delta_\perp/d \quad (4:8)$$

where ε=compression strain perpendicular to the 0.13 m wide fracture

Combining Eqns 4:6 and 4:8 yields Eqn 4:9.

$$M=d\cdot K_n \tag{4:9}$$

Applying d=0.13 m and K_n=638 000 MPa/m yields

- M = 82 940 MPa

The relation between the bulk modulus, the shear modulus, and the compression modulus is

$$E=\frac{M(1+\nu)(1-2\nu)}{1-\nu}=2(1+\nu)G \tag{4:10}$$

which yields

$$\nu=\frac{M-2G}{2(M-G)} \tag{4:11}$$

Using the calculated values of G and M one gets

ν=0.4995
E=225 MPa

for the elastic deformation of the fracture element.

The Mohr-Coulomb parameters ϕ_r and c can be converted to Drucker-Prager parameters β, K and σ_c^0 (σ_c^0= start value for the yield function) by use of Eqns 4:12 to 4:14 /3-3/.

$$\tan\beta=\frac{6\sin\phi_r}{3-\sin\phi_r} \tag{4:12}$$

$$K=\frac{3-\sin\phi_r}{3+\sin\phi_r} \tag{4:13}$$

$$\sigma_c^0=2c\frac{\cos\phi_r}{1-\sin\phi_r} \tag{4:14}$$

These equations yield:

β=54°
K=0.69
σ_c^0=0.112 MPa

However, since K cannot be less than 0.778, K=0.8 is applied.

No information was given about the plastic behaviour of the fractures. In the present study, the yield function in Table 4-1 has been used.

Table 4-1. Yield function for the fracture model

q (MPa)	ε_y
0.112	0
5.5	0.02

The yield function defines the plastic strain. The total strain is the sum of the elastic and plastic strains. The yield function is chosen to give a total shear strain that is about twice the elastic strain.

Fig 4-3 shows an example of the stress-strain relation for a fracture with a normal stress of 2.6 MPa corresponding to the in situ stress. In this example the fracture is sheared to q=5.5 MPa and then unloaded to q=0. The strain will be elastic until q=3.6 MPa, which corresponds to the yield stress at p=2.6 MPa for β=54°. The strain will then be elastic and plastic until shearing is stopped. The unloading will be elastic and a non-recoverable strain of 0.0065 will remain after removal of shear stress.

The Drucker-Prager model gives a very high shear strength at low average normal stresses. This could be a problem close to the floor. However, the calculations show that the plastic strain is too small to be affected by this.

4.3.3 Fracture model input

The input of the fractures is thus:

Thermal and thermo-mechanical

Identical to the input of the rock block.

Mechanical

For the fracture model the input is the following:

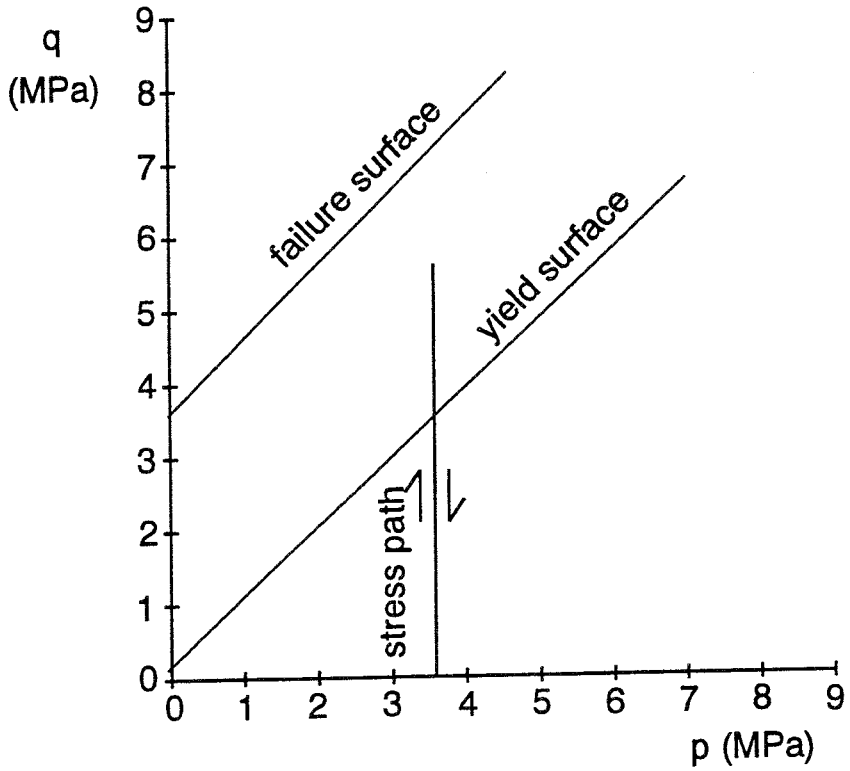

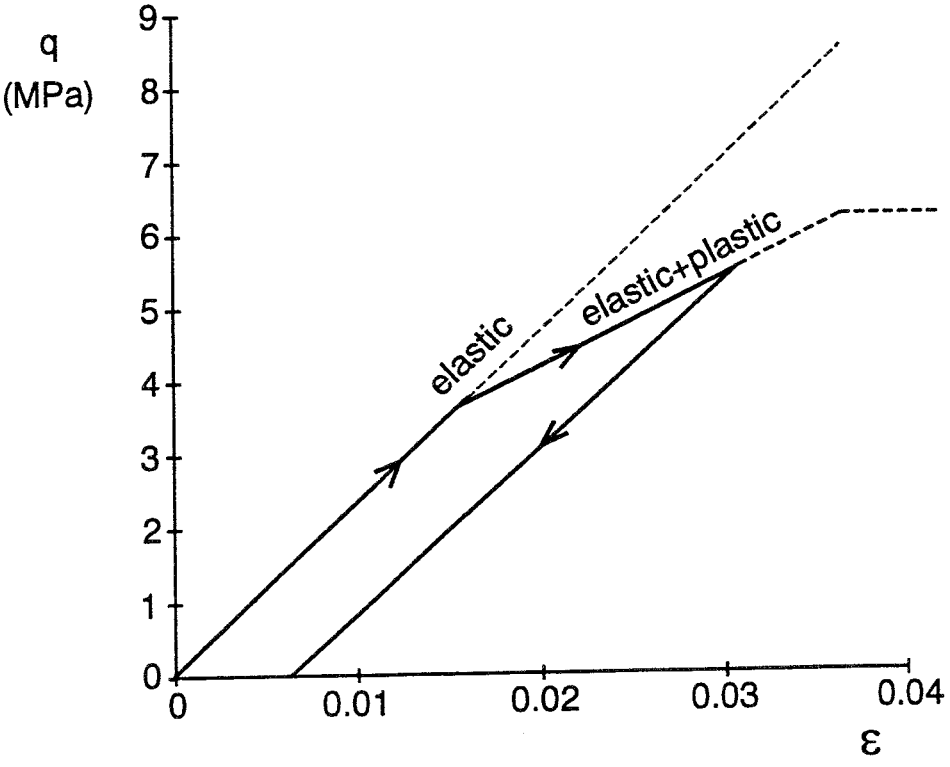

Figure 4-3. Example of the stress-strain relation for the fracture element when the element is sheared until q=5.5 MPa and then deloaded under constant average stress p=2.6 MPa.

Elastic part

ν=0.4995
E=225 MPa

Plastic part

β=54°
K=0.69
$\psi=\phi_d$=47°
Yield function according to Table 4-1

For the elastic non-fractured model the input to the fracture elements is identical to the input to the rest of the rock block.

5 STRUCTURE MODELLING

5.1 GENERAL

According to the fracture mapping, shown in Fig 2-3, the rock block contains a large number of discontinuities. However, since only about 10 of them are unsealed fractures a simplified model consisting of only 6 main breaks has been proposed by INERIS. This model, which is shown in Fig 5-1, has been used in the calculations accounted for in this report.

5.2 FRACTURES

The rock block at $z \leq 0$

The fractures are quite steep with a dip varying between 50° and 86°. The orientations, described in the data collection, have been adapted to the finite element model of the rock block. The extension of the fractures is unknown and they have been modelled to be limited by the boundaries of the rock block, which implies the following dimensions of the block: z=0 to z=-5.0 m, x=–5.0 m to x=+5.0 m, and y=–5.0 m to y=+5.0 m. As indicated by Fig 5-1 they are truncated according to the following specification:

- Fracture 2 is the only unlimited fracture. It intersects the entire block.
- Fracture 1 is limited by fracture 2 at the north side.
- Fracture 3 is limited by fracture 1 and further down also by fracture 2.
- Fractures 6, 7, and 10 are limited by fracture 2 at the south side.

The direction of the fractures are accounted for in Table 5-1.

Table 5-1. Fracture orientations

Fracture No	Strike	Dip
1	N174E	71W
2	N25E	86W
3	N92E	76N
6	N83E	50N
7	N92E	56N
10	N86E	73N

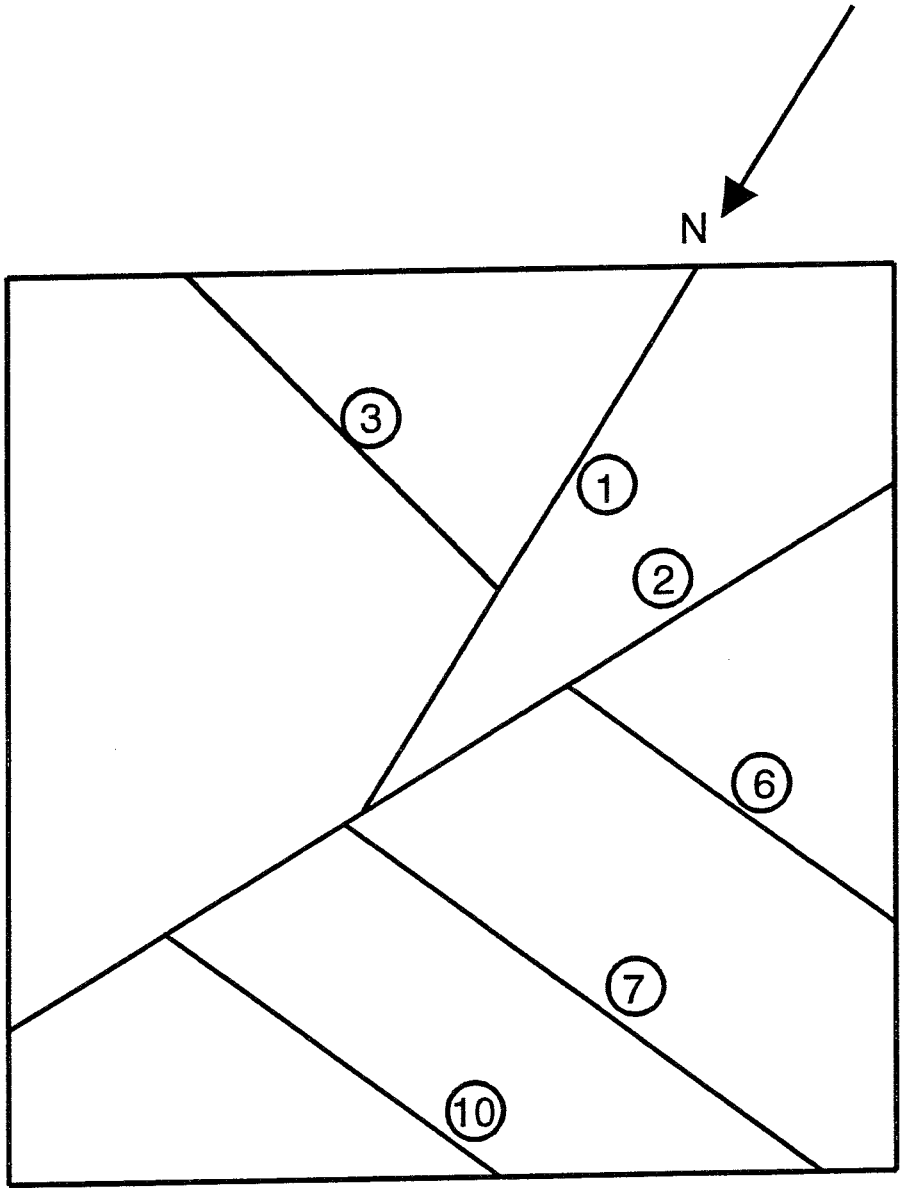

Figure 5-1. *Fracture model proposed by INERIS and applied in the calculations. The location of the fractures in the floor are shown.*

The excavated rock block at z≥0

Before excavation the fractures are assumed to extend into the rock with the same orientation and properties as in the block.

The surrounding rock

No fractures were modelled in the surrounding rock at -5m≥x≥+5m, -5m≥y≥ +5m, and -5m≥z≥+5m.

5.3 FINITE ELEMENT MESH

The rock structure was constructed by 3-dimensional solid elements with 8 nodes. The total volume of the model was 40mx40mx40m. The total amount of elements in the model was 7 180.

Fractures

Fig 5-2 shows the mesh of the fractures in the lower block viewed in the same fashion as in Fig 2-4. All **view plots** are seen from this point if not otherwise noted.

Rock block

The modelling of the rock between the fractures was quite difficult due to the inclinations of the fractures and the intersections between them. Since the fractures were modelled by use of elements, all nodes in the fractures must coincide with the nodes in the rock outside the fractures The lower block was modelled as a sandwich structure composed of 11 layers with a thickness of 0.2-0.5 m. Fig 5-3 shows a view plot of the lower rock block. The final mesh used in the calculations, was made after a large number of test calculations and changes. The final mesh was not altogether perfect due to problems with strange element shapes but considered to be acceptable. A check of the fitness of the mesh was given by elastic calculations of displacements at application of the initial stresses. The displacements of the nodes in the mesh should be zero while the calculated maximum displacements were a few μm. The accuracy of the calculations is thus about +/- 4 μm.

The upper block, which was excavated, was modelled with only 3 levels. The fractures in the upper 2 levels were adjusted to be oriented in the vertical direction.

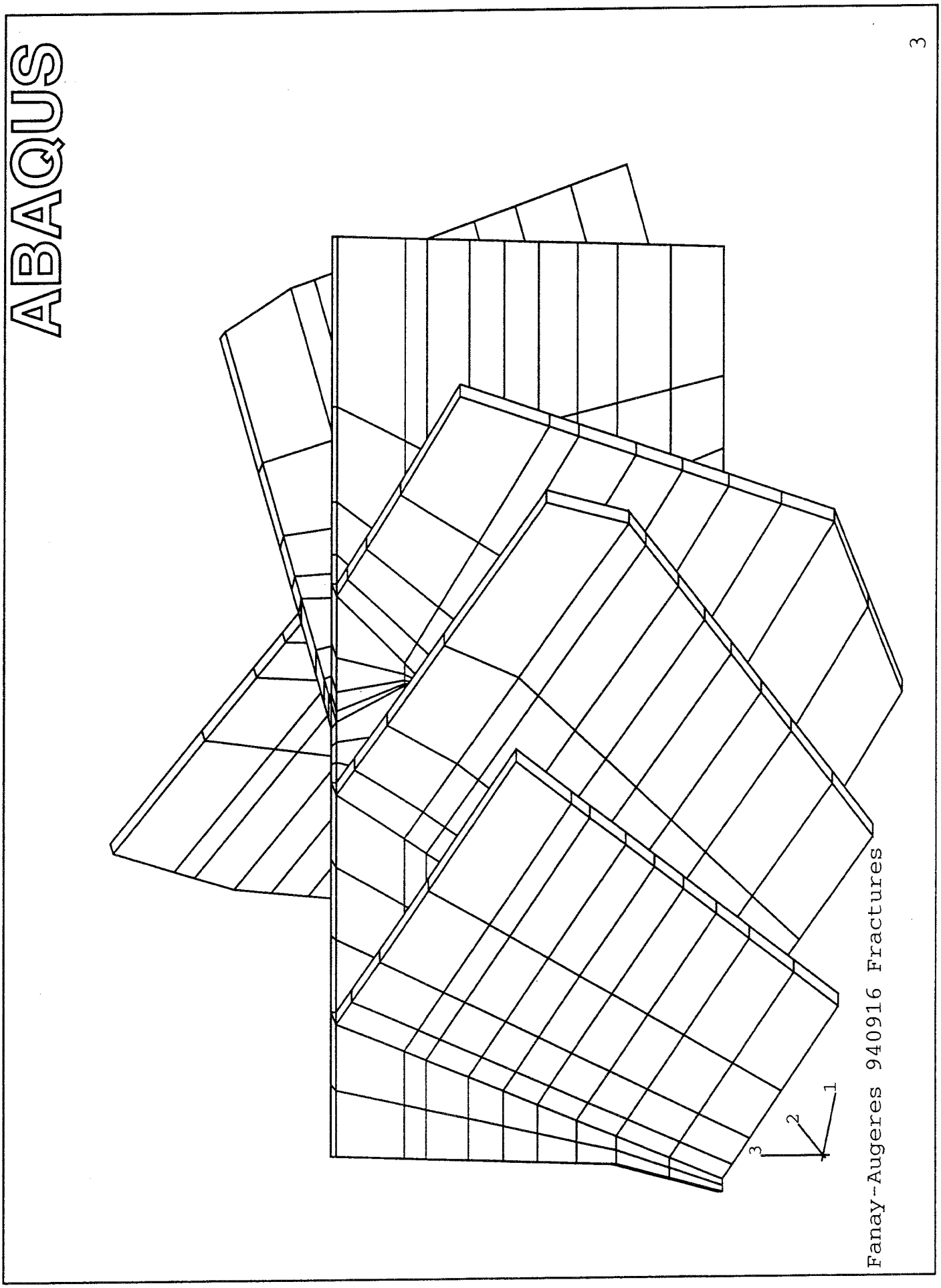

Figure 5-2. *Element model of the fractures in the lower block.*

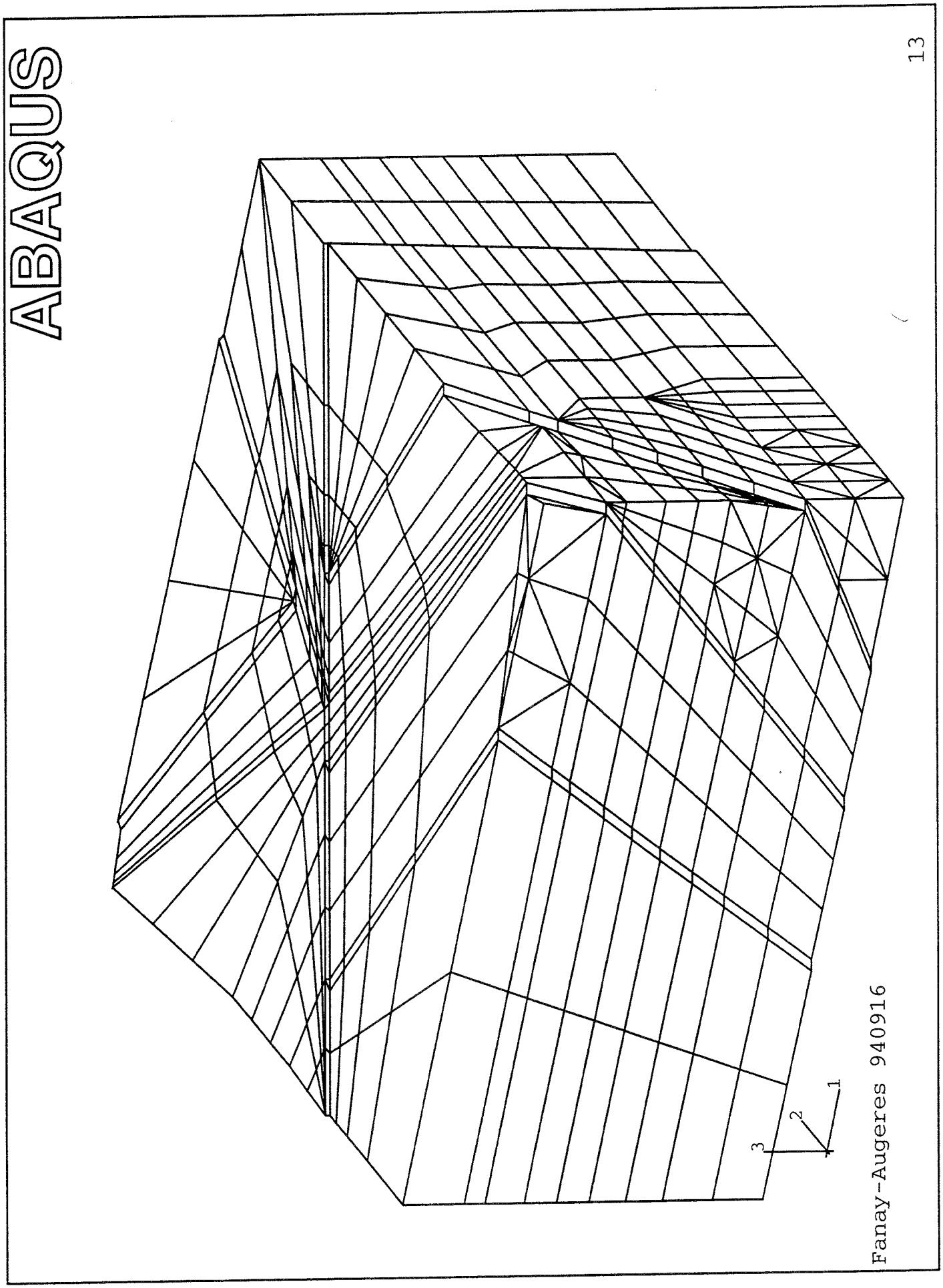

Figure 5-3. *Element mesh of the lower rock block.*

Surrounding rock

The surrounding rock was modelled by four element rows in all six surrounding blocks, the thickness of which was 15 m. Fig 5-4 shows the surrounding rock at level z=0.

The excavation was made by removing the elements in the upper block and the first row of elements in the surrounding rock in x- and y-directions. This gave an opening with the dimension 13mx13m and the height 5m. The shape of the excavated floor differs a little from the real shape but the total square measure is the same as the total square measure of the real excavation.

Fig 5-5 shows a view of the element mesh after excavation with the elements hiding the excavation at $x \leq -5$m and $y \geq +5$m removed.

5.4 BOUNDARY CONDITIONS

Thermal

The outer thermal boundary was assumed to be adiabatic, i.e. perfectly insulated. The calculations showed that no temperature increase took place at the boundary which means that the boundary was located at sufficient distance from the heaters for making the calculations relevant.

Heat convection boundary condition was applied to the inner boundary, i.e. the roof, floor and walls of the excavated room was equipped with heat transfer film coefficients and the air in the room was prescribed to yield a decreasing temperature with time. The following input values were used:

- Heat transfer coefficient: 10 W/m^2,K
- Air temperature at start of the heating period: 13 °C
- Air temperature at the end of the cooling period: 9 °C
- Linear decrease in air temperature during the test

Mechanical

The outer mechanical boundary was simulated as being completely fixed. It was found to be sufficiently far away to make the influence of the assumed boundary conditions insignificant (see chapter 7).

The inner boundary was mechanically free in all directions.

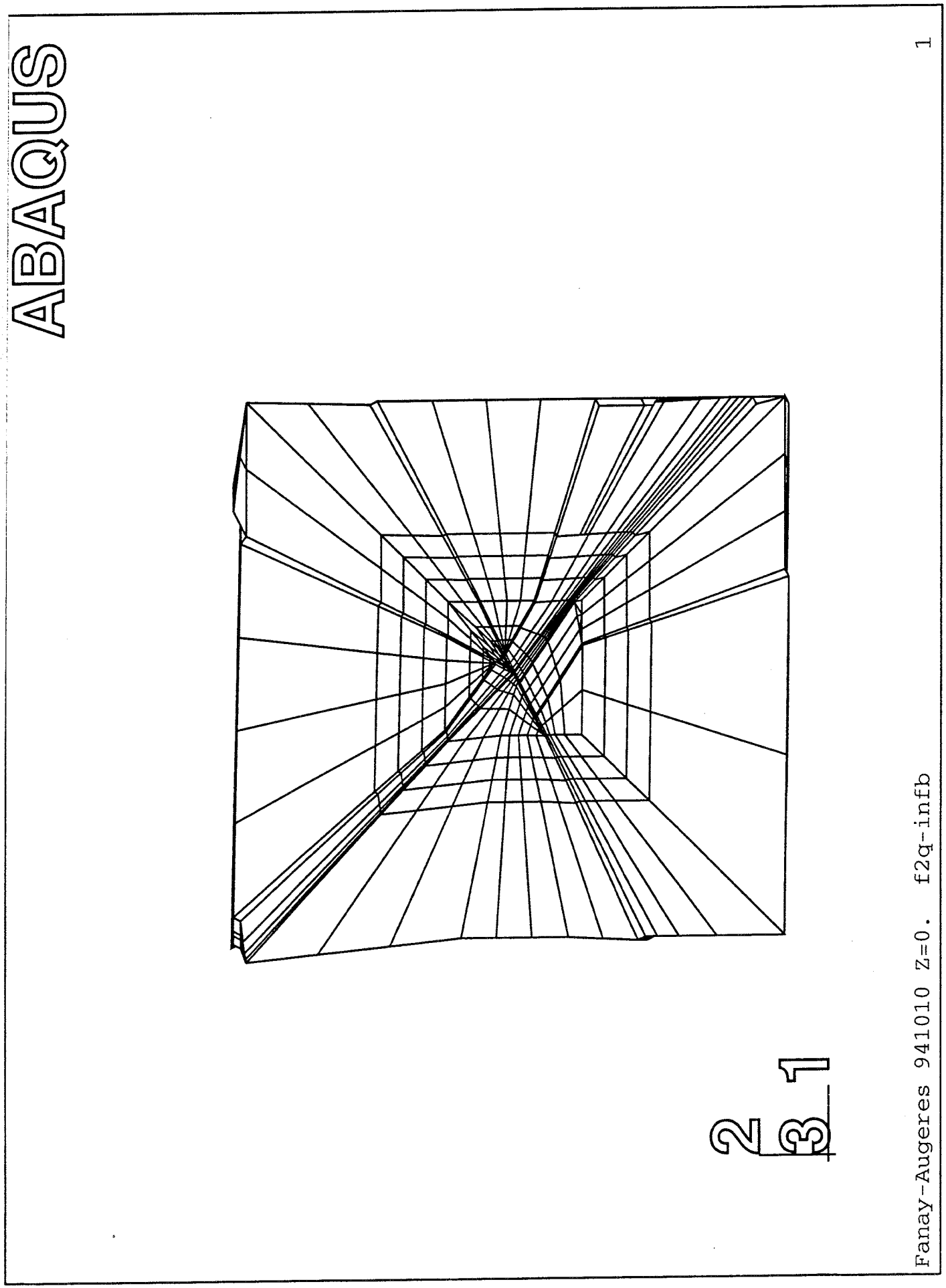

Figure 5-4. *Element mesh of the surrounding rock at the floor level (z=0).*

Figure 5-5. *View of a part of the model after excavation. The outer 10 m thick element row is not shown.*

5.5 INITIAL CONDITIONS

Before running the calculation, the external stresses must be applied to yield the initial, starting conditions and the model must be mechanically in equilibrium. The applied initial in situ stresses were non-isotropic with the following values /1-1/:

$$\sigma_v = \rho z \ (\approx 2.6 \text{ MPa}) \quad (5:1)$$
$$\sigma_{h1} = 1.35\sigma_v \quad (5:2)$$
$$\sigma_{h3} = 0.92\sigma_v \quad (5:3)$$

where σ_v=vertical stress
ρ=2 620 kg/m^3 bulk density
σ_{h1}= horizontal major principal stress
σ_{h3}= horizontal minor principal stress

The direction of the horizontal major principal stress is N150°E (defined as strike).

The initial temperature was 13°C in the entire structure.

5.6 HEATERS

The 5 heaters were modelled by applying the power 1000 W evenly distributed among 8 nodes located in an area of 1.2 m^2 in the centre of the level z=-3m. The heater geometry is not simulated in detail and the temperature will not be very accurate in the vicinity of the heaters (within the radius of about 1 m), partly because of the heater geometry but partly also because of the rather large elements. It has not been considered to be very important to simulate this small volume with a high precision.

The heat was applied for 52 days and the cooling period lasted for 73 days.

6 CALCULATIONS

6.1 GENERAL

A large amount of calculations have been performed before the final ones were made. The pilot calculations were made in order to check the geometry, element mesh, influence of boundary conditions and several other parameters (see chapter 7). No changes have been made in order to fit the measured data better.

The results from two main calculations will be shown. One of them implied linearly elastic strain with no simulation of fractures. The other assumed elasto/plastic behaviour with simulation of fractures.

The results are shown in a large number of figures. In order to keep the text legible, the figures are placed after the references.

6.2 CALCULATION SEQUENCE

The calculations were made in the following 4 steps:

1. Application of in situ stresses and stress adjustment to reach equilibrium
2. Excavation of test room
3. Heating phase
4. Thermomechanical response to the heating

The temperature calculation was made independently of the mechanical calculations, and was hence uncoupled. Coupling was not required since the thermal performance does not depend on the mechanical processes. The temperature calculation was thus the same for both the fracture-free and the fractured conditions.

6.3 TEMPERATURE CALCULATION

The results of the temperature calculation are presented in the form of:

- time-history plots (temperature as a function of time for different nodes)
- contour plots (temperature iso-lines at different sections just before cutting off the power).

Figs 6-1 to 6-3 show time-history plots for five different levels at the same x and y coordinates. Each figure represents the temperatures at the four measuring points in the extensometer holes F1 to F3. The fifth curve is the surface temperature. The coordinates of the different points are given in the figures. The figures show typical temperature-time curves with more

pronounced peak values for the spots close to the heater than away from it. The heat pulse was delayed at large distance from the heater as demonstrated by the diagrams. The surface temperature decreased with time due to the linear decrease in room temperature.

Figs 6-4 and 6-5 show contour plots of the temperature. Fig 6-4 shows the temperature in fracture 2, which intersects the entire test block. The calculated temperatures are very high in the 6 elements that surround the heater due to linear interpolation between the nodes, and those higher than about 50°C are not correct. Fig 6-5 shows the temperatures around the excavated room with the roof and two walls removed. The cooling effect of the room is clearly seen. The temperature of the surrounding rock decreases from the original 13°C a few meters into the rock to about 11.5°C on the surface of the walls. At the surface of the floor the temperature increases slightly from 11.5°C in the corners to about 12.5°C in the centre due to the heaters.

6.4 RESULTS FROM CALCULATIONS WITH ELASTIC NON-FRACTURED ROCK

6.4.1 General

The elastic calculation is important for reference purposes. In particular, it can be used for comparing it with the plastic calculation in order to investigate the impact of fractures in the model. It can also be used for sensitivity analyses, i.a. for investigating the influence of the boundary conditions and other factors. In this chapter only the results of the reference calculation will be reported.

The input of the calculation is given in chapter 4.2, meaning that the fractures are given properties identical with those of the rock.

The results are shown by using the same two techniques as in the temperature calculation; namely contour plots and time-history plots. The contour plots, which show iso-lines of specific stresses and deformations, refer to three different stages:

1. After excavation
2. After heating
3. After cooling

The contour plots show the accumulated values from the start of the calculation. They represent many different sections seen from different angles in order to illustrate the results. A selection of results will be shown here.

The time-history plots will show displacements as a function of time at locations identical to measuring points. The following functions will be shown:

1. Vertical displacement of the floor
2. Strain in the floor
3. Opening of fractures 1 and 2
4. Shear displacement along fractures 1 and 2
5. Expansion of the rock block

6.4.2 Contour plots

All contour plots show the accumulated values from start, i.e. before excavation.

Vertical displacement (U3)

The most characteristic effect is the vertical displacement, since the heave of the floor is considerable. Figs 6-6 to 6-8 show the vertical displacement of the floor. Only the test block is shown and the 1.5 m wide zone around the floor that was also excavated is not seen. The heave after excavation is about 600 μm at the centre of the floor and about 280 μm at the corners (Fig 6-6). At heating, the heave in the centre increases to about 750 μm while the corners hardly move at all (Fig 6-7). After cooling, the floor returns to an almost identical level as before heating due to the elastic behaviour (Fig 6-8). The iso-lines are almost concentric due to the symmetry conditions and the homogenous rock. The small deviations are caused by imperfections in the element mesh.

The vertical displacements are also shown in an almost vertical section of the block that coincides with fracture 2 and in a view that only contains the 6 fractures (Figs 6-9 to 6-13). Figs 6-9 to 6-11, visualising U3 after excavation, after heating and after cooling show that:

- the elastic rebound is not complete (due to incomplete recovery of the temperature)
- the heave below the heater (the centre of the fracture at 3 m depth) is up to 300 μm after excavation and changes very little by the heating.
- the effect of heating is thus primarily an expansion of the rock above the heaters

Vertical stress (S33)

The vertical stress, which was 2.6 MPa before excavation, drops significantly in the rock block at the excavation. Fig 6-14 shows the stresses after excavation in a view with the front walls removed. The stress reduction reaches below the 5 m thick test block and is also seen in the roof.

The vertical stresses after heating in a horizontal plane at z=-2.6 m are shown in Fig 6-15. The increase in stress due to the thermal expansion is very strong close to the heater with values up to 10 MPa.

Principal strain (EP1, EP3)

The strain in the surface of the floor was measured and is thus of interest. Figs 6-16 and 6-17 show the main principal strain in the floor after excavation and after heating. It is quite small with values lower than 10^{-5} (10 μm/m) after excavation and lower than $4 \cdot 10^{-5}$ (40 μm/m) after heating.

6.4.3 Time-history plots

Time history plots of the displacements measured in the extensometer holes (F1-F3 according to chapter 2.4) and at the spots shown in Fig 2-5 have been produced.

Heave of the floor (V0 to V7 in Fig 2-5)

Fig 6-18 shows the vertical displacement of the floor as a function of time from the start of the heating. The locations of the nodes correspond to spots V2 to V7 and V0 corresponds to the rotating laser (reference level). The exact coordinates of the nodes are noted in the figure.

The starting level 550 μm is caused by the excavation. The heave from the heating (100 μm to 170 μm) is thus much smaller. The reference point does not move during the heating period but settles by 14 μm in the cooling period due to the decreased surface temperature.

Displacement of fractures 1 and 2

The following relative fracture displacements have been calculated:

1. Horizontal shear displacement corresponding to the fracture shear displacement in the x/y direction (ux)
2. Opening of the fracture in the normal direction (uy)
3. Vertical shear displacement corresponding to the fracture shear displacement in the z direction (uz)

Fig 6-19 shows the location of the nodes in the fractures for which these displacements have been calculated. The figure shows an enlargement of the element mesh in the floor. The nodes shown in Fig 6-19 correspond to the measuring points in Fig 2-5 according to Table 6-1.

Table 6-1. Measuring points in fractures 1 and 2

Fracture number	Nodes in Fig 6-19	Measuring points in Fig 2-5	Termed in Figs 6-20 to 6-22 (6-42 to 6-44)
2	70/78	L21	1p01
2	71/79	EV4	1p02
2	101/102	EF2	1p03
2	105/106	L23	1p04
2	126/110	EV3	1p05
2	136/146	L22	1p06
2	137/147	EV1	1p07
1	38/28	EF1	2p01
1	39/29	L11	2p02
1	8/18	EV2/L12	2p03

Since no fracture properties have been used in the elastic calculation the results in the fractures are of minor importance. However they will be accounted for in Figs 6-20 to 6-22 for comparison with the fracture calculation.

The diagrams show that the shear displacements and openings vary between 0 μm and 22 μm.

Strain in the floor

Strain representing 8 spots in x and y directions in the floor were calculated and found to be as specified in Table 6-2.

Table 6-2. Locations of points in the floor were strain is calculated

Termed in Fig 2-5	Coordinates (x;y)	Termed in Fig 6-23 (6-45)
EL9/ET10	0;-4	ex/y-6p01
EL7/ET8	0;-2	ex/y-6p02
EL3/ET4	0;+2	ex/y-6p03
EL1/ET2	0;+4	ex/y-6p04
EL11/ET12	-4;0	ex/y-6p05
EL13/ET14	-2;0	ex/y-6p06
EL15/ET16	+2;0	ex/y-6p07
EL17/ET18	+4;0	ex/y-6p08

Fig 6-23 shows the calculated strain in these points. The strain due to the heating vary between $4 \cdot 10^{-5}$ and $34 \cdot 10^{-5}$ (40 μm/m and 340 μm/m).

Expansion of the rock block

The change in distance from the floor and different points in the rock block has been measured at four depths in the extensometer holes F1-F3. Corresponding displacements have been calculated with the exact location and terming according to Table 6-3.

Table 6-3. Location of the points for which expansion has been calculated

"Bore hole"	Coordinates (x;y)	Depth	Termed in Fig 6-24 (6-46)
F1	-1.0;0	-2.5	3p01
F1	-1.0;0	-3.0	3p02
F1	-1.0;0	-4.0	3p03
F1	-1.0;0	-4.5	3p04
F2	+1.0;+1.1	-2.5	4p01
F2	+1.0;+1.1	-3.0	4p02
F2	+1.0;+1.1	-3.5	4p03
F2	+1.0;+1.1	-4.0	4p04
F3	0;-3.0	-2.0	5p01
F3	0;-3.0	-2.5	5p02
F3	0;-3.0	-3.0	5p03
F3	0;-3.0	-3.5	5p04

Fig 6-24 shows the calculated expansion of the rock. It varies between 180 μm for the deepest location in hole F1 to 15 μm for the most shallow location in hole F3.

6.5 RESULTS FROM CALCULATIONS OF FRACTURED ROCK

6.5.1 General

The final calculation, that simulates also the fractures in the test rock block, was made in the same way as the elastic calculation, the only difference being the introduction of elasto-plastic properties of the fractures (cf. chapter 4.3).

The results will be accounted for with same plot types as the elastic results, i.e. contour plots after excavation, after heating, and after cooling, and time history plots.

6.5.2 Contour plots

All contour plots show the accumulated values calculated from start, i.e. before excavation.

Vertical displacement (U3)

Figs 6-25 to 6-27 show the vertical displacements of the floor. Only the test block is shown, while the 1.5 m wide zone around the floor that was also excavated is not plotted in the figure. The heave after excavation is up to 1000 μm at the intersection between fractures 2 and 6 and fractures 2 and 7, and about 280 μm at the corners (Fig 6-25). The strong influence of the fractures is obvious and the shear displacement in some fractures very large, especially in fracture 6, were it is up to 400 μm. On heating, the heave in the centre is increased to over 1000 μm while the corners have hardly moved at all (Fig 6-26). The shear displacement due to the heating is not very large. After cooling, the floor has returned to a similar position as before heating, which indicates that the plastic displacements in the fractures are negligible.

The vertical displacement is shown in an almost vertical section of the block that coincides with fracture 2 and in a view that only contains the 6 fractures (Figs 6-28 to 6-32). Figs 6-28 to 6-30, visualising U3 after excavation, after heating, and after cooling show that

- there is a small but obvious difference between the displacements after excavation and after cooling, which is partly due to a slight change in temperature and partly to plastic strain in the fractures
- in concordance with the elastic calculation, almost all the expansion takes place above the heater (placed in the centre of the fracture at 3 m depth).
- there is a substantial shear displacement in the three fractures, especially of fracture 6. The shear displacement increases close to the floor.

Figs 6-33 and 6-34 show a 3-dimensional picture of the floor with the displacements enlarged 1400 times. The view is taken from "behind" with the large fracture 2 traversing the floor and fractures 6, 7, and 10 oriented away from the observer. The additional expansion due to the heating can be seen when comparing the pictures.

Plastic strain of the fractures

Some plastic strain takes place along the fractures as can be seen in the plots of PEEQ (equivalent plastic strain) in a view of only the fractures in Figs 6-35 and 6-36. The maximum plastization takes place in fracture 6 with a maximum plastic strain that is 0.14 % ($\delta^p_{//}$=0.182 mm) after excavation and 0.17% ($\delta^p_{//}$=0.221 mm) after heating and after cooling. The plastization is thus small and does not imply failure, which takes place at a strain of 2%, corresponding to a plastic shear displacement of $\delta^p_{//}$=2.6 mm.

Vertical stress (S33)

The vertical stress, which was 2.6 MPa before excavation, dropped significantly in the rock block at the excavation and was locally increased at heating. Fig 6-37 shows these stresses after excavation and Fig 6-38 the stress conditions after heating, at the level z=-2.6 m. In the latter figure the maximum stress is about 8 MPa in the centre, which is less than for the elastic conditions

Principal strain (EP1, EP3)

Figs 6-39 and 6-40 show the major principal strain EP1 in the floor after excavation and after heating. It is smaller than for the elastic calculation with values below $2 \cdot 10^{-5}$ (20 μm/m) after excavation and below $4 \cdot 10^{-5}$ (40 μm/m) after heating.

6.5.3 Time-history plots

Time history plots of the displacements measured in the extensometer holes (holes F1-F3 according to chapter 2.4) and in the floor according to Fig 2-5 have been produced.

Heave of the floor (V0 to V7 in Fig 2-5)

Fig 6-41 shows the vertical displacement of the floor as a function of time from the start of the heating. The locations of the nodes correspond to spots V2 to V7 and V0 to the rotating laser (reference level). The exact coordinates of the nodes are given in the figure.

The heave caused by excavation, representing the start values in the field measurements, varies from 500 to 850 μm. The heave emanating from heating (70 μm to 280 μm) is thus much smaller. The reference point heaves 300 μm during excavation but does not move during the heating period, and settles by 14 μm at the cooling period due to the decreased surface temperature.

Displacements in fractures 1 and 2

The following relative fracture displacements have been calculated:

1. Horizontal shear displacement corresponding to the tangential shear displacement in the x/y directions (*ux*)
2. Opening of the fracture in the normal direction (*uy*)
3. Vertical shear displacement corresponding to the tangential shear displacement in the z direction (*uz*)

The location of the nodes in the fractures for which these displacements have been calculated is shown in Fig 6-19. The nodes corresponding to the measuring

points in Fig 2-5 are given in Table 6-1. The fracture displacements are shown in Figs 6-42 to 6-44.

The opening (curve 2 termed *uy* in the diagrams) is negative for point 1p03 (nodes 101/102 in Fig 2-5 and EF2 in Fig 2-5) in fracture 2, which means closure. All other parts of fractures 1 and 2 open. The expansion of fracture 2 is quite small, i.e. between 0 and 50 μm. Fracture 1 expands significantly more, i.e. by 20 μm to 160 μm.

The horizontal shear displacement (curve 1 named *ux* in the diagrams) in fracture 2 varies between 20 μm and 70 μm and between 15 μm and 50 μm in fracture 1.

The vertical shear displacement (curve 2 named *uz* in the diagrams) in fracture 2 varies between 10 μm and 70 μm and between 40 μm and 180 μm in fracture 1.

Strain in the floor

The strain is calculated for 8 points in x and y directions in the floor according to Table 6-2 in chapter 6.4.3. Fig 6-45 shows that the strain varies from 10^{-5} (10 μm/m) to $8 \cdot 10^{-5}$ (80 μm/m).

Expansion of the rock block

The change in distance between the floor and different points in the rock block has been measured at four depths in the extensometer holes F1-F3. The corresponding displacements have been calculated with the exact location and terming according to Table 6-3 in chapter 6.4.3. Fig 6-46 shows the calculated expansion of the rock block. Each diagram correspond to one hole. The diagrams show that:

- the maximum expansion in hole F1 varies between 20 μm and 200 μm
- the maximum expansion in hole F2 varies between 20 μm and 100 μm
- the maximum expansion in hole F1 varies between 10 μm and 60 μm

7 INFLUENCE OF VARIOUS FACTORS

7.1 GENERAL

Several elastic calculations were made before the final one in order to investigate the influence of different boundary conditions and parameter values as well as of the size of the excavated room. A few of these calculations and a selected number of plottings will be shown here.

7.2 INFLUENCE OF BOUNDARY CONDITIONS

The final element mesh had the dimension 40x40x40 m^3 with mechanically fixed boundaries. The following calculations were made to investigate if the dimensions and boundary conditions were satisfying:

A) Infinite boundaries

ABAQUS has the ability to simulate infinite boundaries. However, since the elements cause certain problems in the temperature calculation they were not used in the final calculations. A calculation assuming elastic conditions and infinite boundaries was performed and compared with the final elastic model. No significant difference between these elastic calculations was found.

B) Total mesh 20x20x20 m^3

Some calculations were made with a total dimension of 20x20x20 m^3 of the element mesh, which means that the fixed boundary was located only 5 m outside the test block and the room. These calculations showed that the heave of the floor was about 4% smaller at excavation and about 8% larger at heating. These results indicate that this mesh was too small. The closely located boundaries made the rock mechanically stiffer and the heave at excavation smaller. Still, the heave caused by the heating was larger, which can be explained by the temperature, which was too high due to the thermally insulated boundary.

C) Mechanically free boundaries

A calculation with the small mesh (20x20x20 m^3) and mechanically free boundaries was also made. It showed that the heave of the floor after excavation was about 7% larger than that obtained from calculations assuming fixed boundaries (*B*). The difference between the results of the calculations at heating was insignificant.

7.3 INFLUENCE OF ROCK PROPERTIES

The influence of the E-modulus and the coefficient of thermal expansion was investigated by performing some calculations.

D) Influence of E-modulus of the surrounding rock

In the given properties of the rock the E-modulus of the surrounding rock was 55 650 MPa, which was higher than the E-modulus of the test rock block (30 000 MPa). This choice was based on the assumption that there are no fractures in the surrounding rock. Since there is a possibility that the E-modulus of this rock is lower, an additional calculation was made with the same low E-modulus of the surrounding rock as of the test rock block.

The results showed that the heave after excavation was up to 15% higher when the low E-modulus was used. However, the heating caused no significant increase in heave in comparison with the base case.

E) Coefficient of thermal expansion (α)

α was given both as a constant and as a function of the temperature, the latter being used as a basic case. The significance of this was investigated by conducting a calculation with the constant value $\alpha=5 \cdot 10^{-6}$ 1/K. The results showed no significant difference between the calculations.

7.4 INFLUENCE OF ROOM DIMENSIONS

The area of the floor of the excavated room was 162 m^2. By mistake, the first calculations were made with a size of the room equal to the size of the test block (100 m^2). The size was then increased to 169 m^2 (13mx13m) and comparison of these calculations illustrated the influence of the room dimensions.

The heave was about 10% smaller for the small room at excavation. The difference at heating was even smaller, probably because the smaller heave of the smaller room was counteracted by a larger heat-induced expansion resulting from less effective cooling.

7.5 CONCLUSIONS

The different calculations and results are summarised in Table 7-1.

Table 7-1. Summary of sensitivity analyses. The comparison is made with the heave of the floor in the final calculation as reference

Calculation	Infl. of excavation Diff. in strain	Infl. of heating Diff. in strain
Infinite boundaries	Insignificant	Insignificant
Small mesh (20^3 m^3)	-4%	+8%
Free boundaries	+7%*	Insignificant
E=30 GPa of surr. rock	+15%	Insignificant
$\alpha=5\cdot10^{-6}$ 1/K (constant)	Insignificant	Insignificant
Smaller room (100 m^2)	-10%	Insignificant

* This comparison was made with the small mesh.

These sensitivity calculations show that most factors have a significant influence on the strain caused by the excavation, but not on the straine caused by heating. It is thus obvious that the thermo-mechanical effect of the heating is very local.

8 COMPARISON WITH MEASURED RESULTS

8.1 GENERAL

A comparison between measured and calculated results entails a lot of work because of the large amount of data. A complete comparison should include a thorough analysis of the following ones:

1. Comparison between the maximum values at each point
2. Comparison of the time history of the measured and calculated values at each point (trends or actually the time derivative *dx/dt* of the measured parameter).
3. A thorough analysis of the relevance of each measurement.
4. A sensitivity analyses of most parameters in the calculation.

A preliminary sensitivity analysis was made in chapter 7. In the present chapter comparison between the maximum values will be made.

8.2 EXPANSION OF THE ROCK

Table 8-1 shows a comparison of the values of expansion measured in the extensiometer holes F1-F3 and calculated by the unfractured and fractured rock versions.

Table 8-1. Expansion of the rock (measured by extensometers)

Location	Depth m	Measured expansion µm	Elastic calculation µm	Fracture calculation µm
F1 EF11	-2.5	55	20	20
F1 EF12	-3.0	80	75	85
F1 EF13	-4.0	145	160	170
F1 EF14	-4.5	170	185	205
F2 EF21	-2.5	50	20	20
F2 EF22	-3.0	100	60	65
F2 EF23	-3.5	135	100	90
F2 EF24	-4.0	165	130	100
F3 EF31	-2.0	12	16	12
F3 EF32	-2.5	-	22	17
F3 EF33	-3.0	32	34	50
F3 EF34	-3.5	40	47	58

The table shows that the measured and calculated expansions are of the same magnitude. The agreement is very good at some points and not so good at others for both rock versions. However, the results from the "elastic" calculation agree a little better with the measured ones than the results from the "fracture" calculation.

8.3 VERTICAL HEAVE OF THE FLOOR

Table 8-2 shows a comparison of the heave of the floor measured with the rotating laser technique, and of the calculated one. V0 represents the location of the laser.

Table 8-2. Vertical heave of the floor

Location	Measured heave μm	Elastic calc. μm	Fracture calc. μm
Laser V0		5	0
V2	200	90	60
V3	400	20	10
V4	340	125	270
V5	280	170	130
V6	415	160	235
V7	543	125	150

Table 8-2 shows that the measured heave is much larger than the calculated one. Since the measured expansion in the rock between the floor and the level 4.5 m deeper down agreed well with the calculations (Table 8-1) and since the values were much smaller than the total heave as shown in Table 8-2, one of the following statements must be valid:

- The rock deeper than 4.5 m underwent strong expansion.
- The measurements are not accurate.

A large expansion of the deep-lying rock has no natural explanation. There had been problems with the laser system and difficulties to evaluate the results, and it is therefore concluded that the difference between theoretically deduced and measured values is caused by inadequate measurements.

8.4 STRAIN IN THE FLOOR

The measured and calculated strain at 8 points in the floor have been compared in Table 8-3. Each row contains strain values in both x- and y-directions. The notation 20/60, for instance, means that the strain is 20 μm/m in x-direction and 20 μm/m in y-direction.

Table 8-3. Strain in the floor

Location Termed in Fig 2-5	Coord. (x;y)	Termed in Fig 6-23 (6-45)	Measured strain μm/m	Elastic calc. μm/m	Fracture calc. μm/m
EL9/ET10	0;-4	ex/y-6p01	20/60	8/14	40/30
EL7/ET8	0;-2	ex/y-6p02	14/125	27/8	18/10
EL3/ET4	0;+2	ex/y-6p03	47/40	27/14	9/37
EL1/ET2	0;+4	ex/y-6p04	17/95	12/12	3/14
EL11/ET12	-4;0	ex/y-6p05	40/8	13/13	22/14
EL13/ET14	-2;0	ex/y-6p06	25/16	13/31	8/32
EL15/ET16	+2;0	ex/y-6p07	18/6	8/34	65/83
EL17/ET18	+4;0	ex/y-6p08	25/23	12/12	25/8

The discrepancy between the calculated and measured strain is very significant and the reason is probably that the surface is structurally much more complex than modelled. The average values of the respective strain are

- Measured average strain (μm/m) *Ex/Ey*=26/47
- Elastic calc. average strain (μm/m) *Ex/Ey*=15/17
- Fracture calc. average strain (μm/m) *Ex/Ey*=24/29

The influence of the fracture systems is manifested by the average strain data. The elastic calculation yields small isotropic strain. The fracture calculation yields larger strain because the fractures make the rock less stiff although without any major difference between the x- and y-directions. The measurements, on the other hand, yield a much larger average strain in the y-direction than in the x-directions. However, the latter agree with those calculated for the fractured rock. The conclusion is thus that the surface is not correctly modelled, an improvement would be to regard it as an anisotropic material with less stiffness in the y- and z-directions.

8.5 FRACTURE OPENINGS

The measured and calculated expansions at some locations in fractures 1 and 2 are compared in Table 8-4. The location of the measuring and calculation points are shown in Figs 2-5 and 6-19. The elastic expansion data are not relevant since they are caused by the large thickness of the fracture elements.

Table 8-4. Fracture openings

Fracture	Location	Measured opening μm	Elastic calc. Opening μm	Fracture calc. Opening μm
1	EF1	35	(8)	150
1	L11	35	(6)	150
1	L12	25	(2)	18
2	L21	4	(-3)	3
2	EF2	56	(-6)	-17
2	L23	20	(-7)	8
2	L22	37	(3)	22

The agreement between the measurements and calculations (with the fracture calculation) is good for two, fairly good for two, and very bad for three of the expansions.

8.6 VERTICAL SHEAR DISPLACEMENTS

The measured and calculated vertical shear displacements are compared in Table 8-5. As in the case of the floor strain the elastic calculation is of course not relevant.

Table 8-5. Vertical shear displacement

Fracture	Location	Measured shear displacement μm	Elastic calc. μm	Fracture calc. μm
2	EV-4	3	(7)	4
2	EV-3	4	(2)	62
2	EV-1	10	(1)	11

The agreement between the measurements and calculations (for the fractured rock) is acceptable for two and unacceptable for one of the shear displacement values. These results and the result of the calculation of the fracture opening thus show that the fractures are not very well modelled for calculation of the performance of the individual fractures.

8.7 TEMPERATURES

When the calculated and measured temperatures are compared (e.g. Figs 2-6 and 6-4 or Figs 6-18 to 6-20 and corresponding measurements) one finds that they do not agree very well close to the heaters where the calculated temperatures are higher than the measured ones. At a distance of more than

about 1 m from the centre of the heaters the agreement is good, however. The reason for the bad agreement close to the heaters is the coarse element mesh and inaccurate heater model as mentioned in chapter 6.3. The rock volume where the temperatures are overestimated is only a small part of the total heated volume and it is concluded that the overestimation of the rock expansion caused by this error is not significant.

9 CONCLUSIONS

The calculations of the TM test in Fanay-Augères accounted for in this report have yielded a lot of experience and information about the behaviour of the near field rock and the possibility to model it with the finite element code ABAQUS in spite of the limited available time. The following conclusions can be drawn from the *calculations*, the *sensitivity* analyses, and the *comparison* with measured results:

Calculations

The very general finite element program ABAQUS is well suited for these 3D modellings since it can take into account all types of boundary conditions, thermal as well as mechanical. The whole process, including the excavation of the room and the change in room temperature with time, was simulated. The problems in the calculation originate from the fracture modelling.

1. The 3D mesh of the test rock block that contains the fractures, was very difficult to generate, due to the inclinations and intersections of the fractures. The mesh used in the calculations was not perfect, since it generated mechanical errors of up to +/-5-10 μm due to uncoupled nodes in the mesh. In spite of this, the mesh was considered to be acceptable.

2. The properties of the fractures were given as parameters, which could not be directly used in ABAQUS. No perfect fracture model is yet available, but the technique to use fracture elements with a substantial width, and to model the properties by applying the Drucker-Prager concept, was useful.

3. The complicated fracture mesh made it necessary to model the 5 heaters in a too simple way for time and cost reasons. This resulted in an overestimation of the temperature close to the heaters, i.e. within a volume of about 4 m^3. Since this is less than 1/100 of the entire fractured experimental rock block, this error was considered to be acceptable.

Sensitivity analyses

Several analyses were made with different boundaries and properties. The following conclusions concerning the effect of the boundaries on the heave of the floor can be drawn from them:

1. The conditions of the outer boundaries were only important for the calculation of the excavation-induced strain and not for the effect of heating. No influence of infinite boundaries compared to fixed boundaries was found.

2. The location of the outer boundary had an influence on the calculation of both strain and temperature. With a boundary located only 10 m outside the centre of the test block the calculated heave deviated by up to 8% from the heave calculated with the final boundary located 10 m further away.

3. A reduction in E-modulus of the surrounding rock by 40% had a significant influence on the effect of excavation but not on the effect of heating.

4. No influence of using a variable coefficient of thermal expansion instead of a fixed value could be found.

5. The size of the room above the rock block had a significant influence on the effect of excavation of the room but not on the effect of heating.

The general conclusion from these calculations was that the boundaries had no influence on the effect of heating but a substantial influence on the effect of excavation. The only calculation that showed an effect of the heating was when the mesh was too small, yielding too high temperatures near the heaters.

Comparisons

Although a complete evaluation of the results from the calculations and the measurements has not been made, the following conclusions can be drawn from the preliminary comparisons made in chapter 8:

1. The expansion of the rock is fairly well modelled by both models.

2. The strain in the surface of the floor is not very well modelled with either of the models. It is obvious that the complicated structure of the floor surface cannot be modelled with only a few fractures. The average measured strain in one direction is twice as large as the calculated strain, while it is about the same in the opposite direction. This shows that fracturing has given the shallow rock anisotropic behavior. The floor can probably be more correctly modelled by introducing an anisotropic zone in the upper decimetres with a lower E-modulus perpendicular to the fracture directions and in the z-direction.

3. Comparison of the calculated and measured displacements of the two dominating fractures yields inconsistent results. Hence, some displacements agree well while others do not. The conclusion is that the fracture models (geometry and properties) are inadequate.

4. The general behaviour of the floor does not seem to be more correctly modelled by use of the fracture model than with the elastic model. A fracture model is of course necessary for estimating the displacements in the fractures but the models used seem to overestimate the displacements.

REFERENCES

1-1 Gros, J.Cl. (1992) - DECOVALEX, phase 2, test-case 2, Fanay Augères THM test. SERGD 92/43

2-1 Rejeb, A. (1992) - Comportement thermomecanique du granite, application au stockage des dechets radioactifs. Doctor thesis, L'ecole de mine de Paris.

3-3 Hibbitt, Karlsson, and Sorensen (1993). ABAQUS manuals, version 5.3. Hibbitt, Karlsson, & Sorensen, Inc.

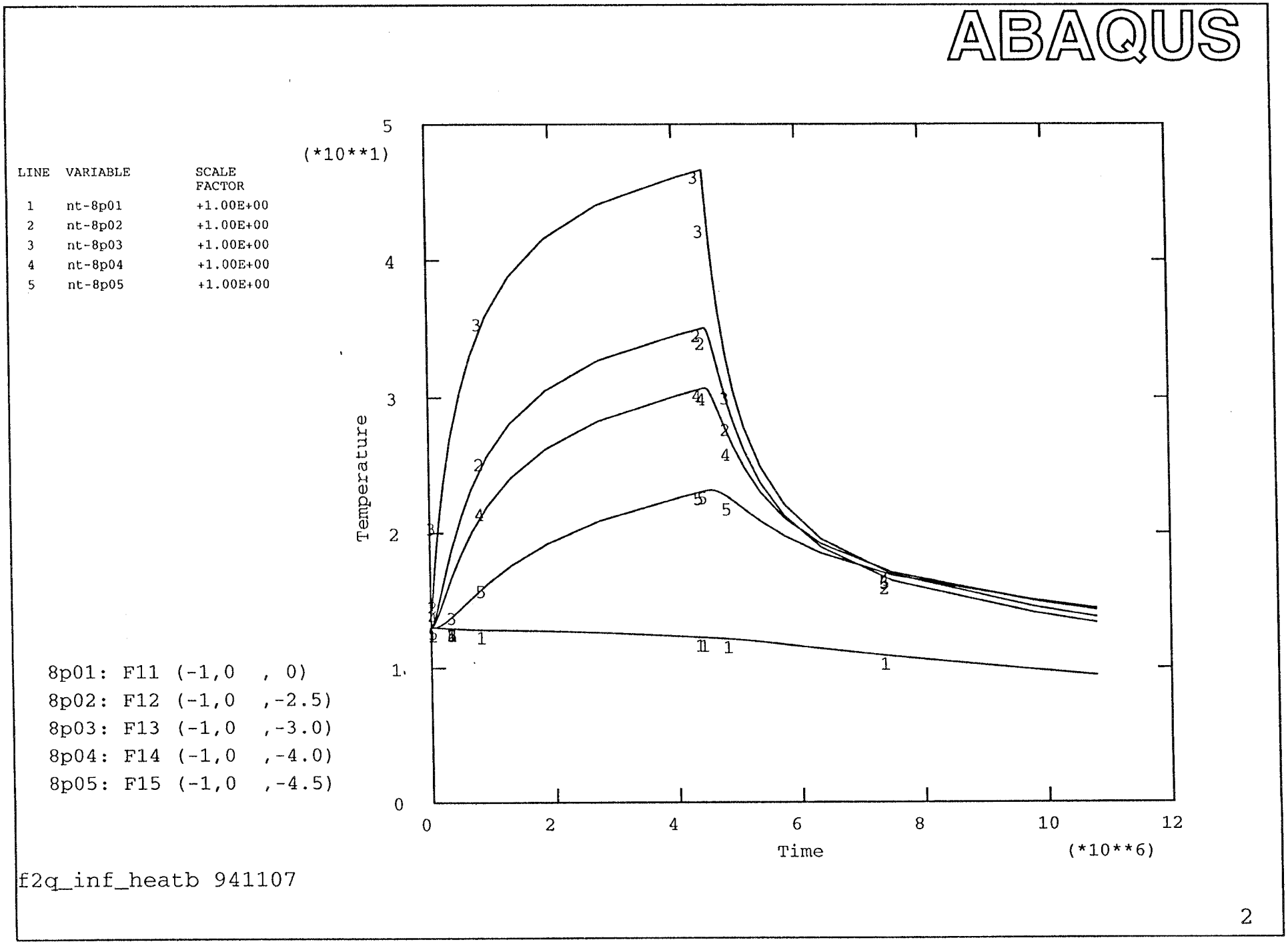

Figure 6-1. *Calculated temperatures in points that approximately correspond to hole F1*

ABAQUS

LINE	VARIABLE	SCALE FACTOR
1	nt-8p06	+1.00E+00
2	nt-8p07	+1.00E+00
3	nt-8p08	+1.00E+00
4	nt-8p09	+1.00E+00
5	nt-8p10	+1.00E+00

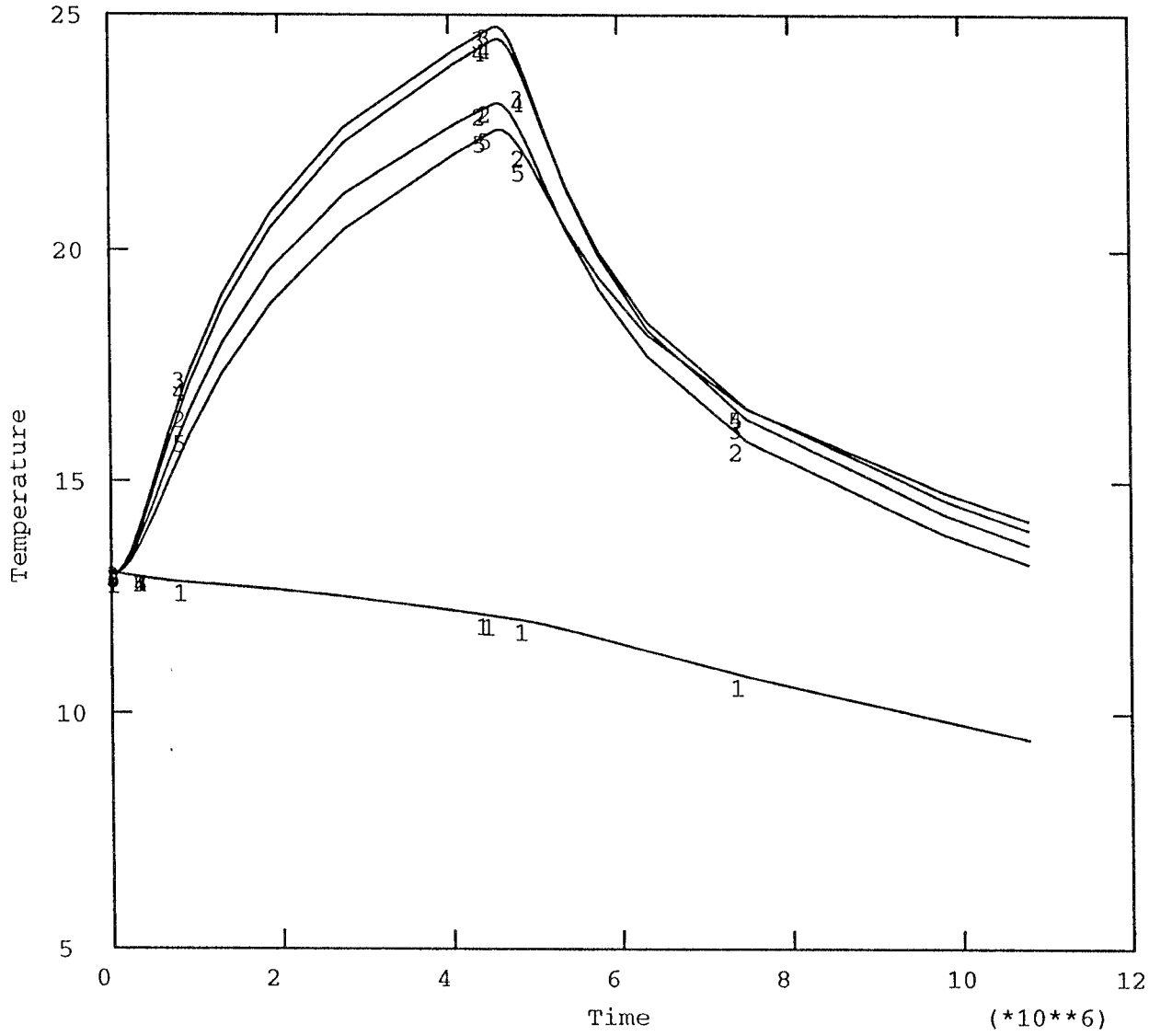

8p06: F21 (1,1.1, 0)
8p07: F22 (1,1.1,-2.5)
8p08: F23 (1,1.1,-3.0)
8p09: F24 (1,1.1,-3.5)
8p10: F25 (1,1.1,-4.0)

f2q_inf_heatb 941107

Figure 6-2. Calculated temperatures in points that approximately correspond to hole F2

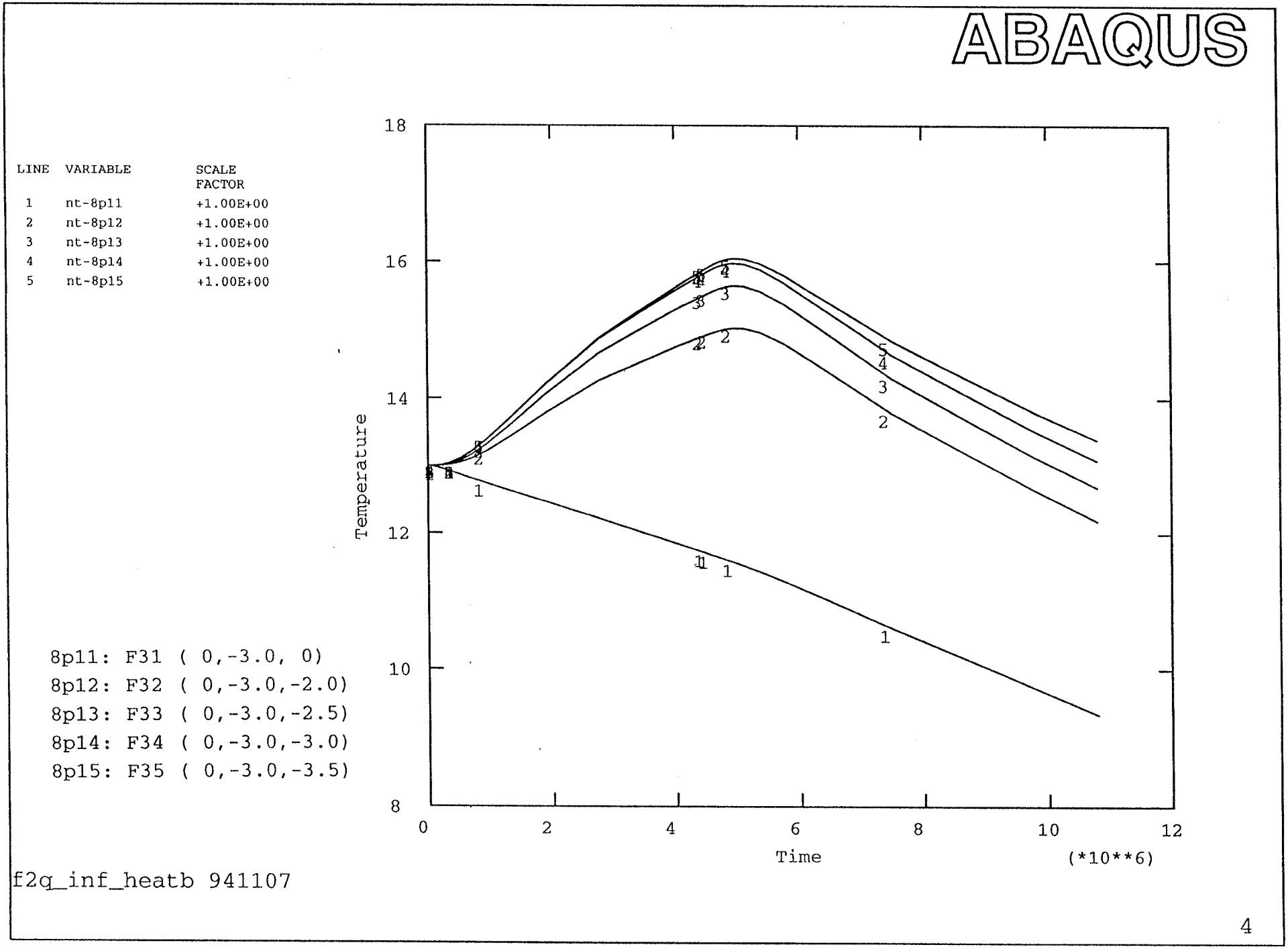

Figure 6-3. Calculated temperatures in points that approximately correspond to hole F3

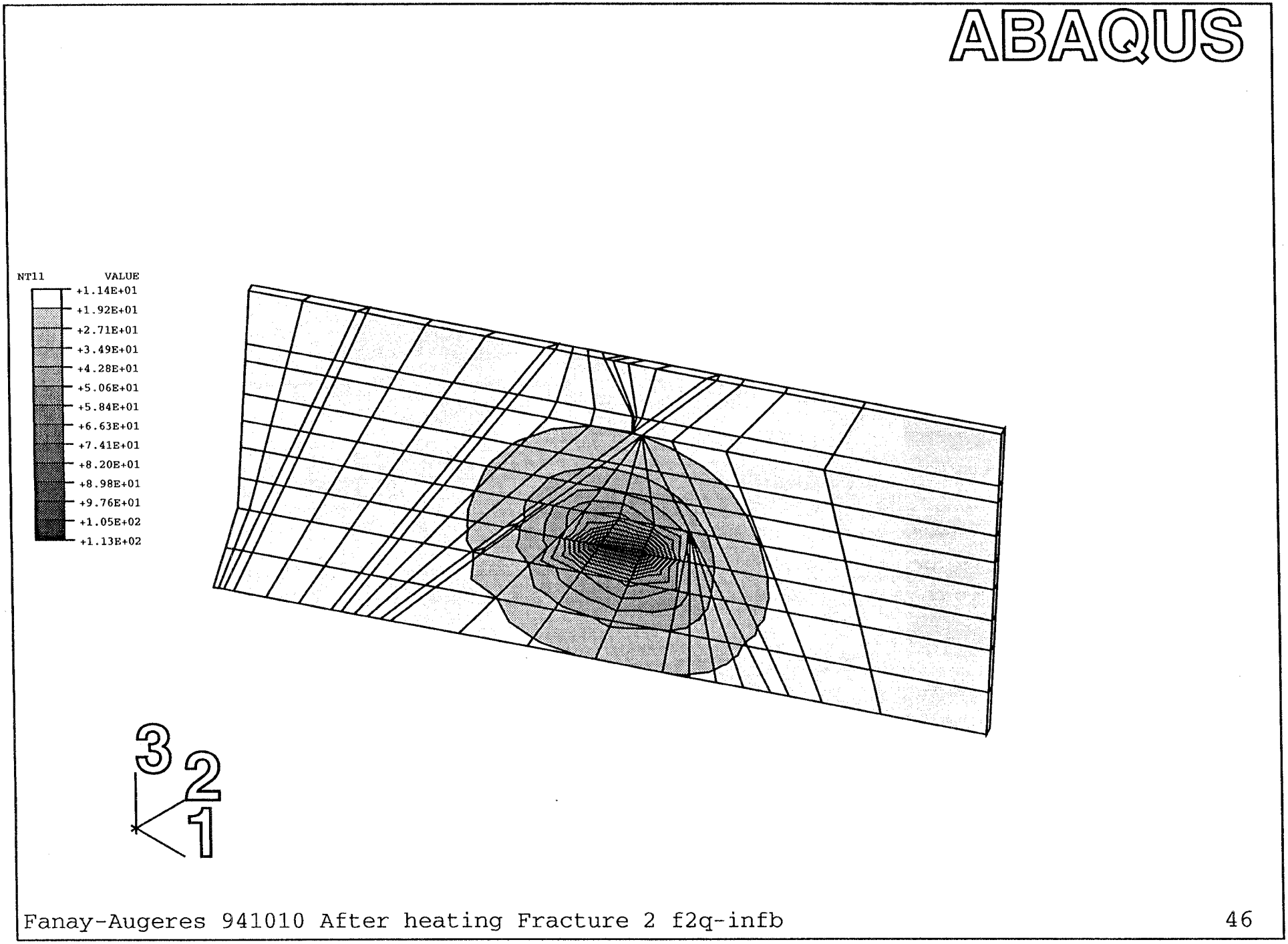

Figure 6-4. Temp. calc. Temperature (NT11) in fracture 2 (°C).

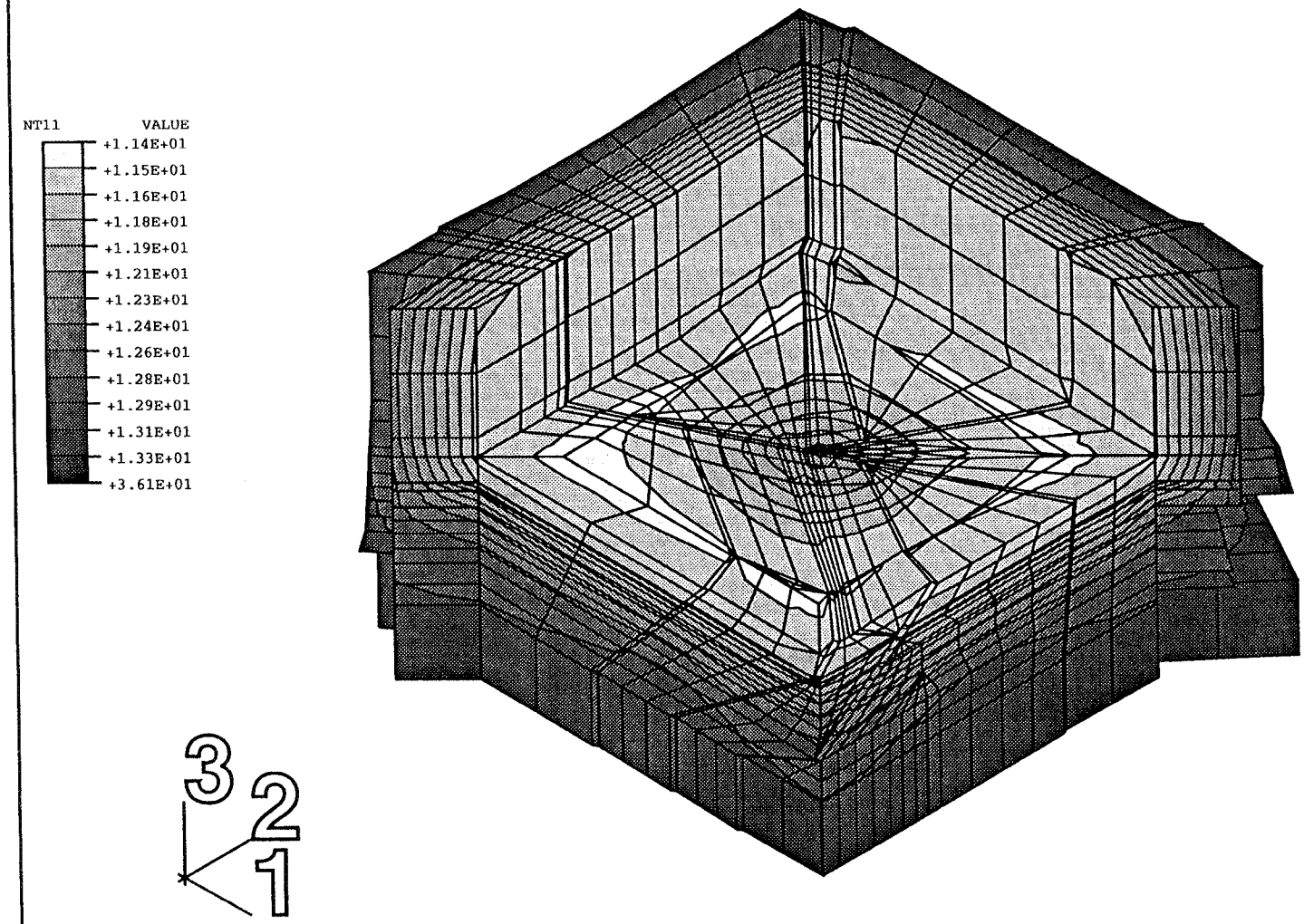

Figure 6-5. Temp. calc. Temperature (NT11) around the excavation (°C).

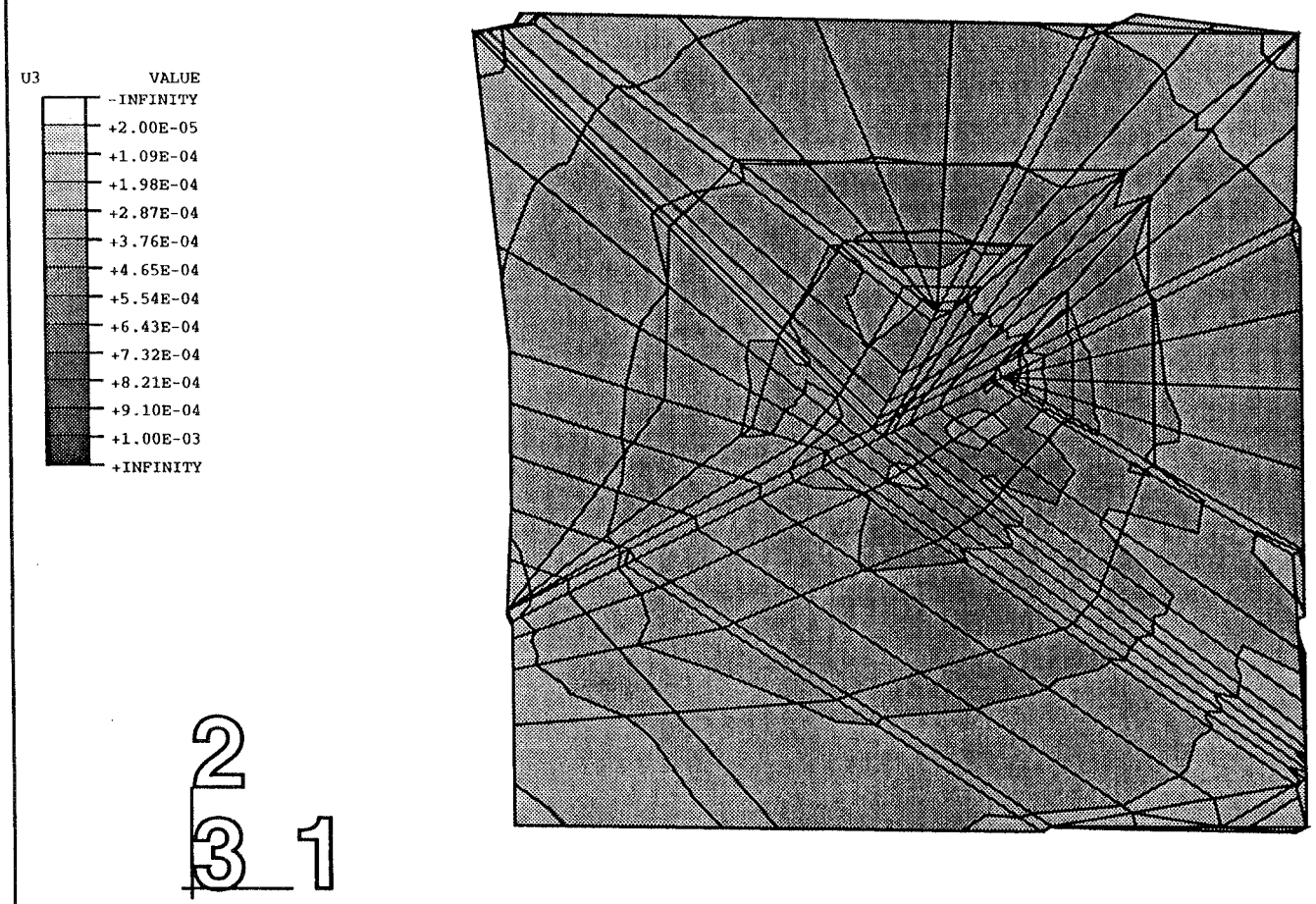

Figure 6-6. Elastic calc. Vertical displacements (U3) of the floor after excavation (m).

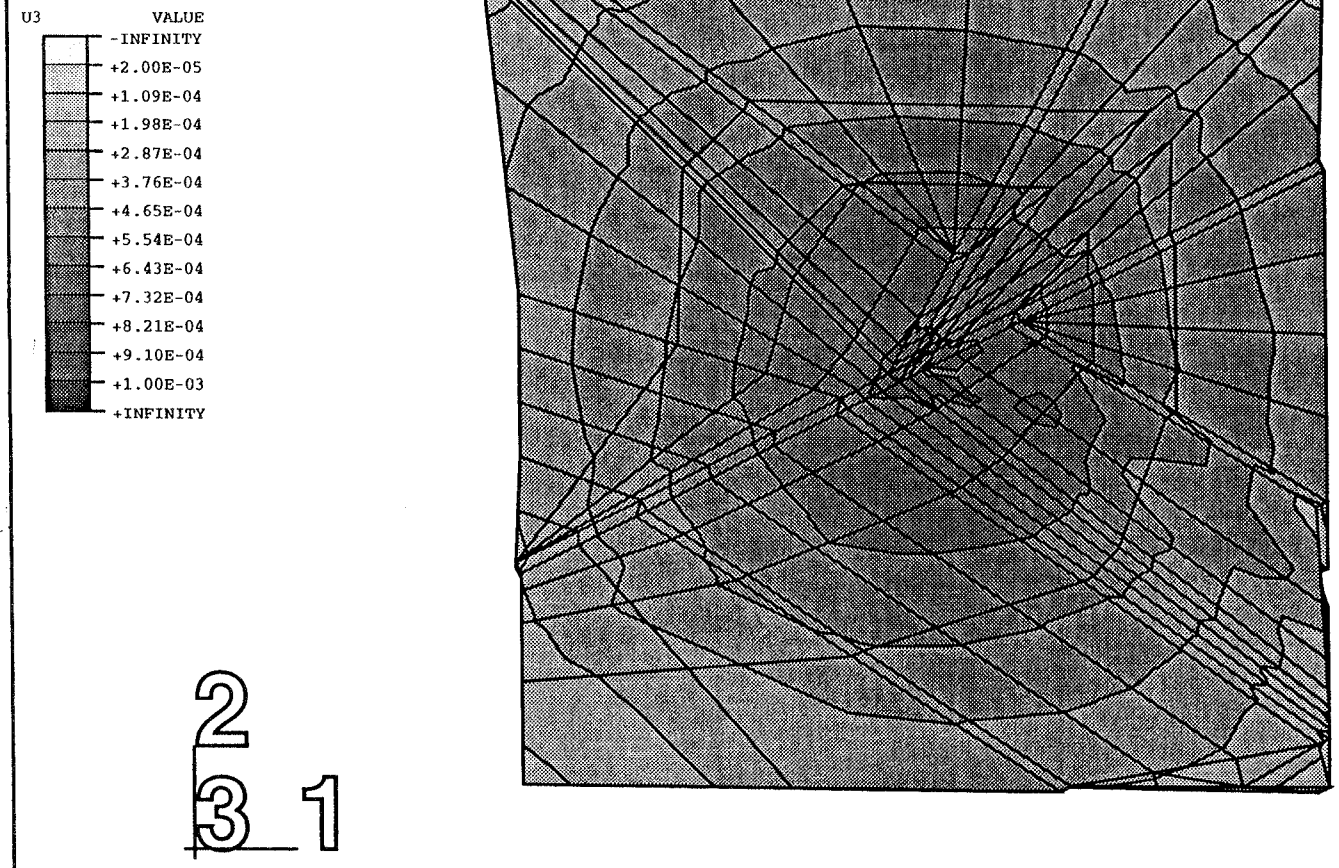

Figure 6-7. Elastic calculation. Vertical displacements (U3) after heating (m).

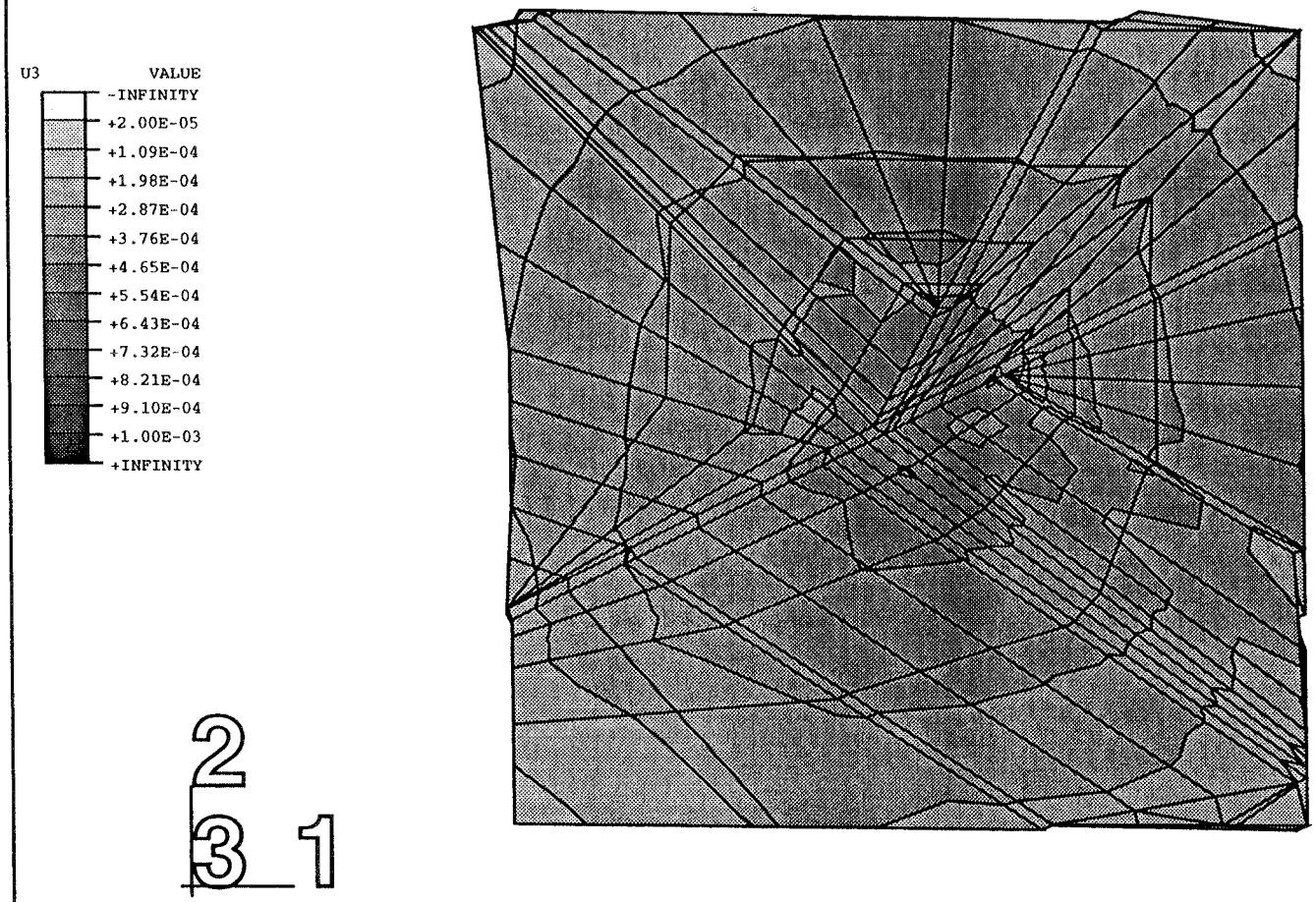

Figure 6-8. Elastic calculation. Vertical displacements (U3) after cooling (m).

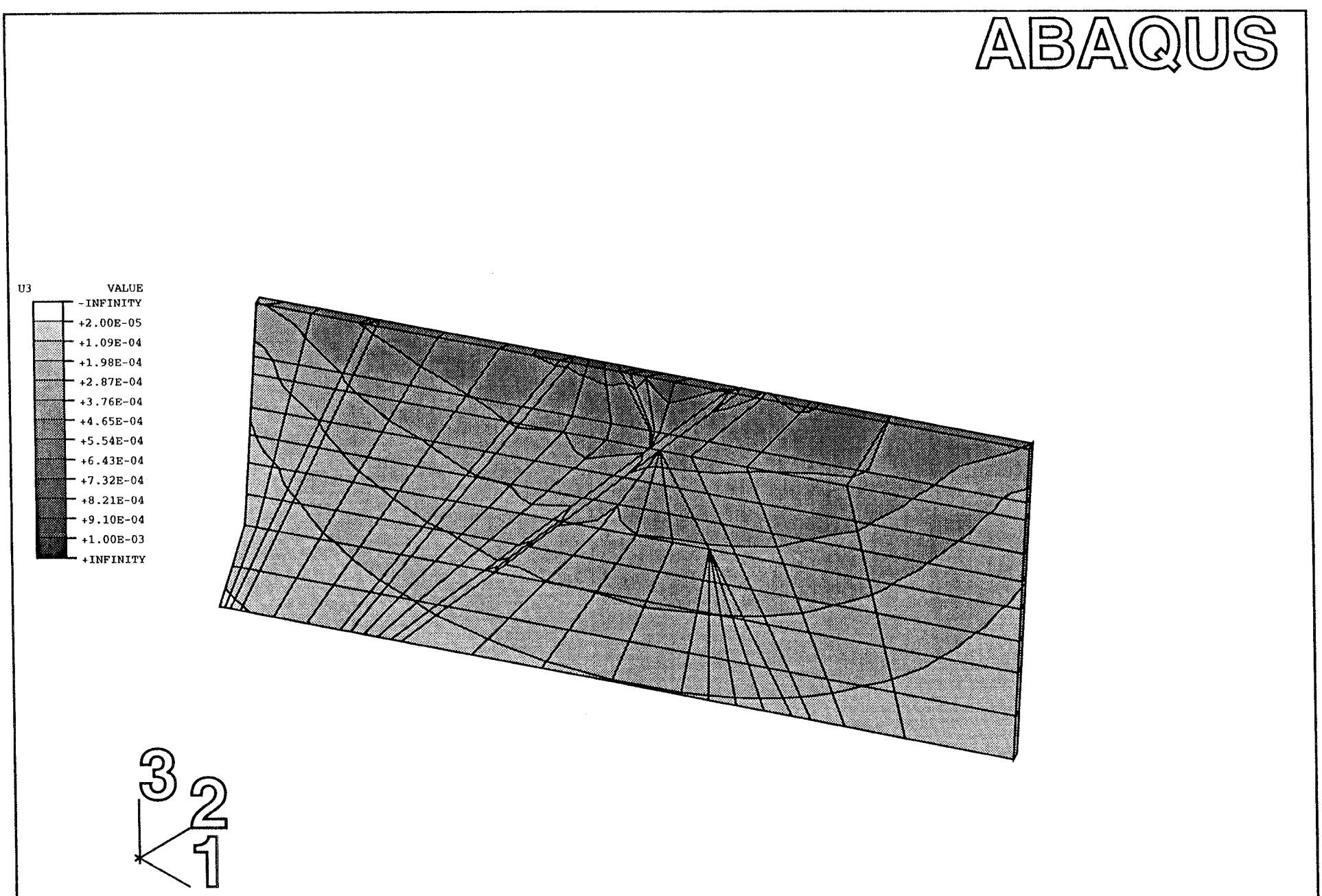

Figure 6-9. *Elastic calculation. Vertical displacements (U3) after excavation (m).*

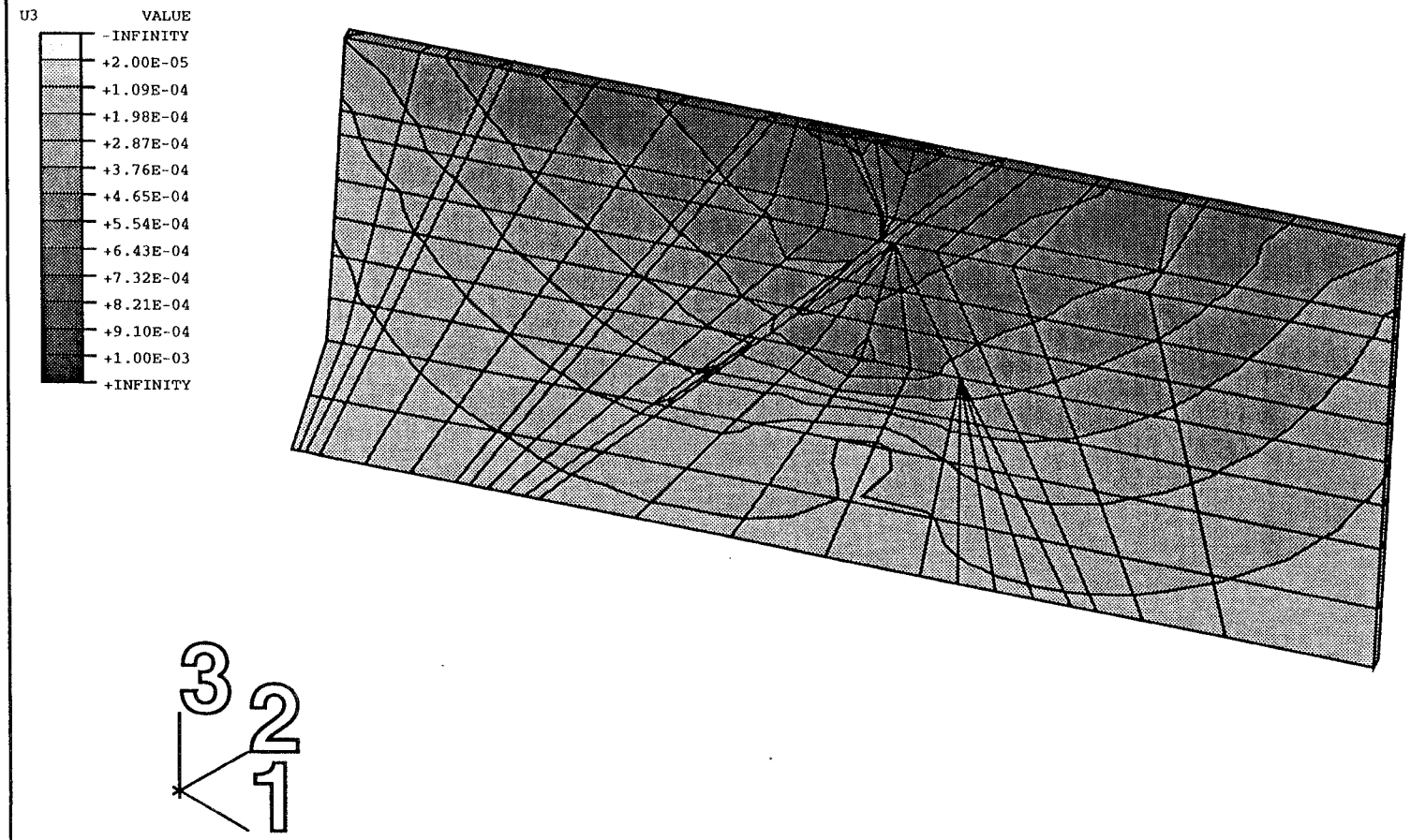

Figure 6-10. Elastic calculation. Vertical displacements (U3) after heating (m).

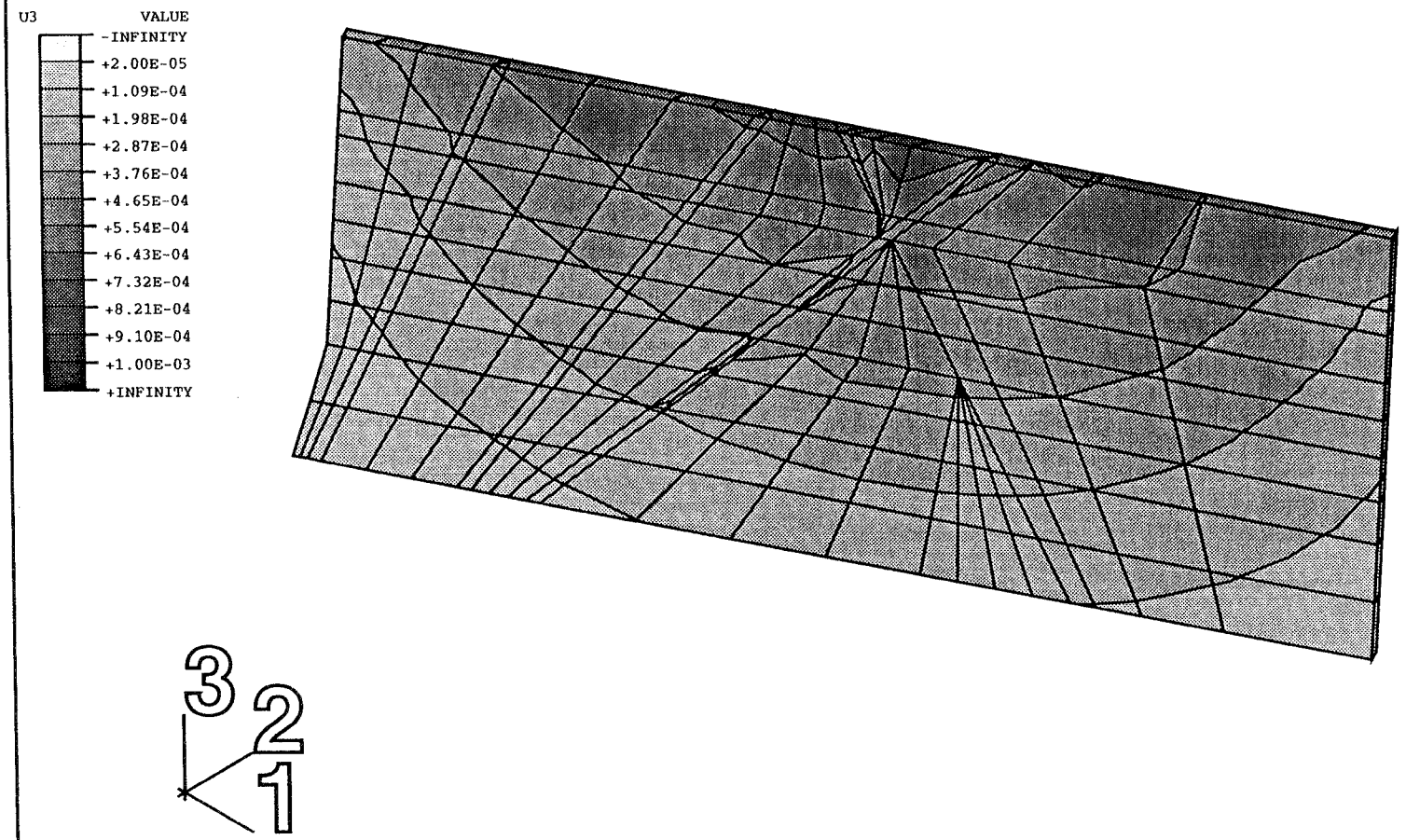

Figure 6-11. Elastic calculation. Vertical displacements (U3) after cooling (m).

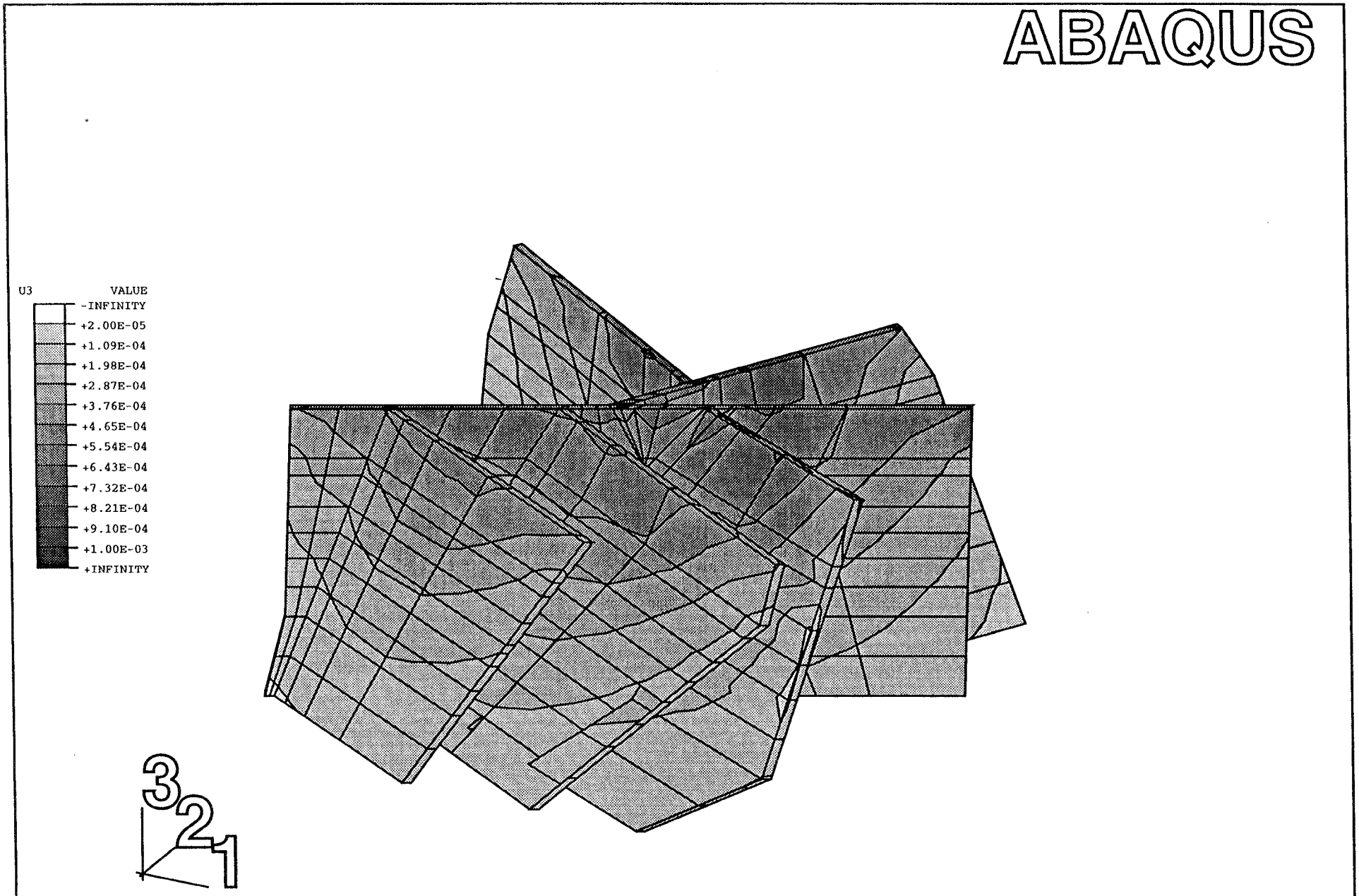

Figure 6-12. *Elastic calculation. Vertical displacements (U3) after excavation (m).*

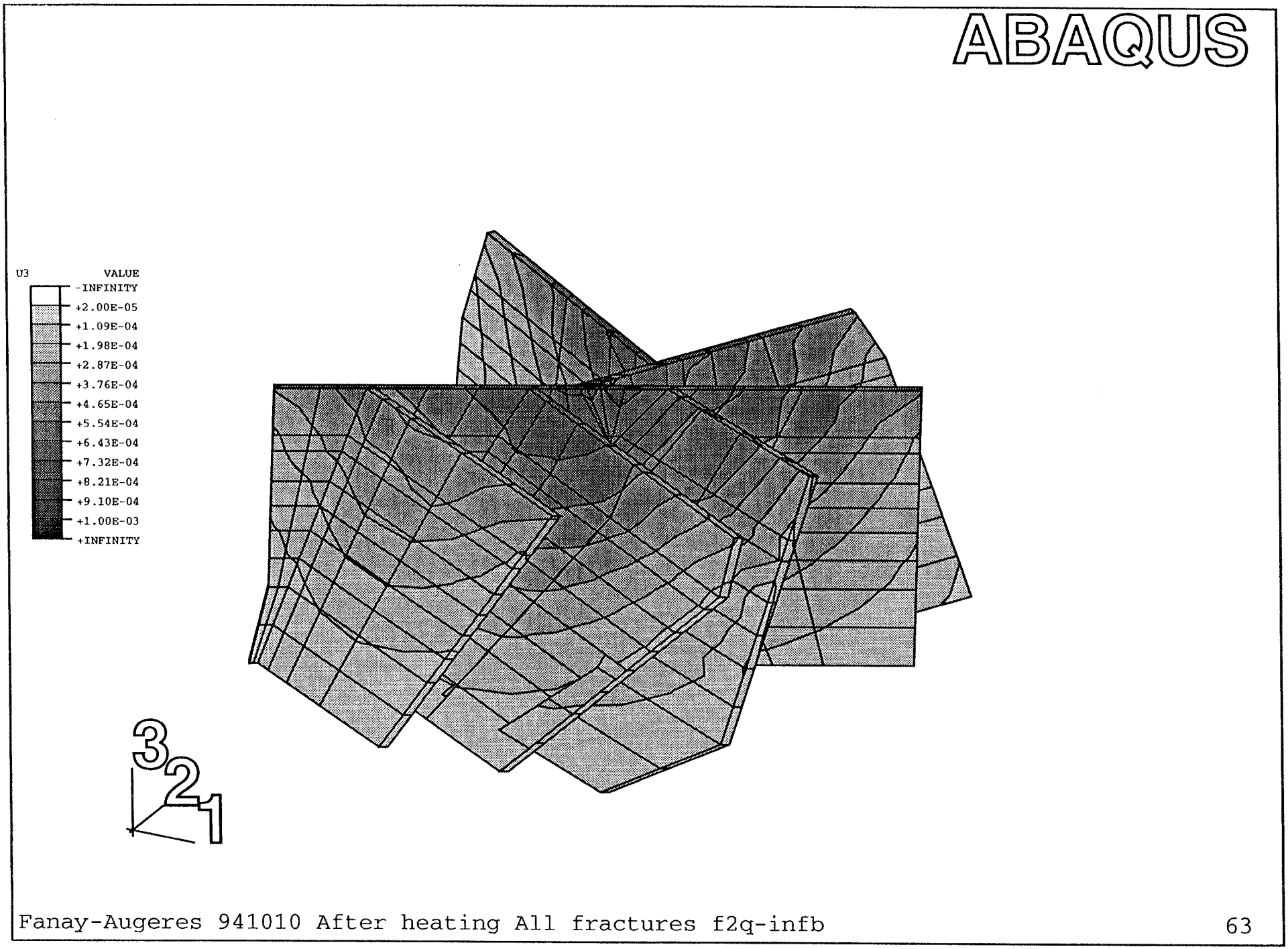

Figure 6-13. Elastic calculation. Vertical displacements (U3) after heating (m).

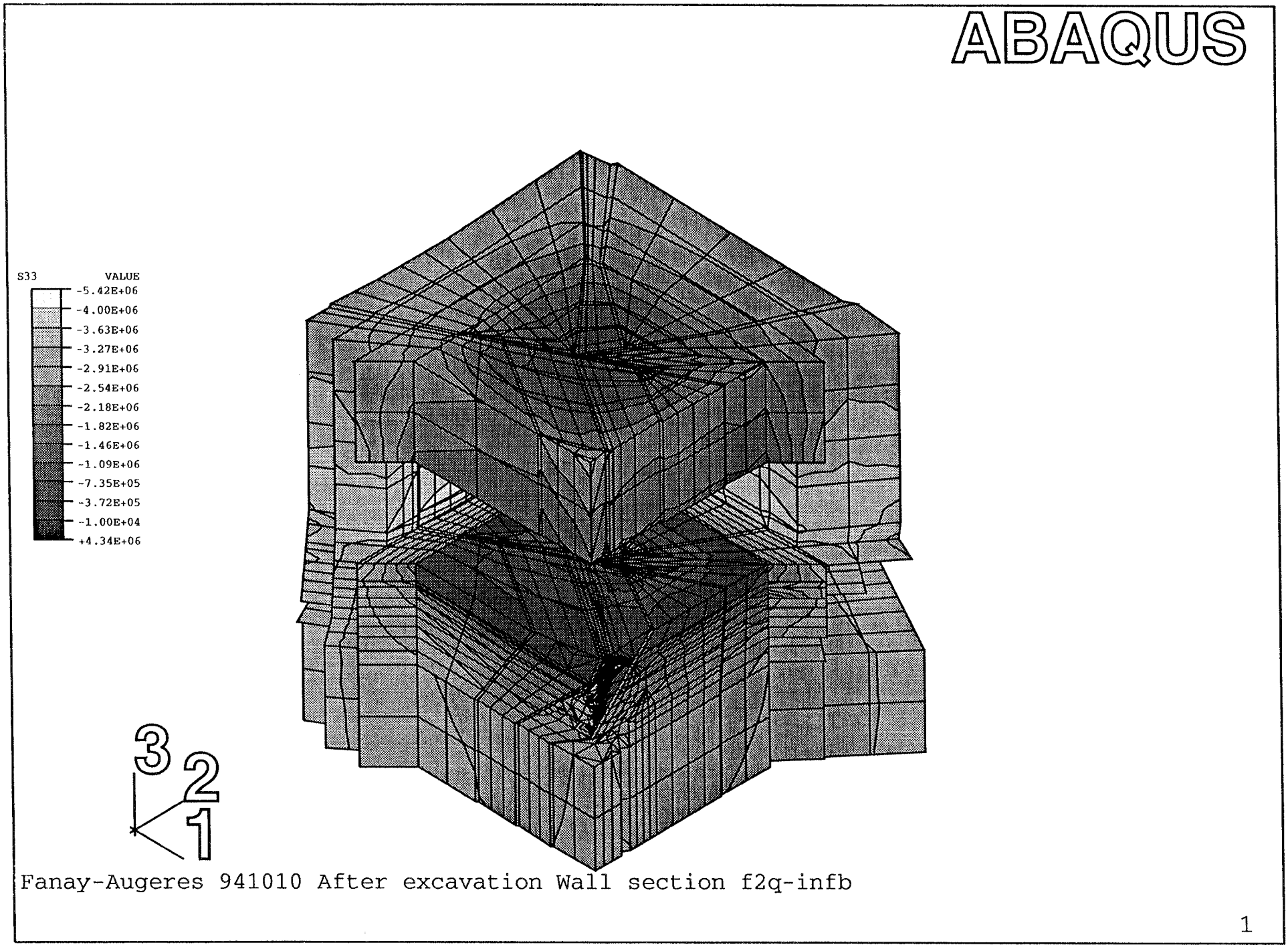

Figure 6-14. Elastic calculation. Vertical stress (S33) after excavation (Pa).

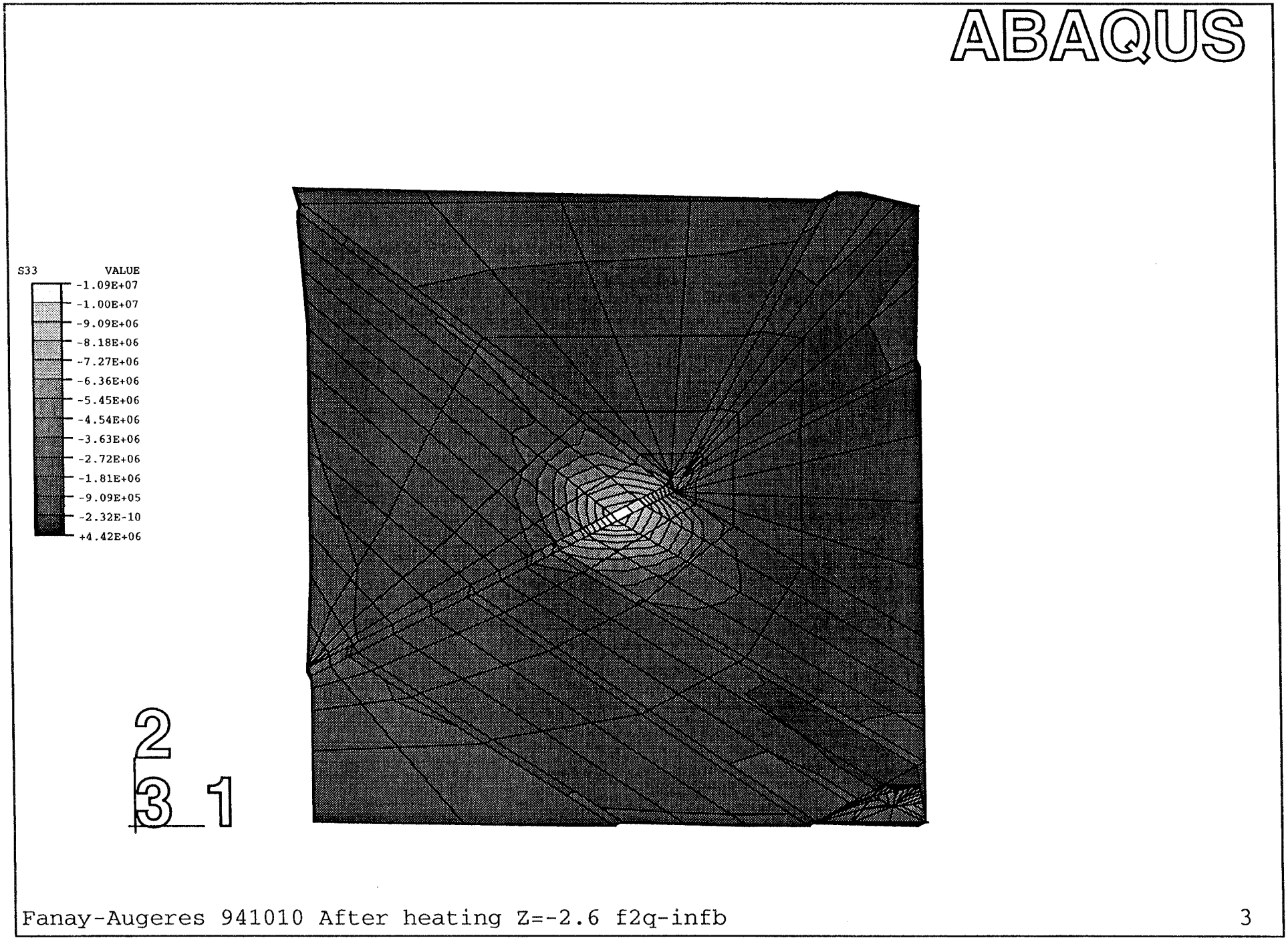

Figure 6-15. Elastic calculation. z=-2.6 m.

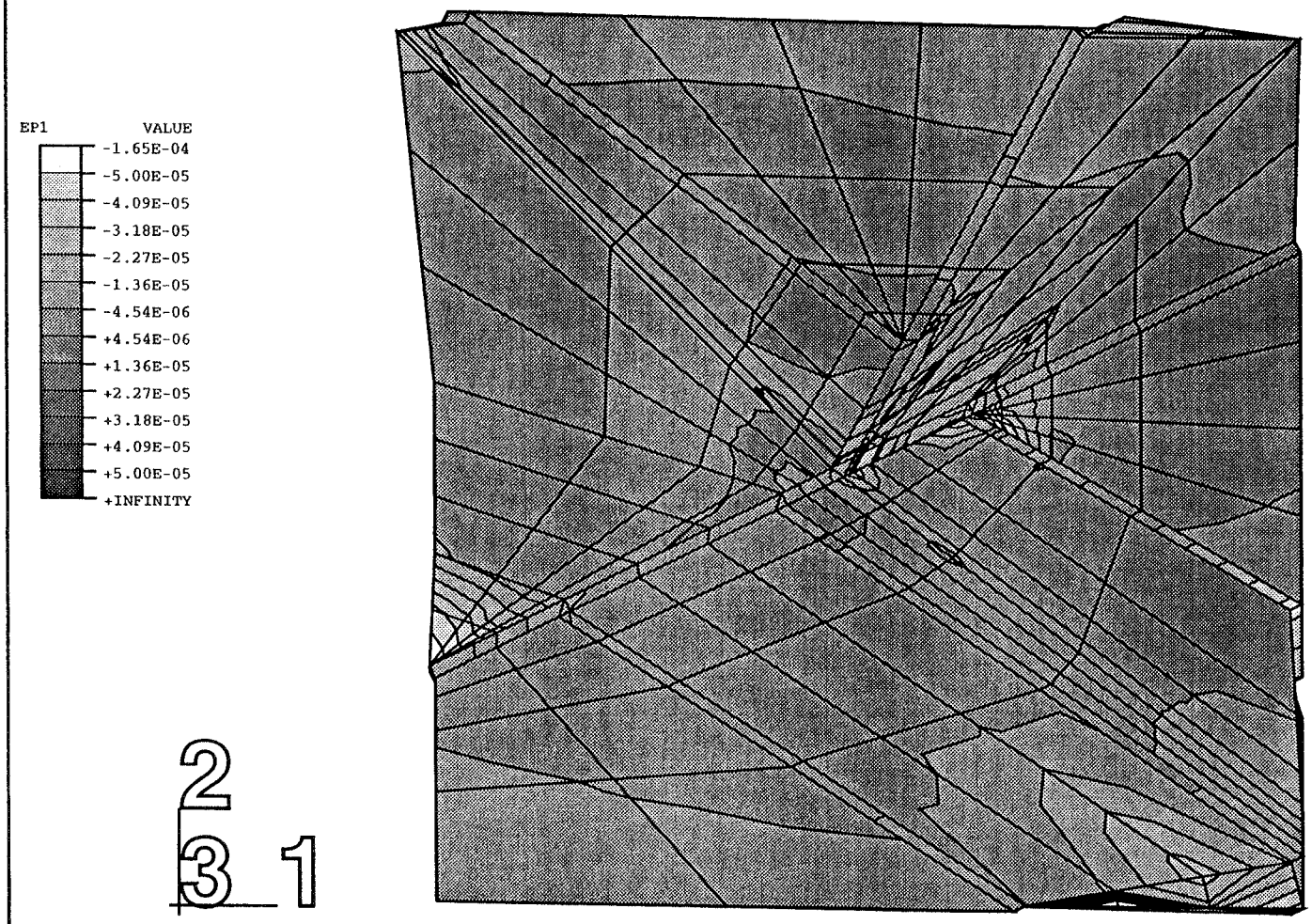

Figure 6-16. *Elastic calculation. Main princ. strain (EP1) in the floor after exc. (m/m)*

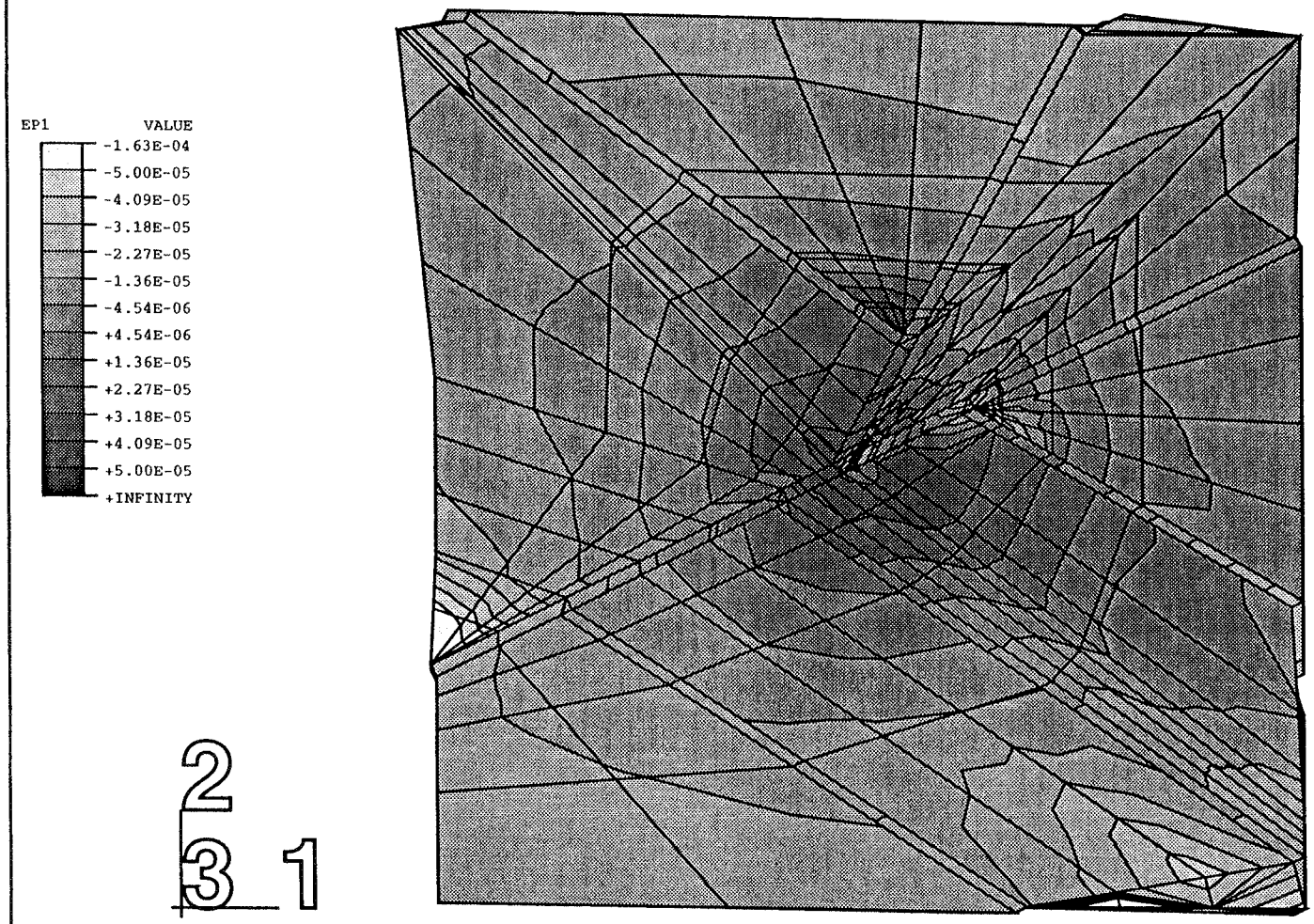

Figure 6-17. Elastic calculation. Main princ. strain (EP1) in the floor after heating (m/m)

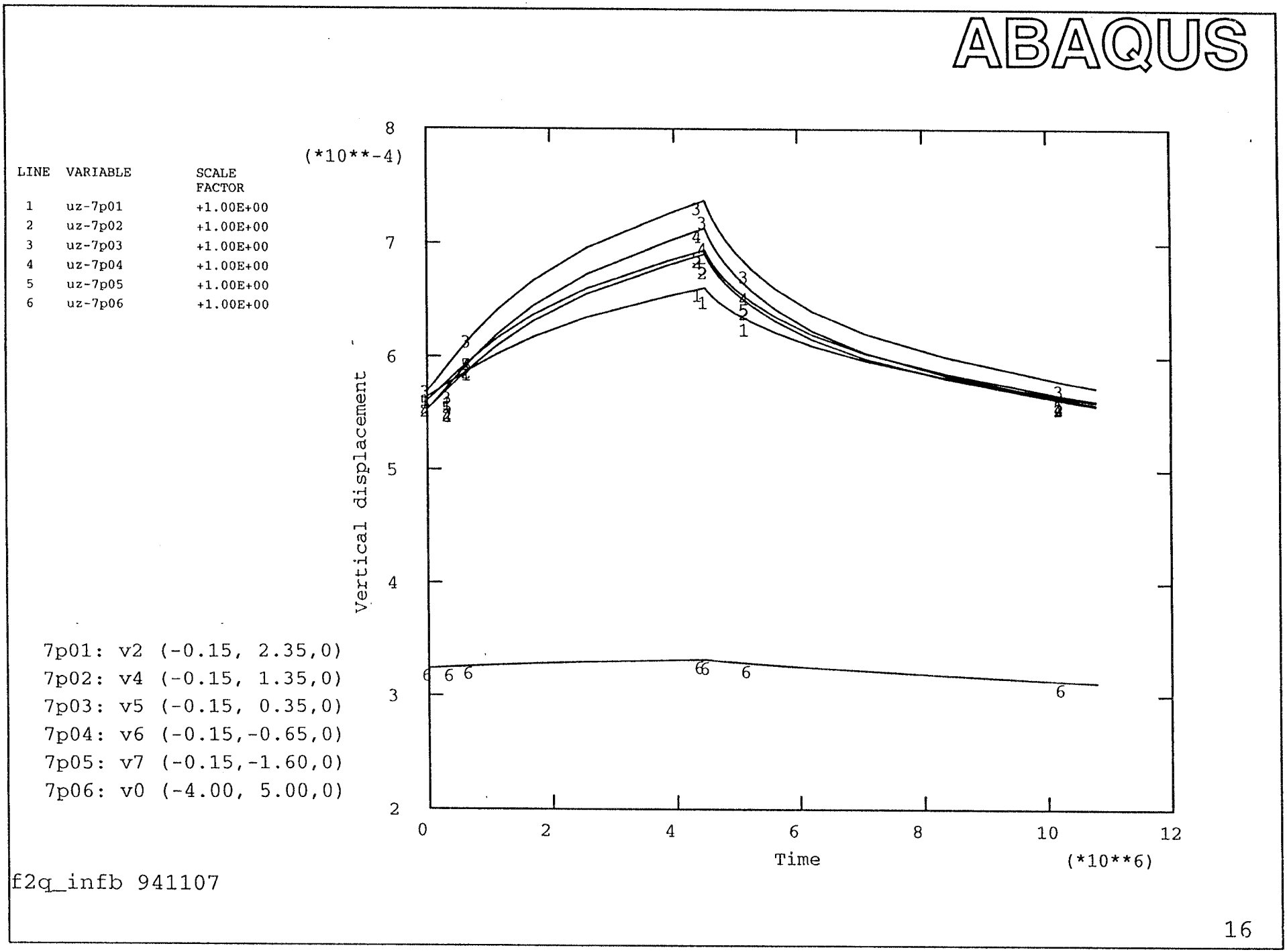

Figure 6-18. *Elastic calculation. Heave (m) of the floor in points V2-V7. (V0=ref.)*

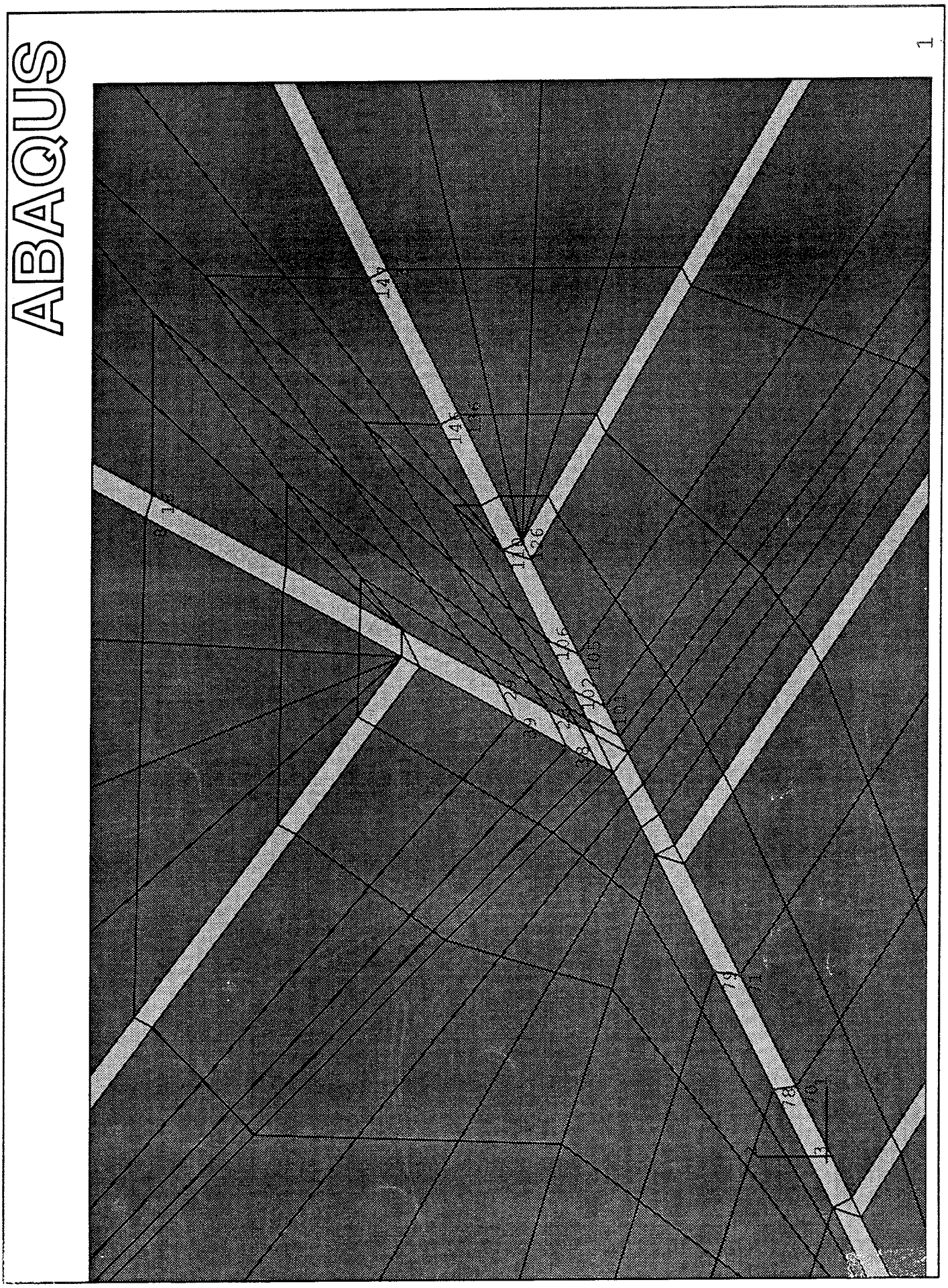

Figure 6-19. *Location of nodes in fractures 1 and 2 where displacements are calculated*

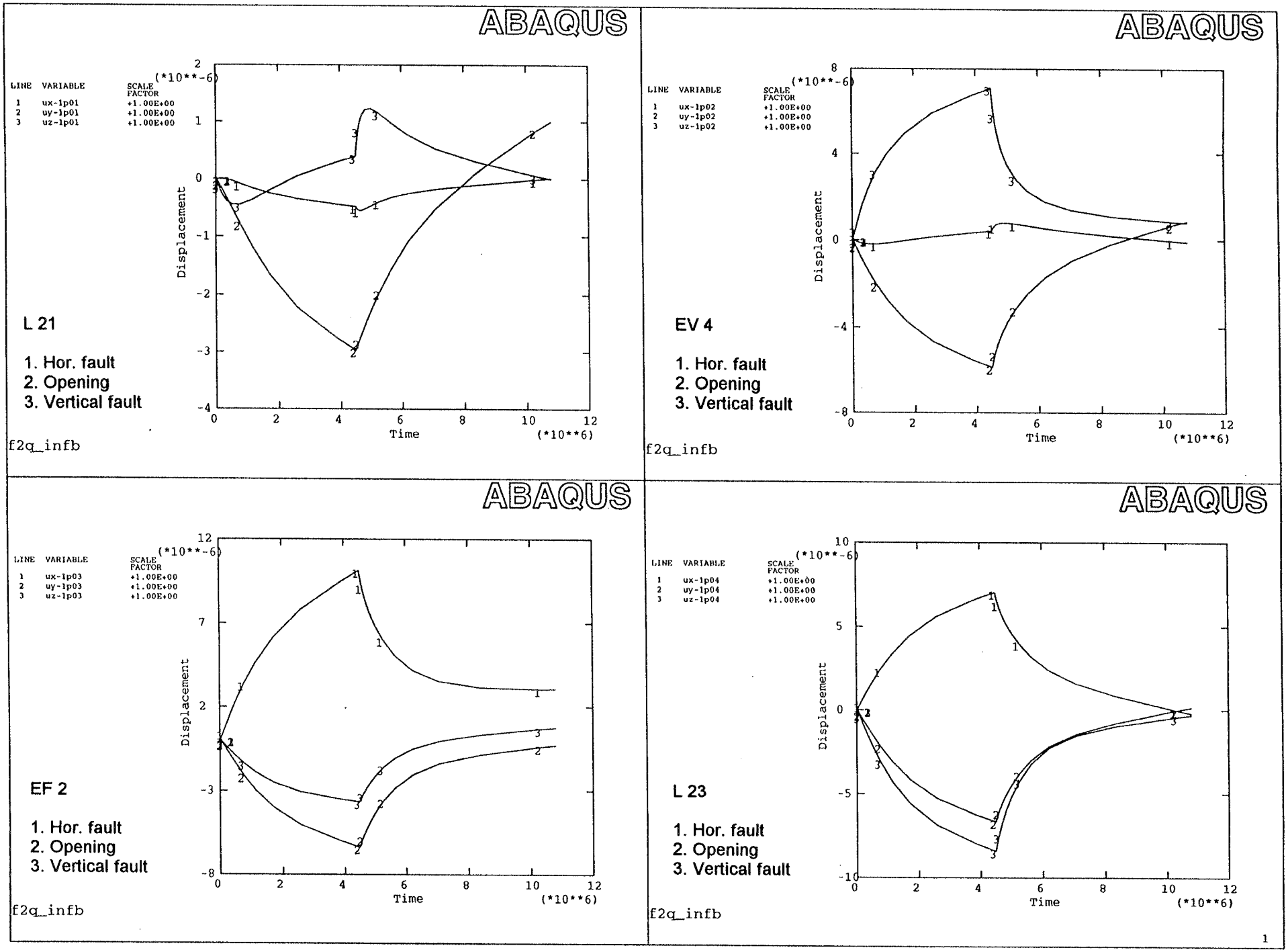

Figure 6-20. Elastic calculation. Fracture displacements (m). See Table 6-1.

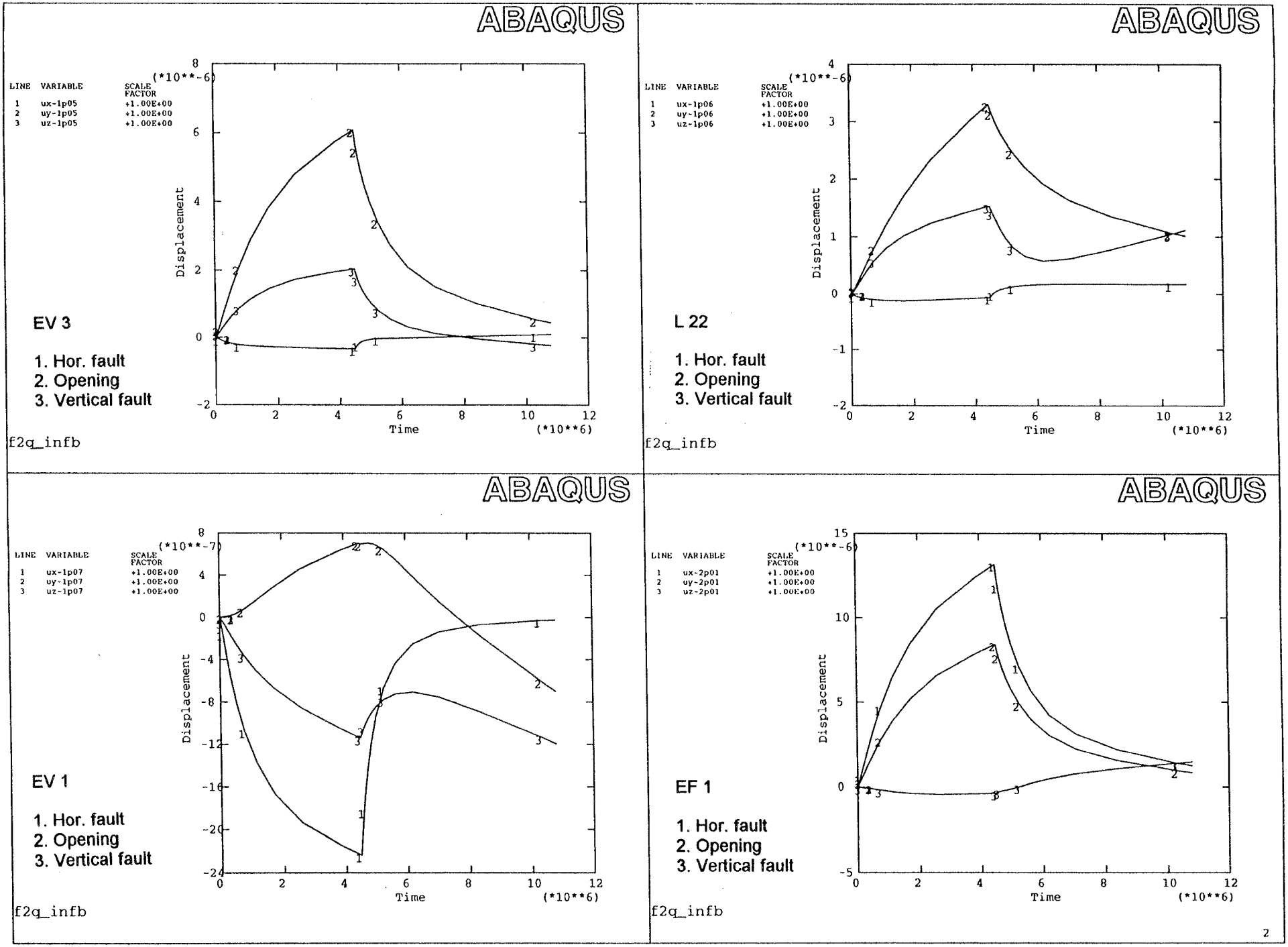

Figure 6-21. Elastic calculation. Fracture displacements (m). See Table 6-1.

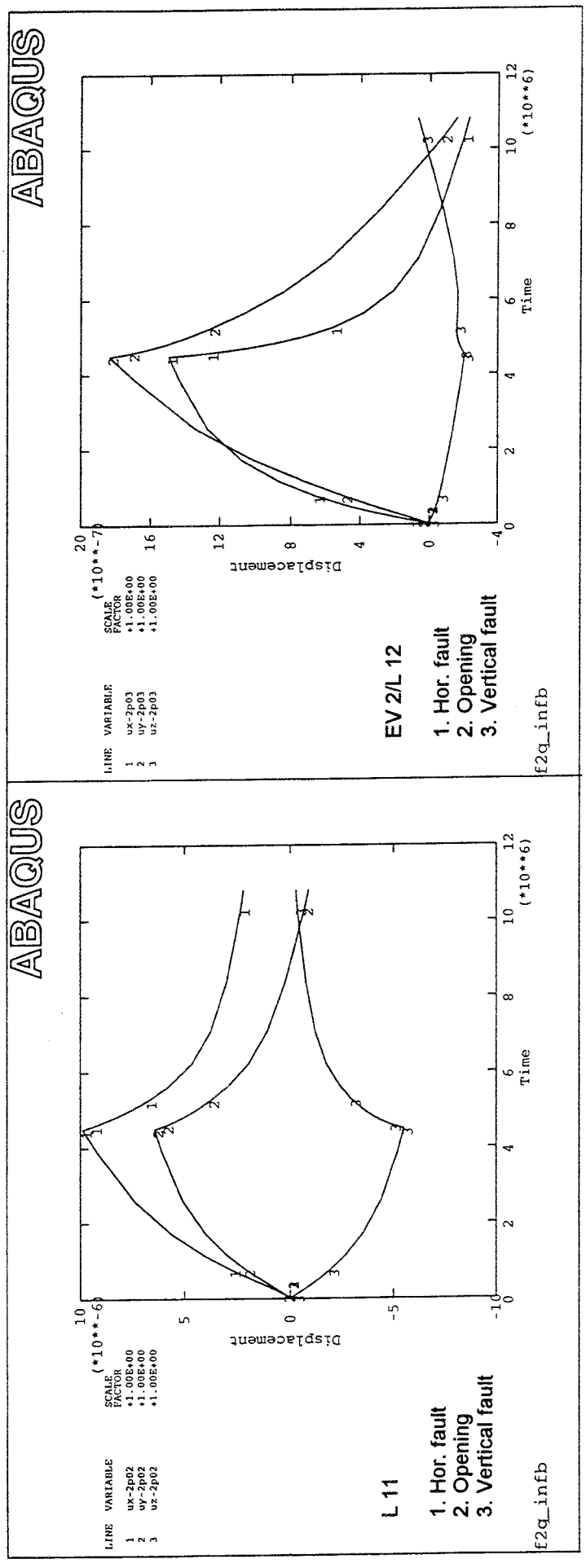

Figure 6-22. *Elastic calculation. Fracture displacements (m). See Table 6-1.*

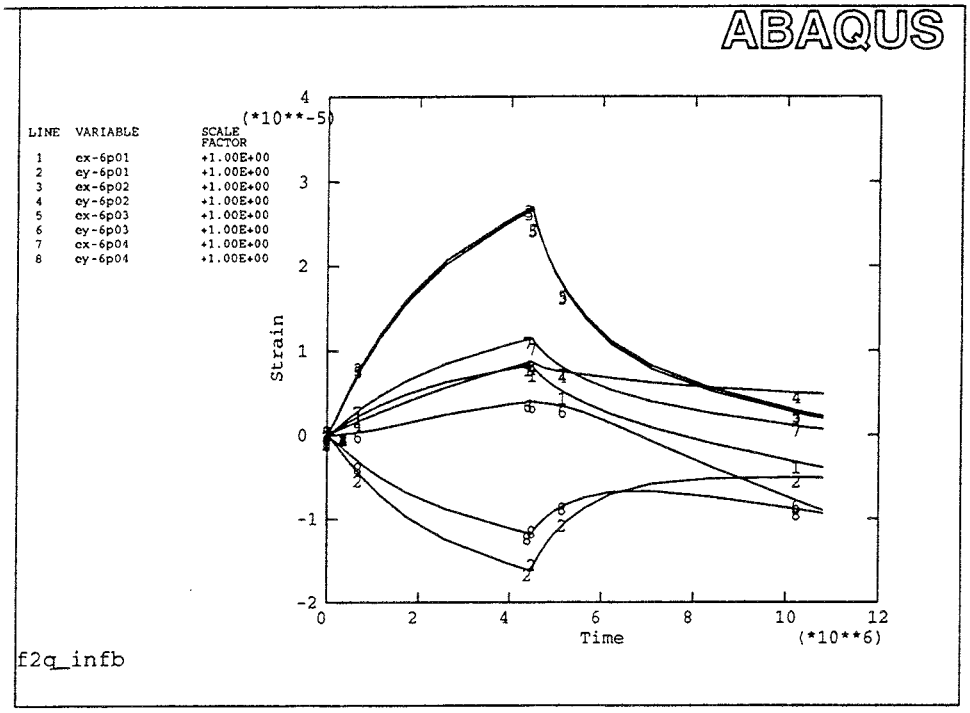

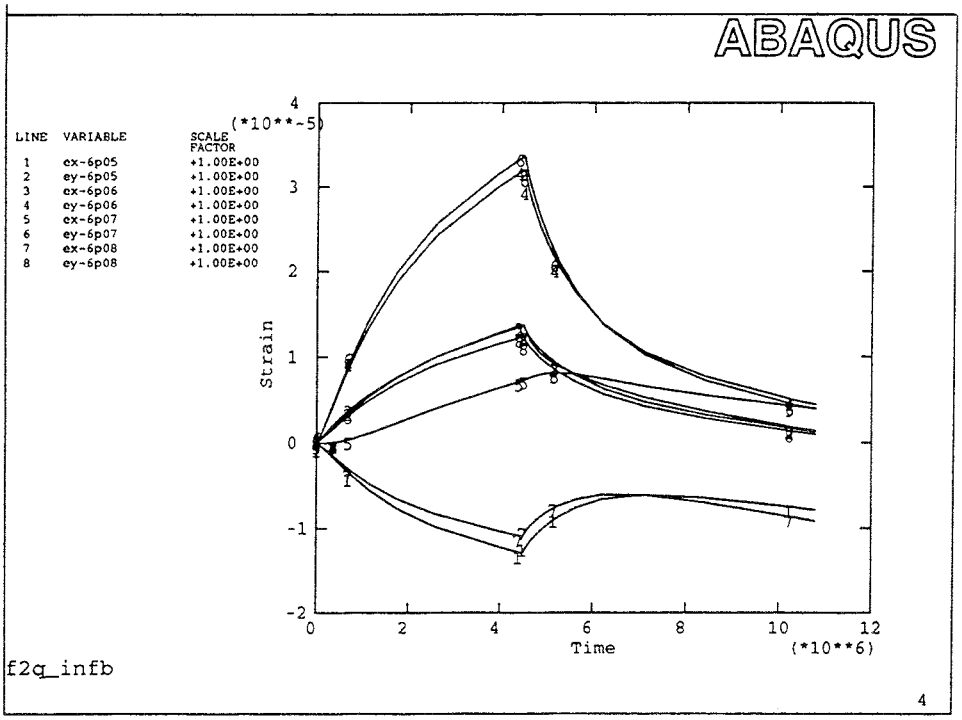

Figure 6-23. *Elastic calculation. Strain in the floor. See Table 6-2.*

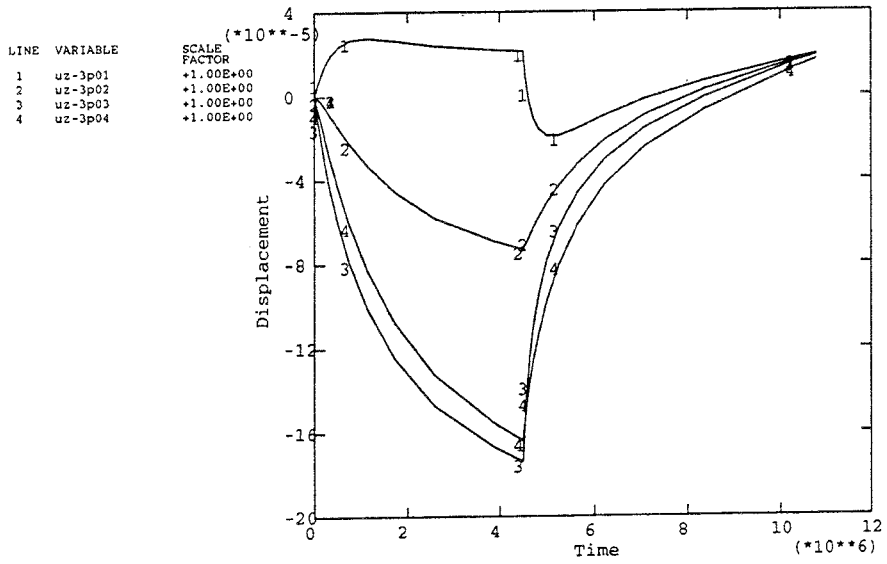

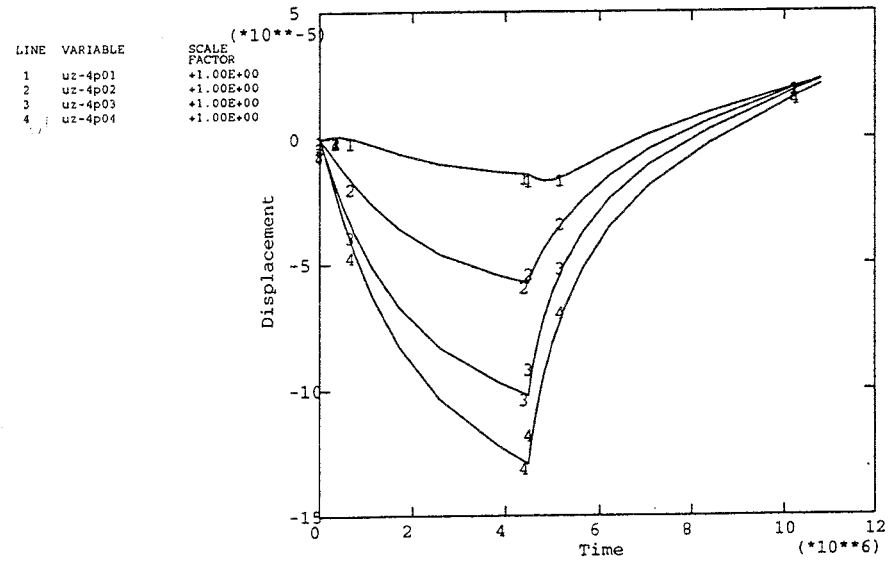

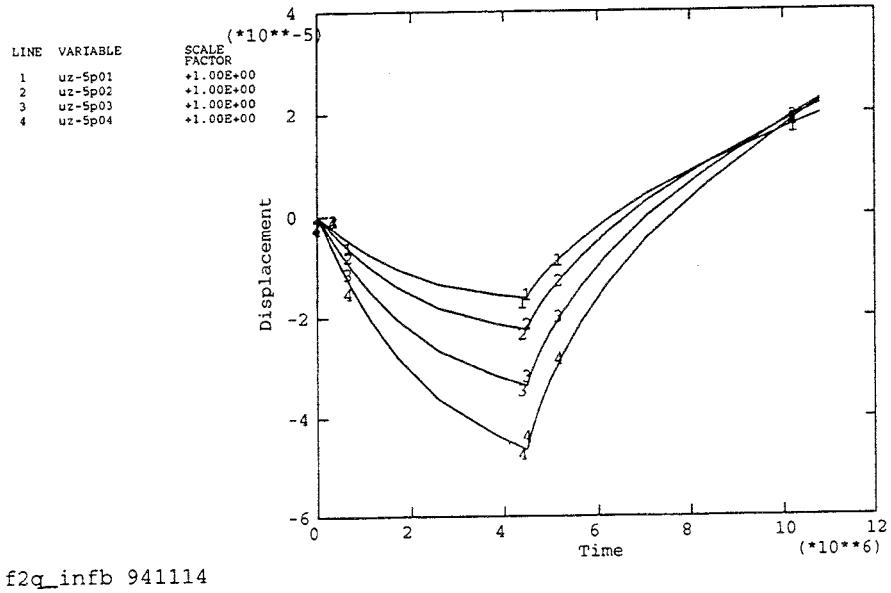

Figure 6-24. *Elastic calculation. Expansion of the rock. See Table 6-3.*

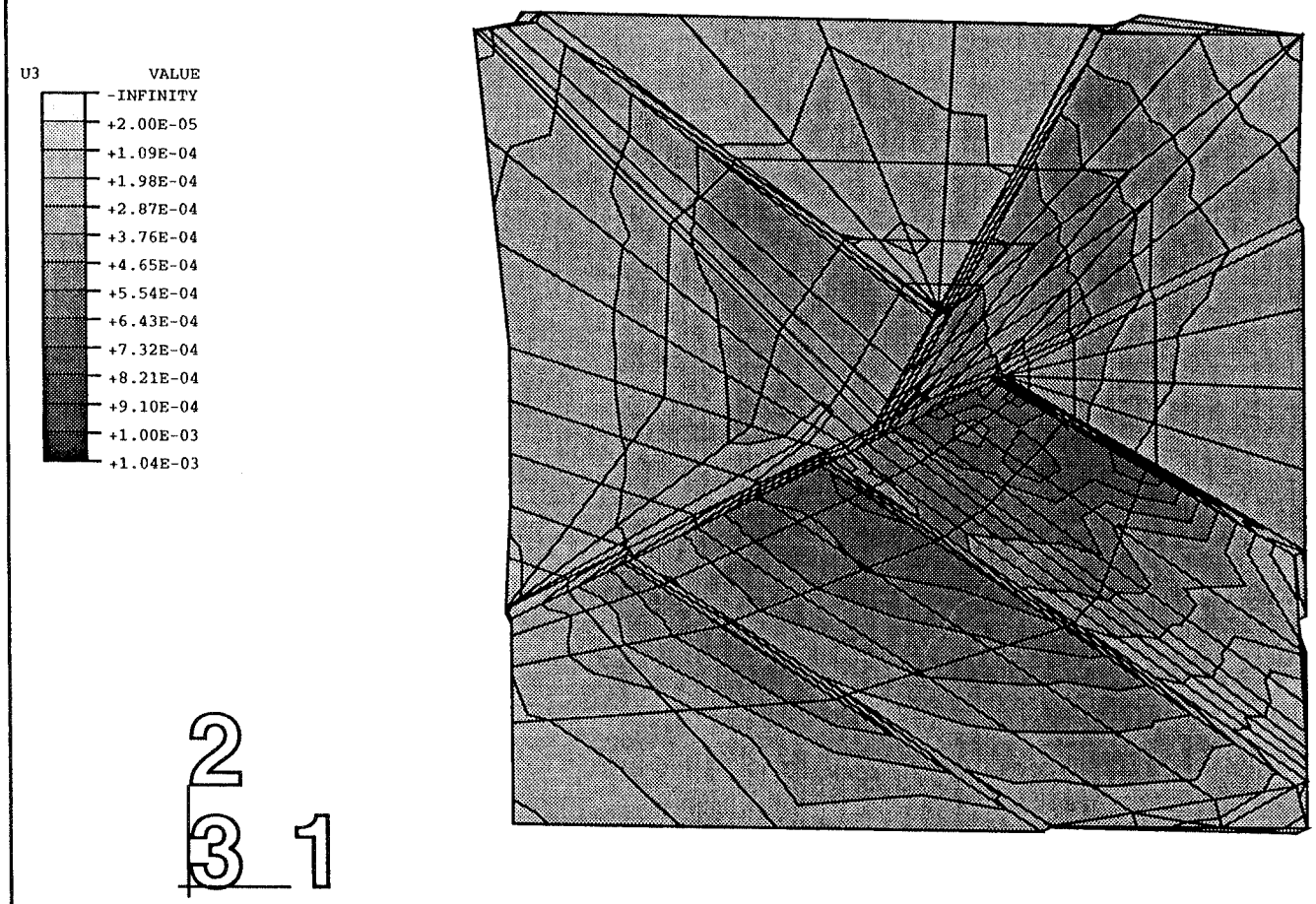

Figure 6-25. *Fracture calculation. Vertical displacements (U3) after excavation (m).*

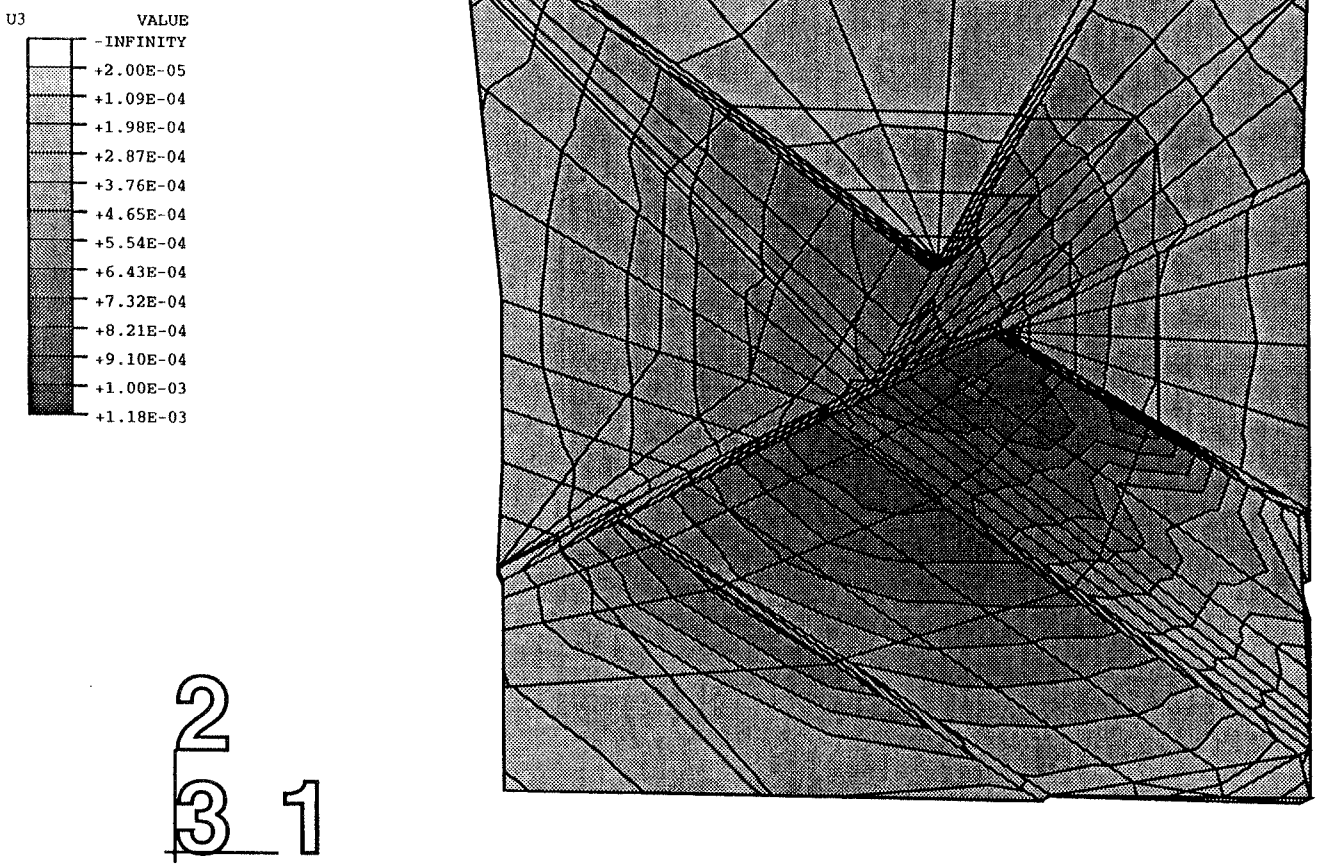

Figure 6-26. *Fracture calculation. Vertical displacements (U3) after heating (m).*

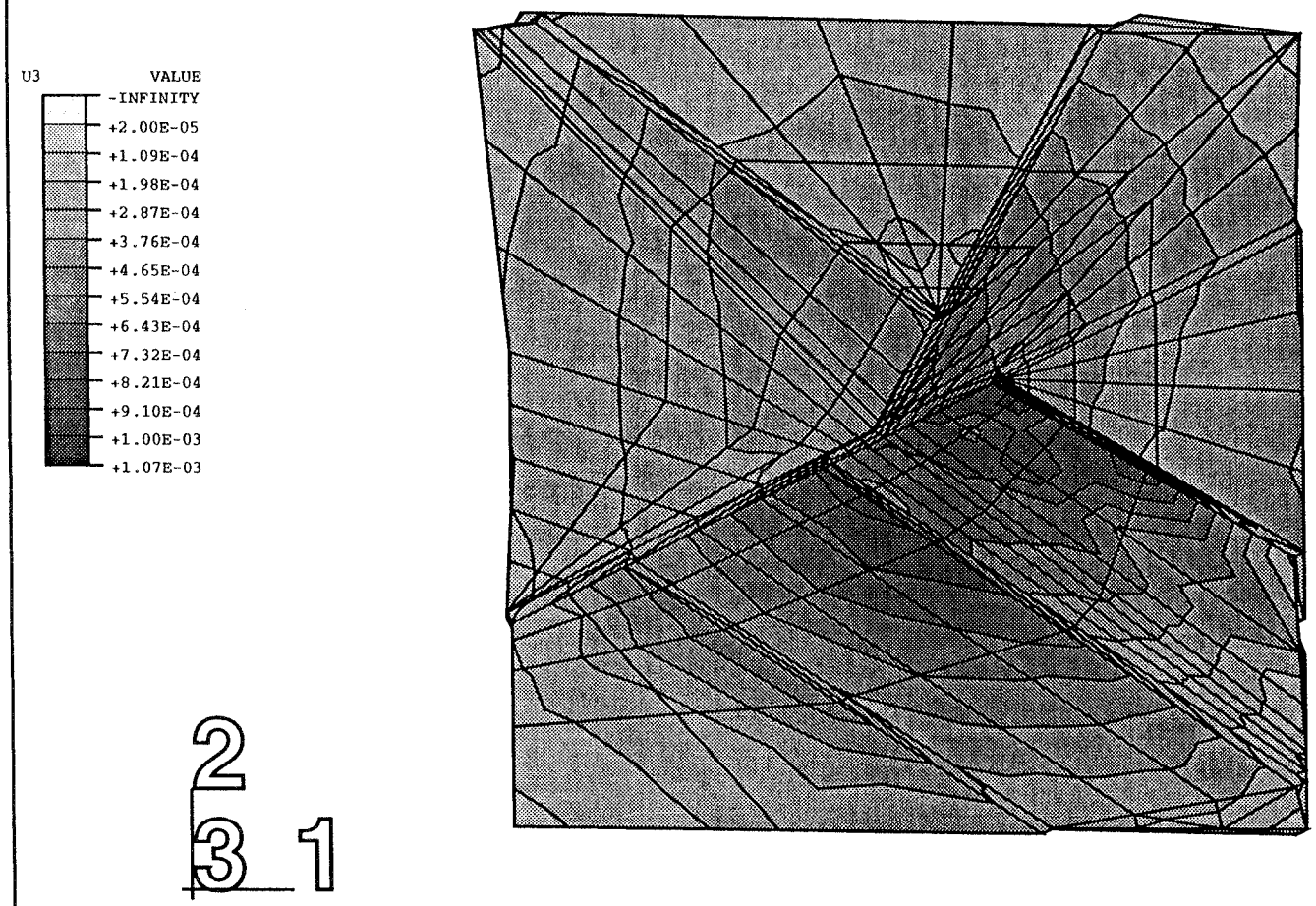

Figure 6-27. *Fracture calculation. Vertical displacements (U3) after cooling (m).*

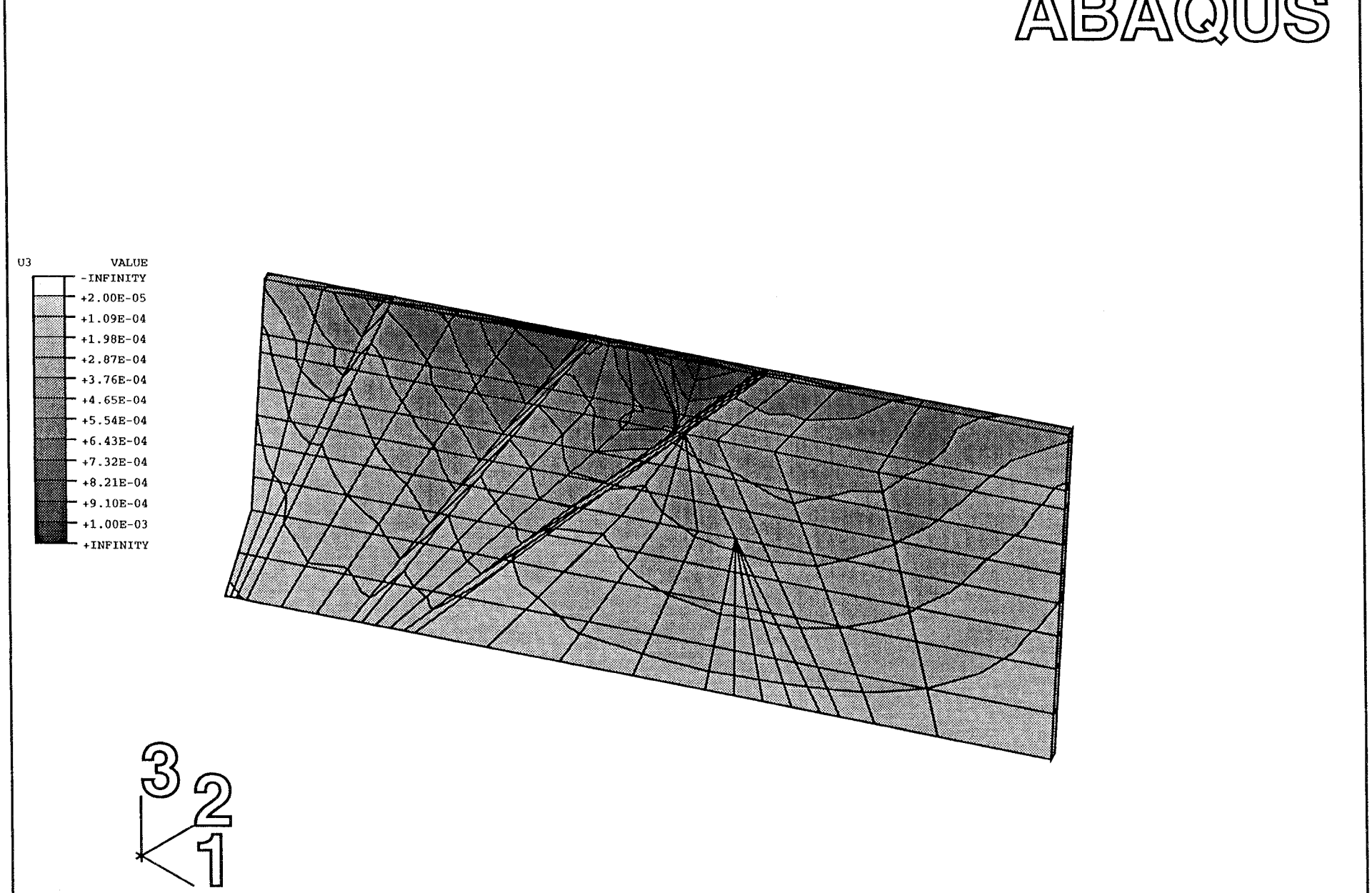

Figure 6-28. *Fracture calculation. Vertical displacements (U3) after excavation (m).*

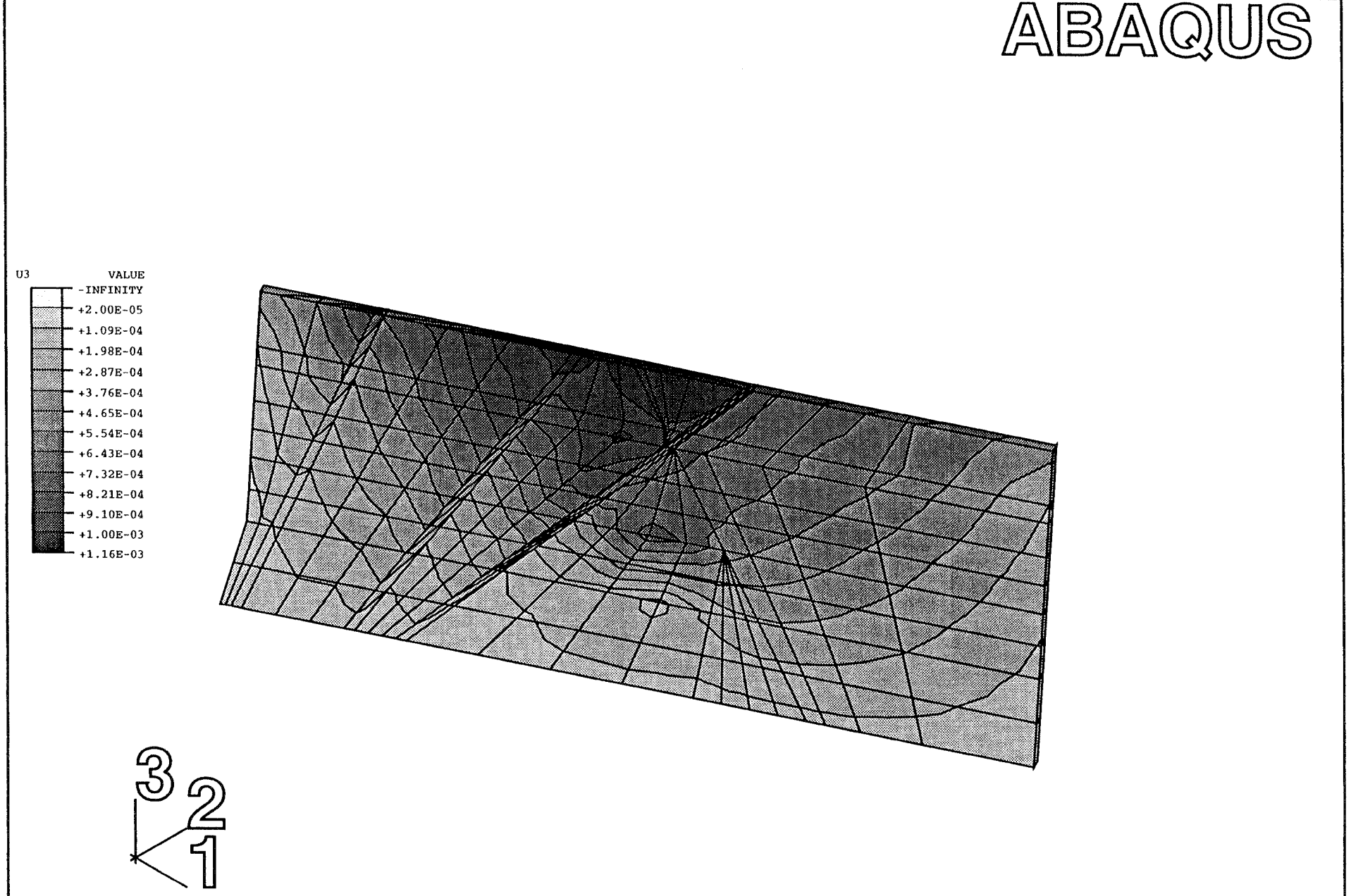

Figure 6-29. *Fracture calculation. Vertical displacements (U3) after heating (m).*

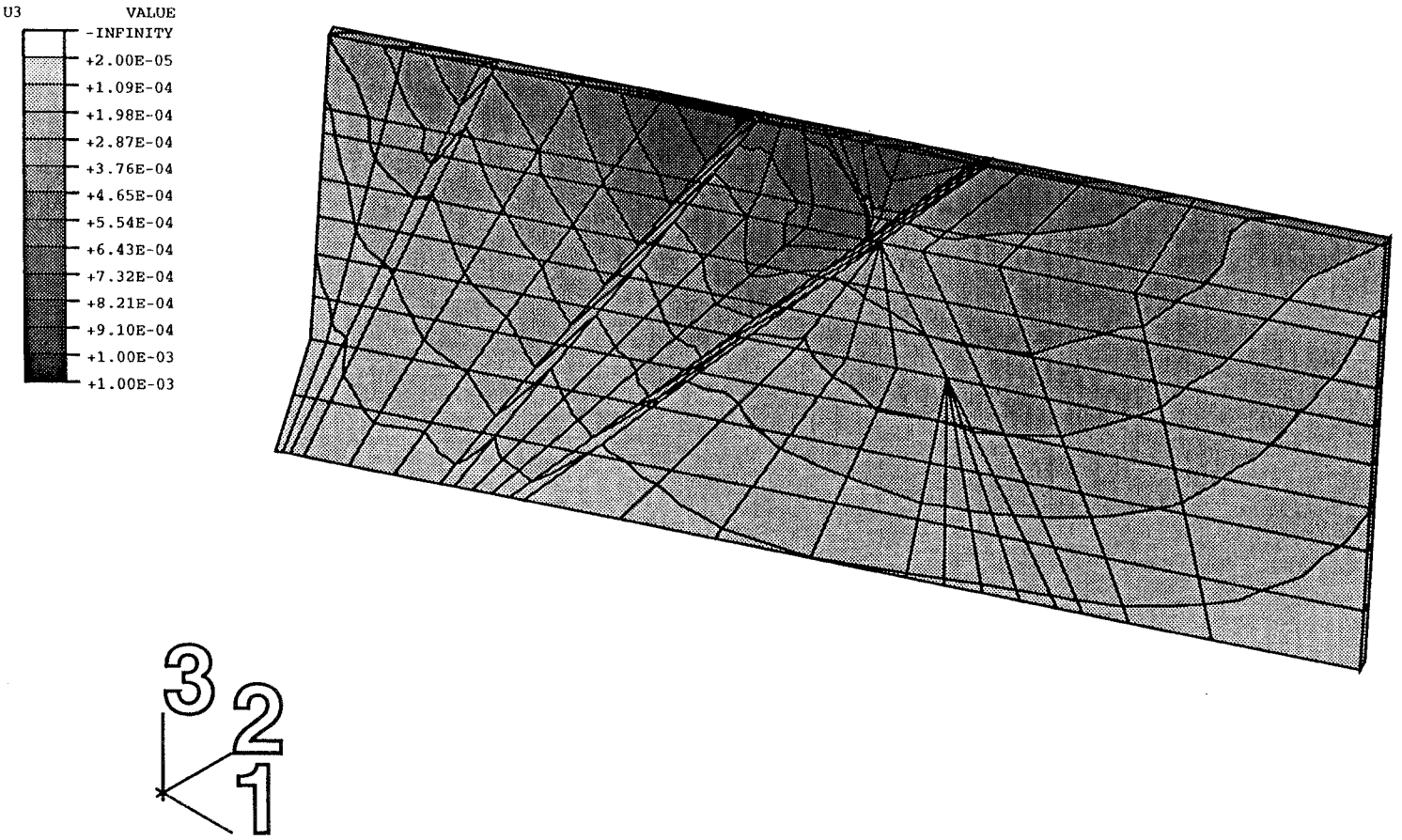

Figure 6-30. *Fracture calculation. Vertical displacements (U3) after cooling (m).*

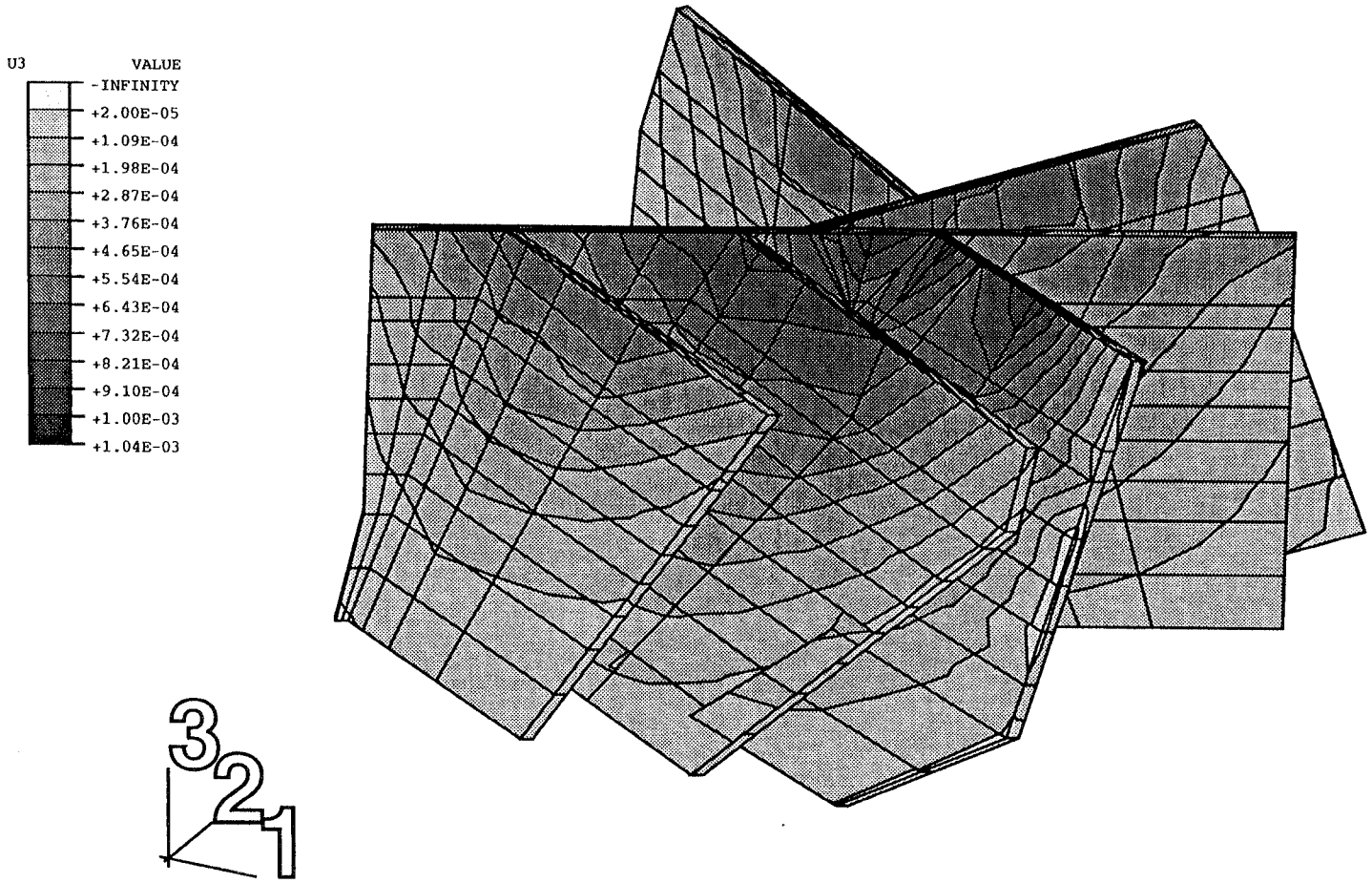

Figure 6-31. Fracture calculation. Vertical displacements (U3) after excavation (m).

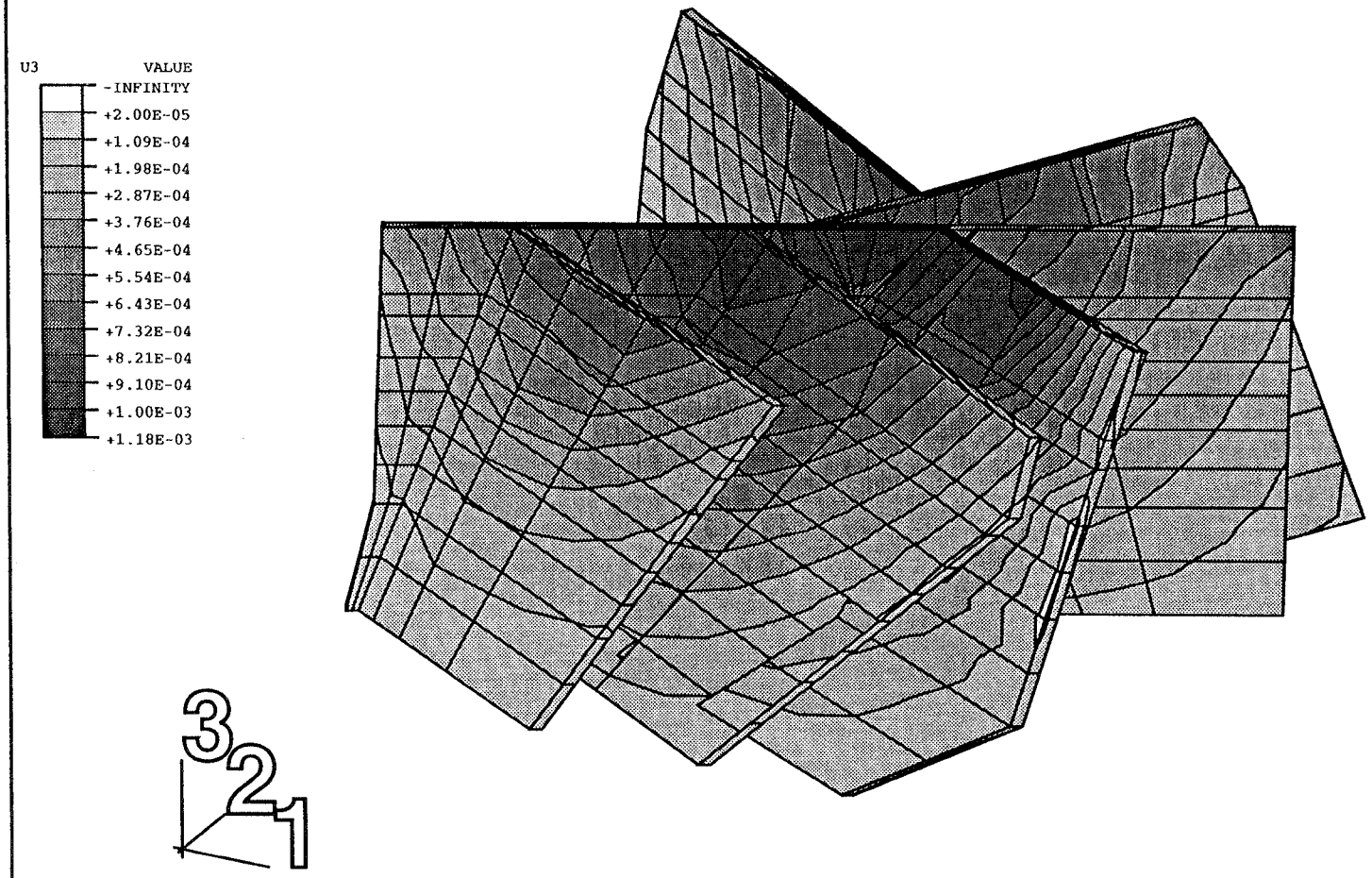

Figure 6-32. *Fracture calculation. Vertical displacements (U3) after heating (m).*

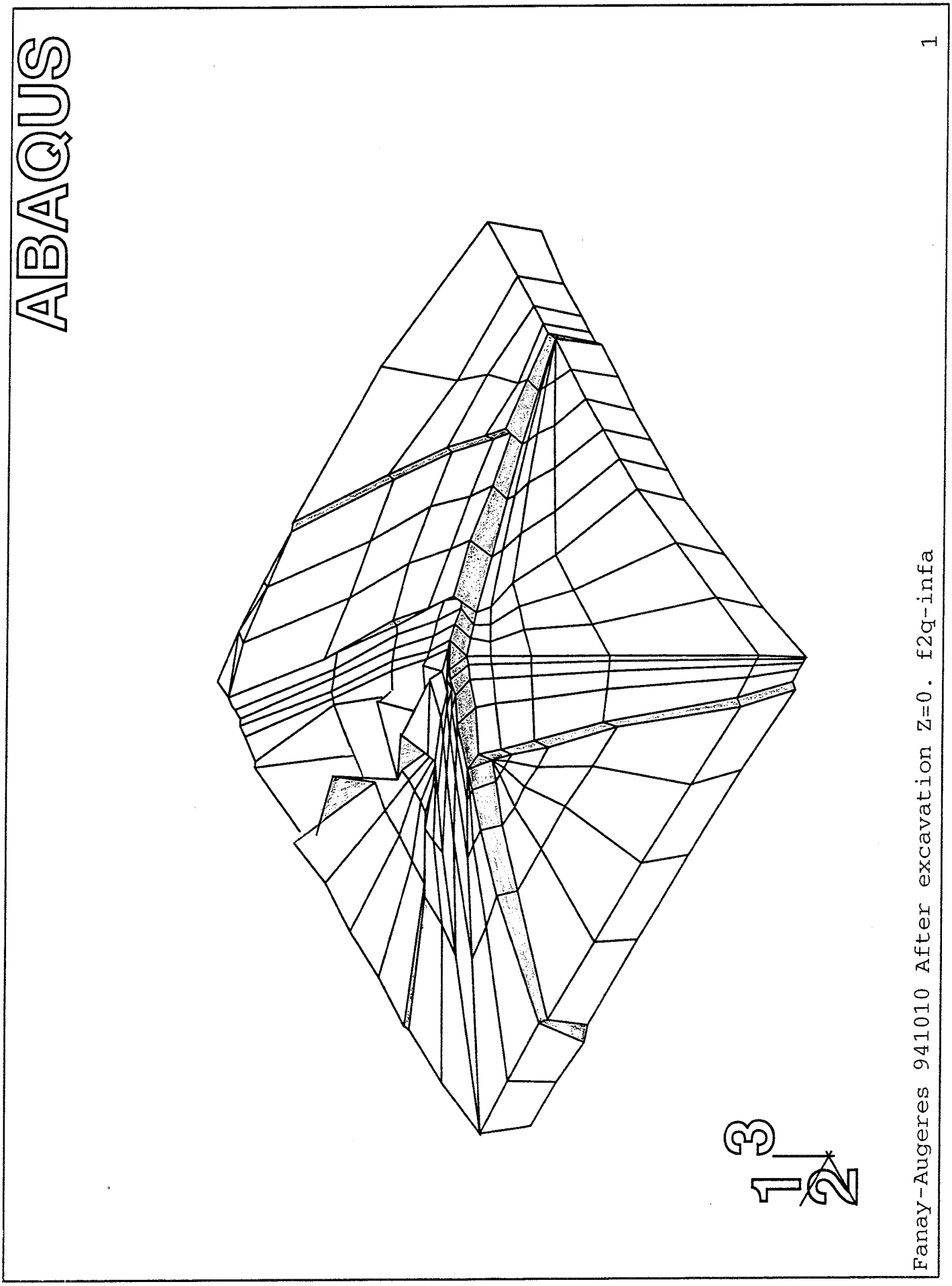

Figure 6-33. *Fracture calculation. View of displaced mesh after excavation.* D_{mag}*=1400*

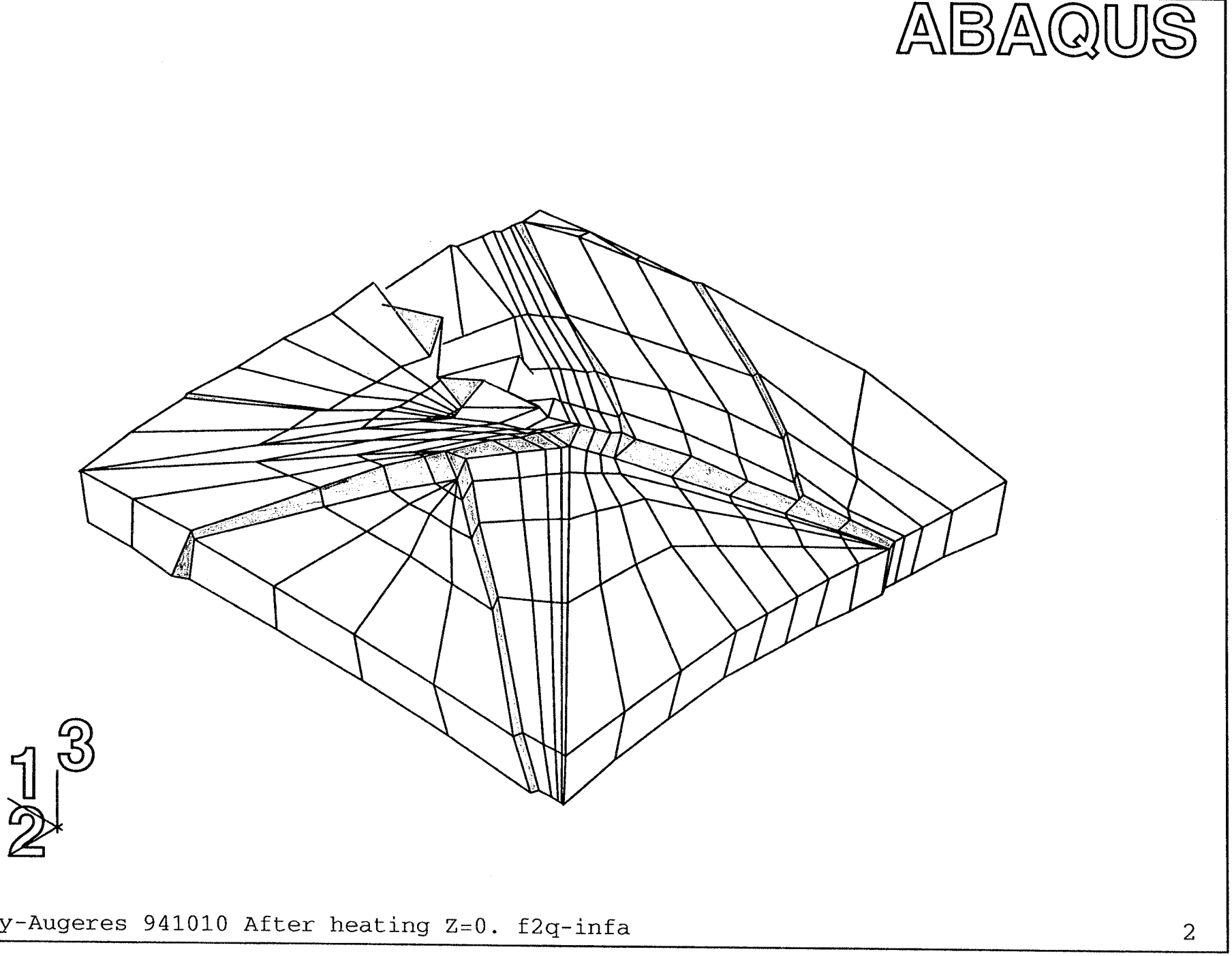

Figure 6-34. *Fracture calculation. View of displaced mesh after heating.* D_{mag}=*1400*

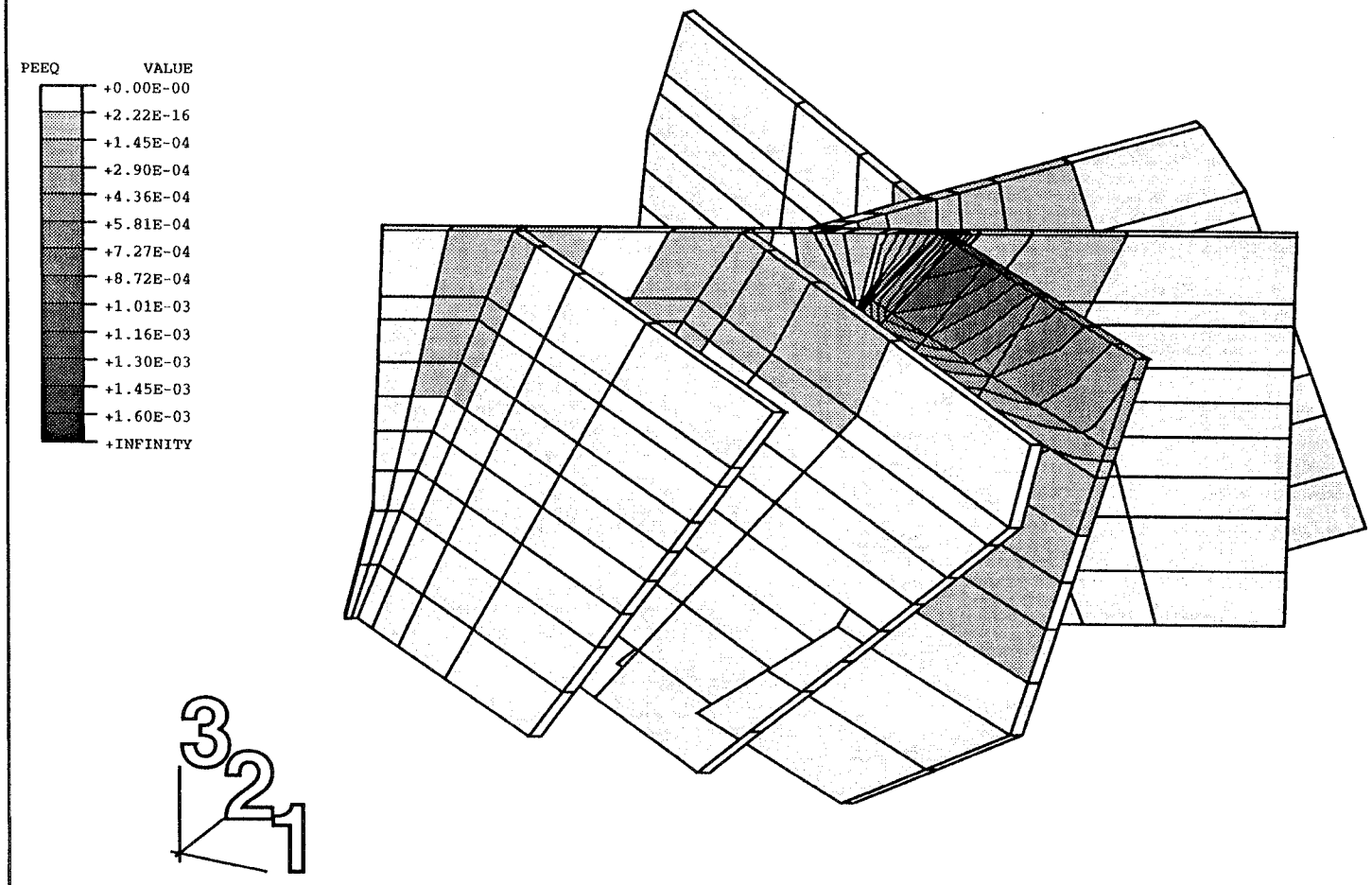

Figure 6-35. Fracture calculation. Plastic strain (PEEQ) in the fractures after excavation

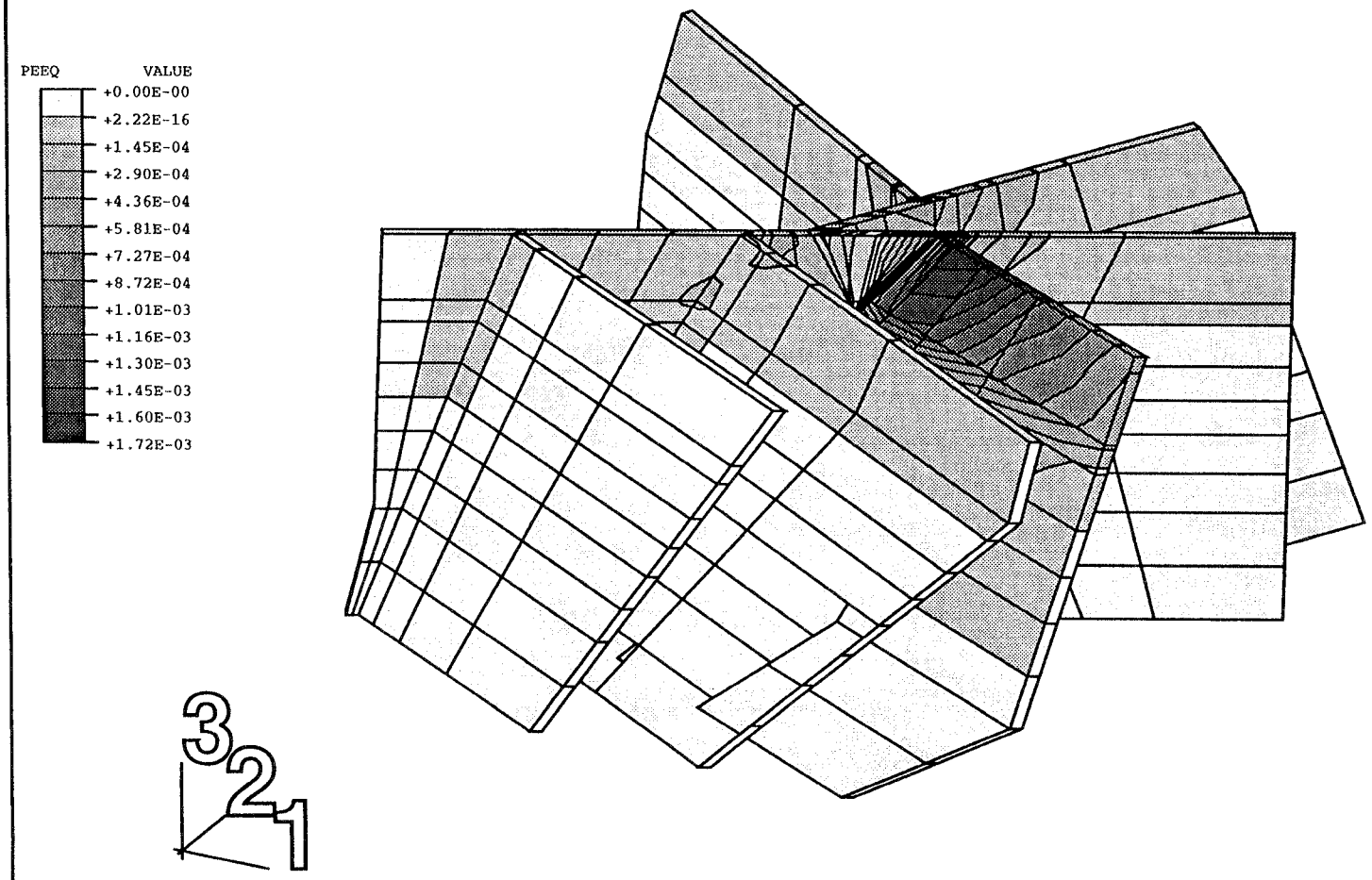

Figure 6-36. *Fracture calculation. Plastic strain (PEEQ) in the fractures after heating*

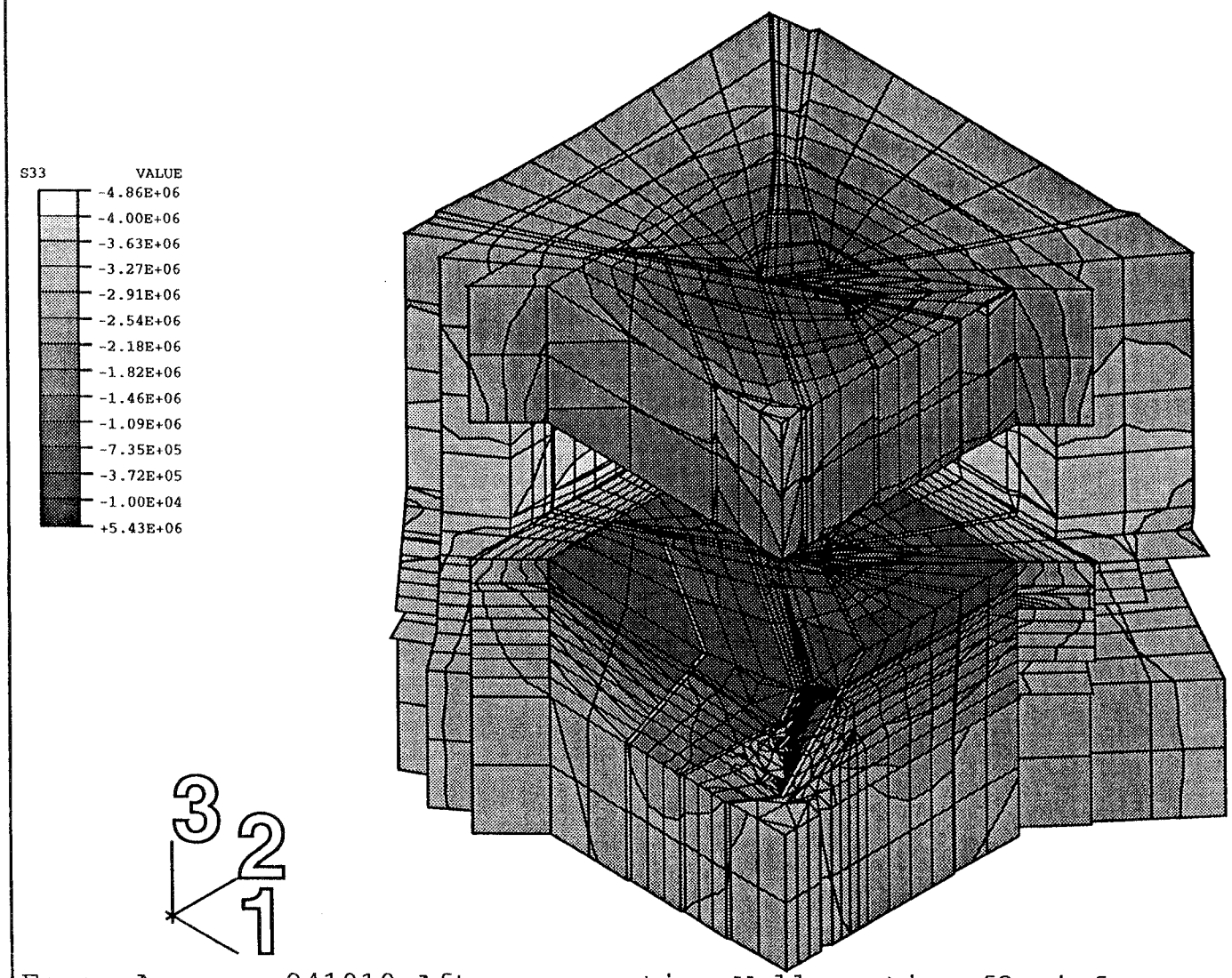

Figure 6-37. Fracture calculation. Vertical stress (S33) after excavation (Pa).

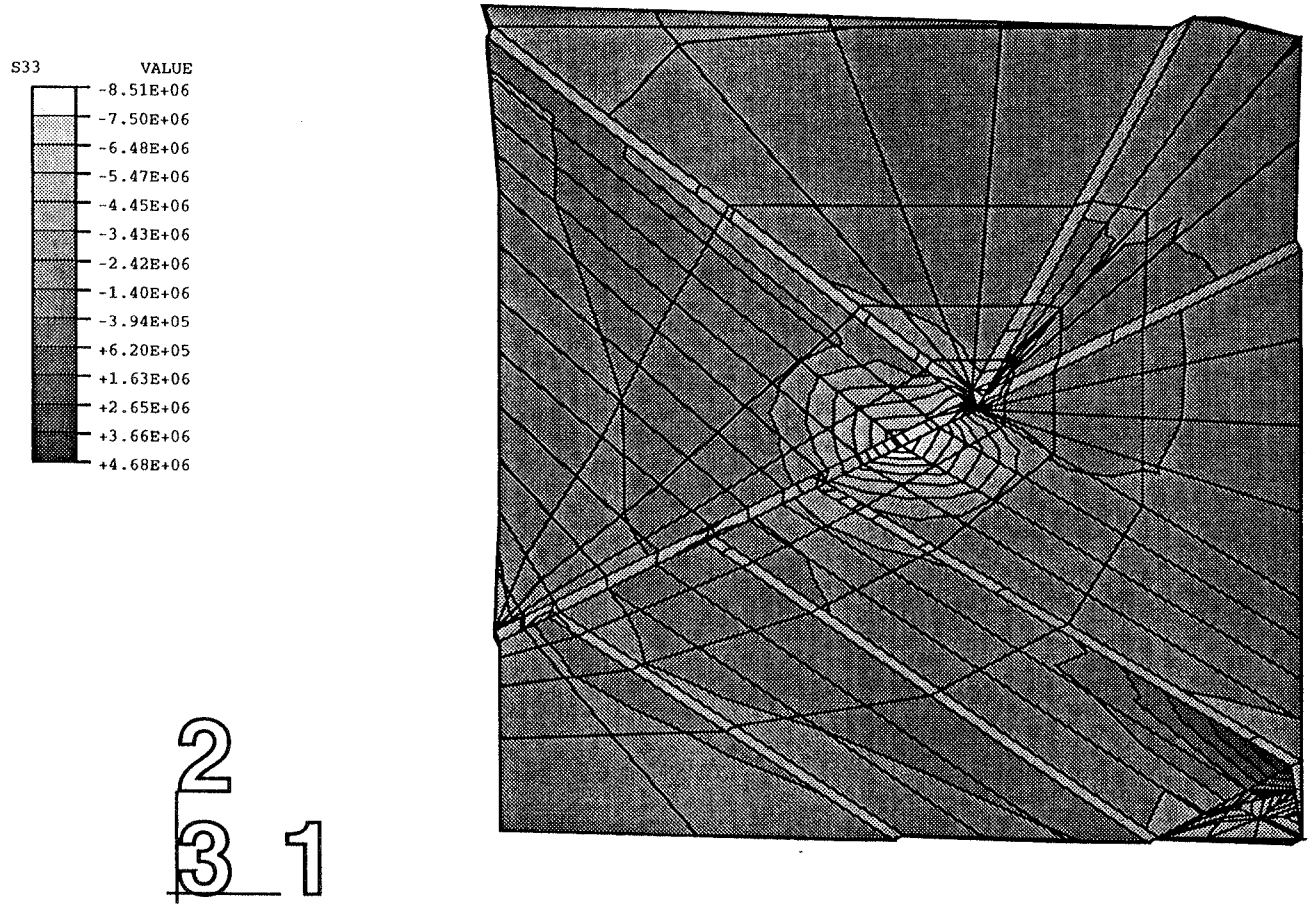

Figure 6-38. *Fracture calculation. z=-2.6 m. Vertical stress (S33) after heating (Pa)*

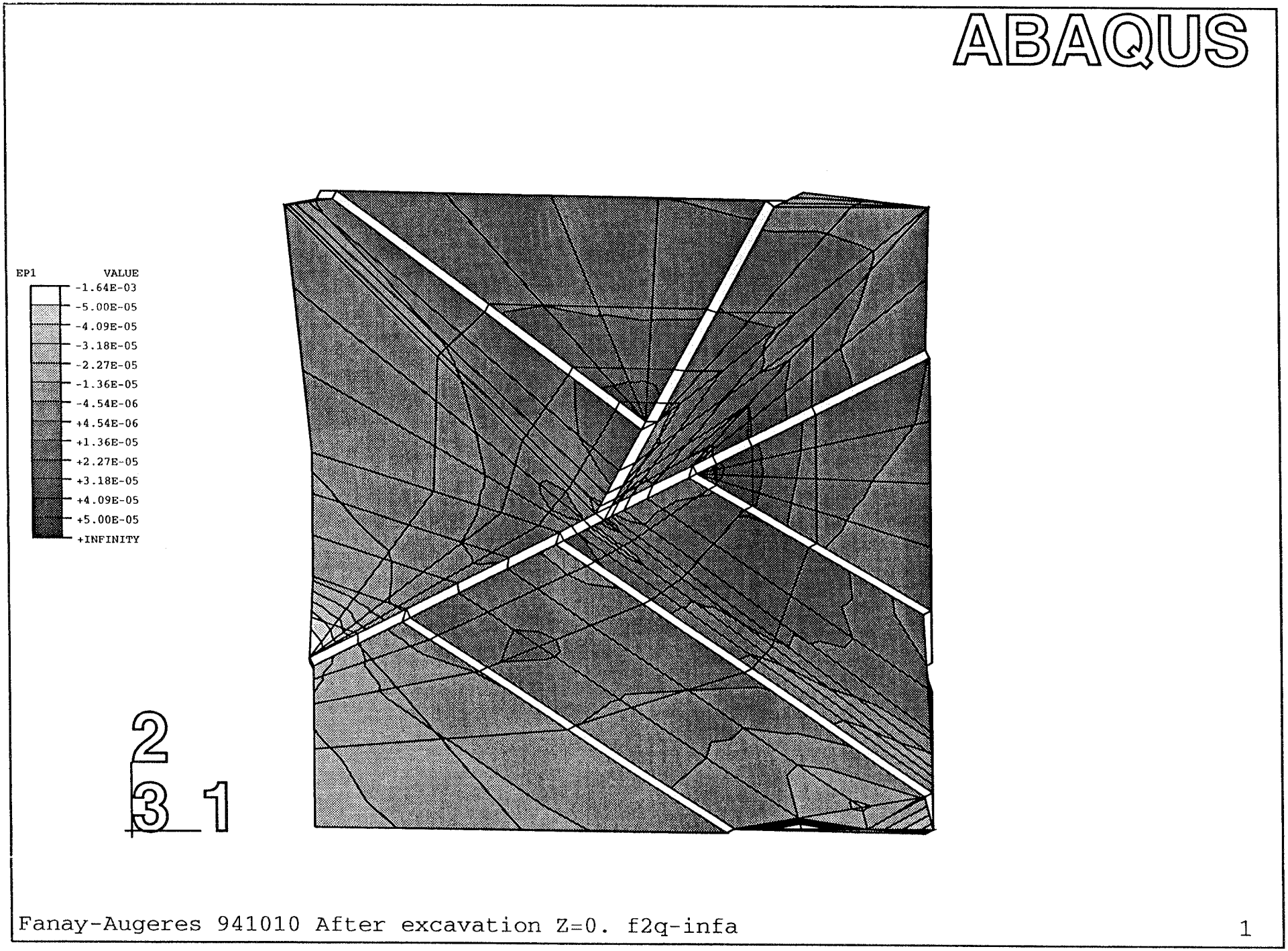

Figure 6-39. *Fracture calculation. Main princ. strain (EP1) in the floor after exc. (m/m)*

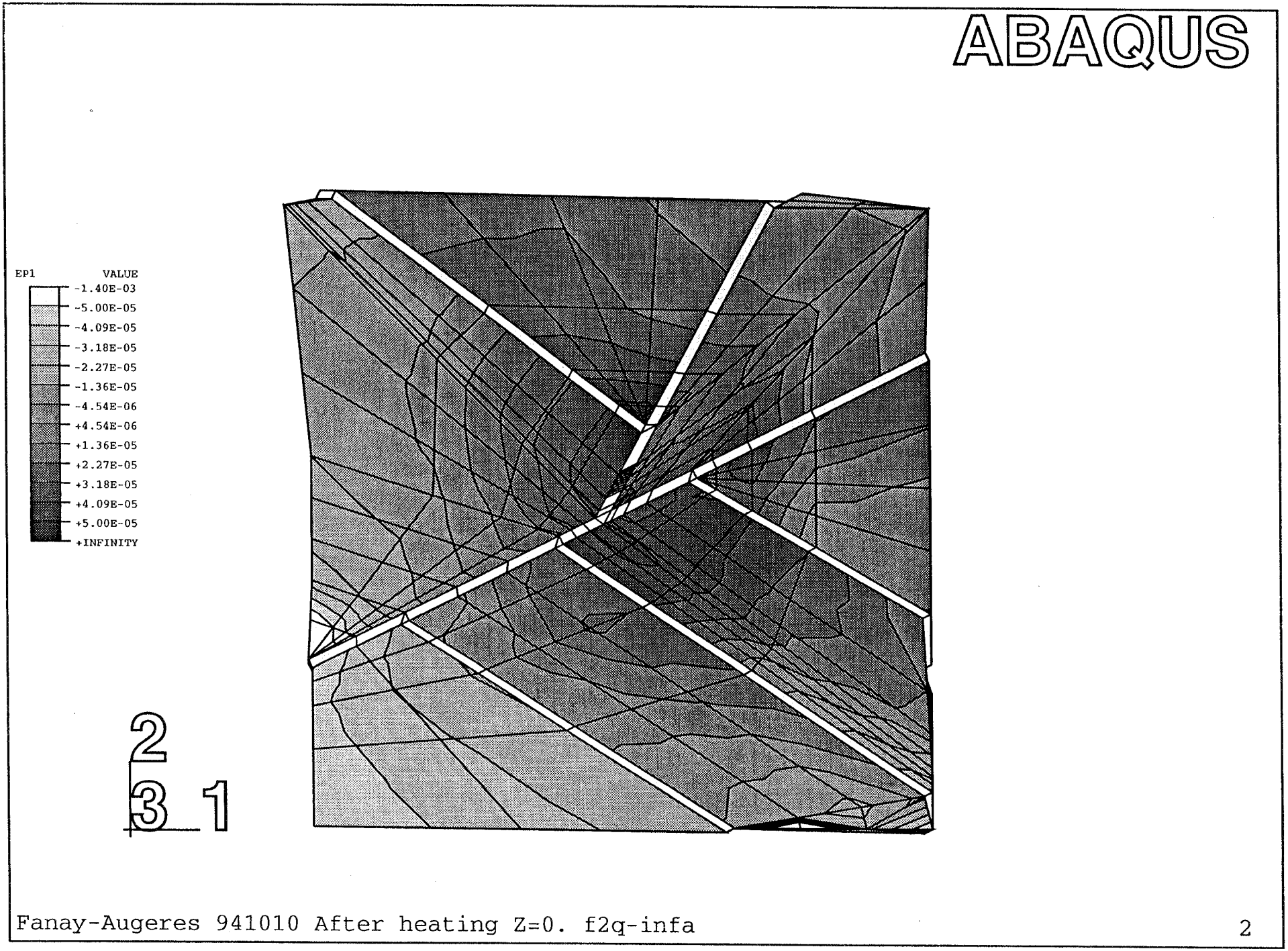

Figure 6-40. *Fracture calculation. Main princ. strain (EP1) in the floor after heating (m/m)*

ABAQUS

LINE	VARIABLE	SCALE FACTOR
1	uz-7p01	+1.00E+00
2	uz-7p02	+1.00E+00
3	uz-7p03	+1.00E+00
4	uz-7p04	+1.00E+00
5	uz-7p05	+1.00E+00
6	uz-7p06	+1.00E+00

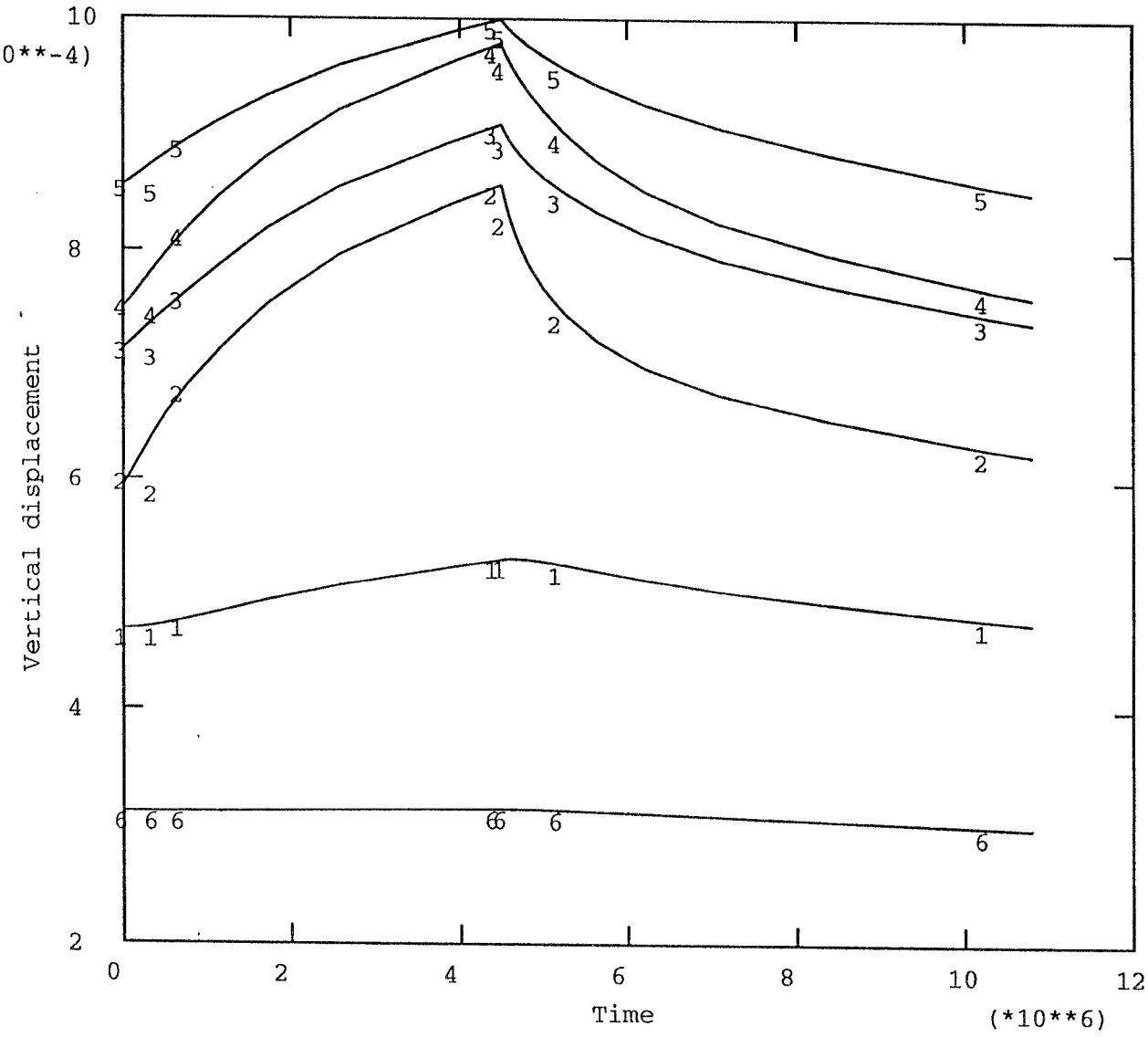

7p01: v2 (-0.15, 2.35,0)
7p02: v4 (-0.15, 1.35,0)
7p03: v5 (-0.15, 0.35,0)
7p04: v6 (-0.15,-0.65,0)
7p05: v7 (-0.15,-1.60,0)
7p06: v0 (-4.00, 5.00,0)

f2q_infa 941107

Figure 6-41. Fracture calculation. Heave (m) of the floor in points V2-V7. (V0=ref.)

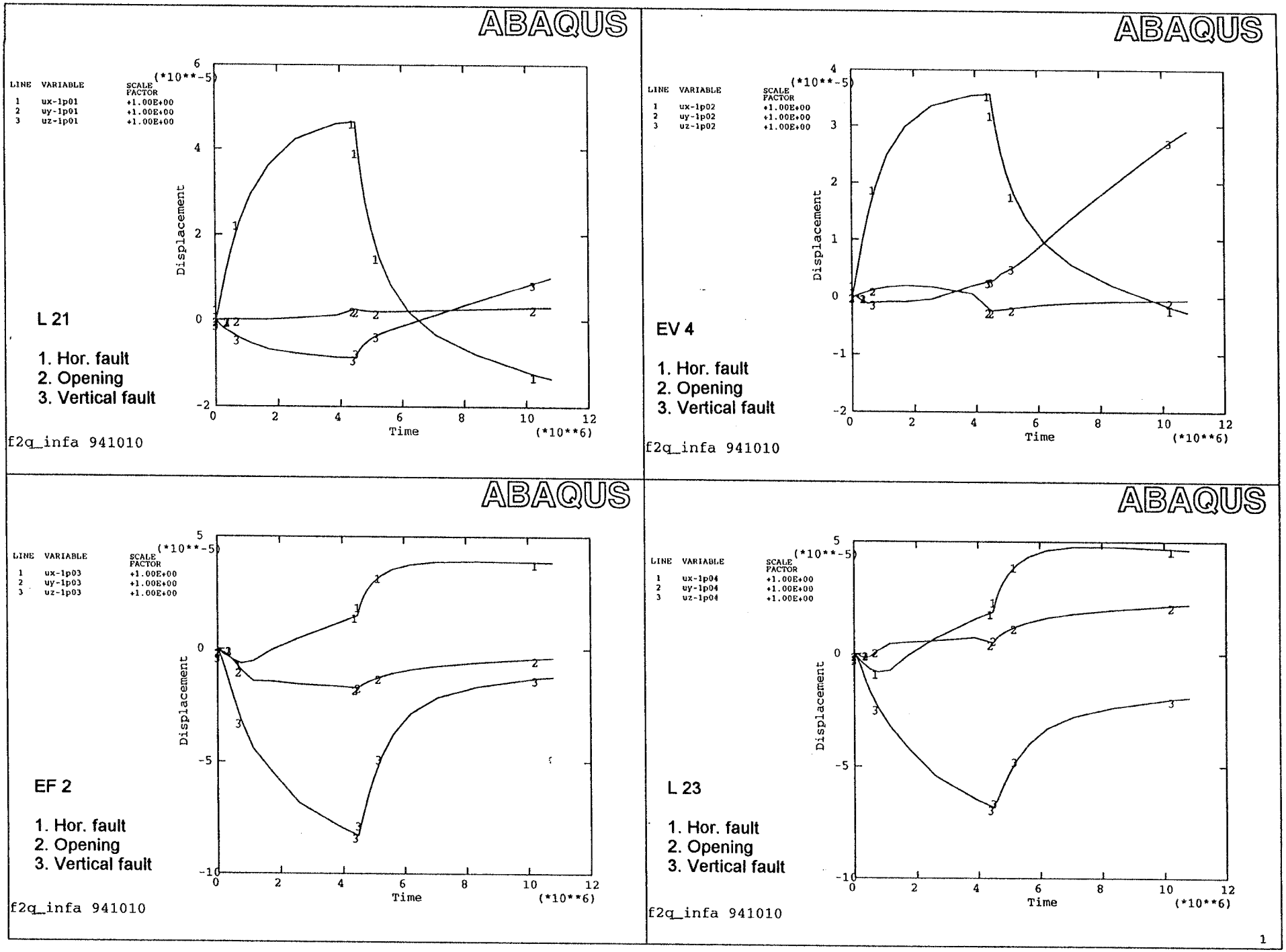

Figure 6-42. Fracture calculation. Fracture displacements (m). See Table 6-1.

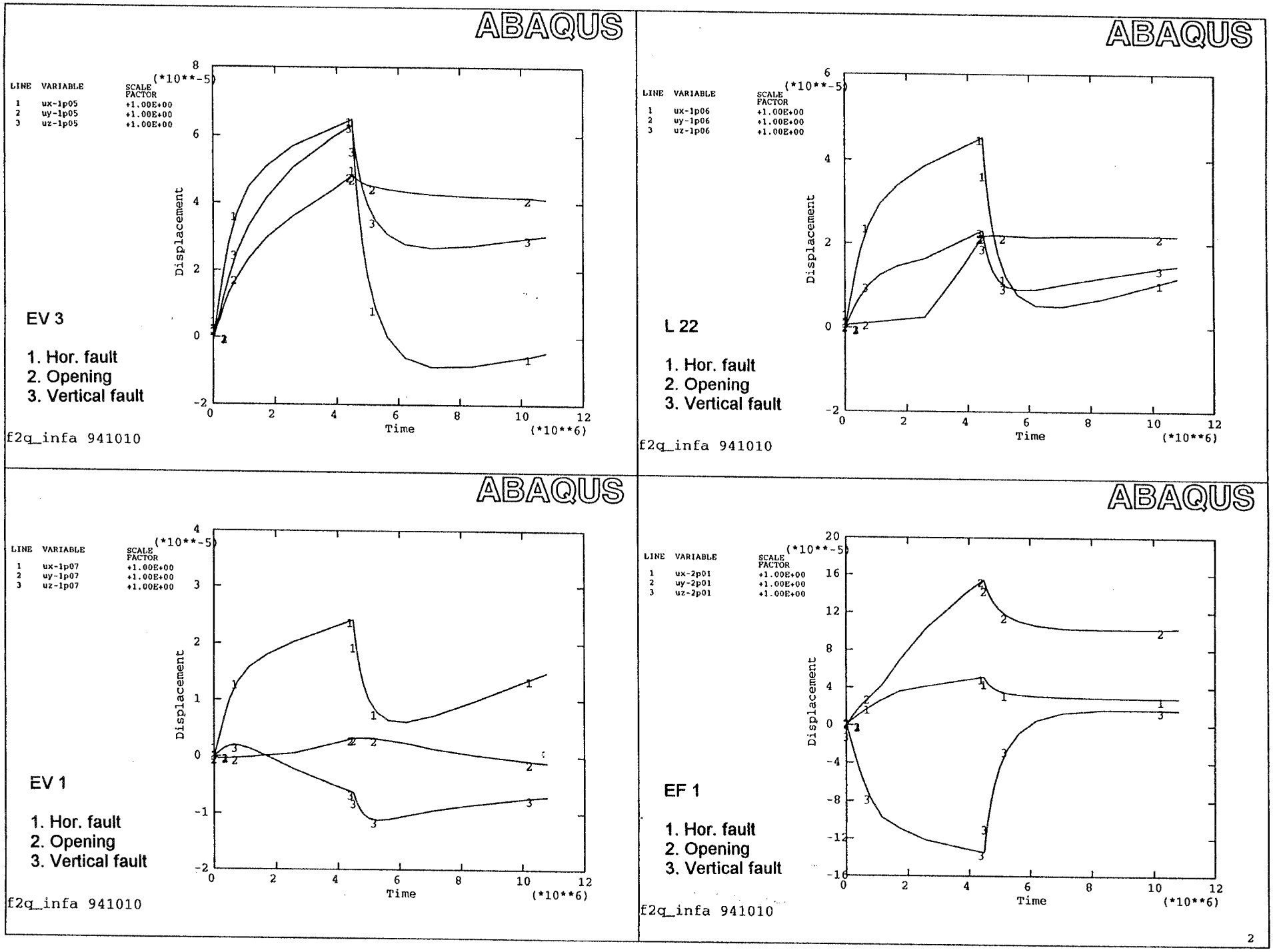

Figure 6-43. Fracture calculation. Fracture displacements (m). See Table 6-1.

Figure 6-44. Fracture calculation. Fracture displacements (m). See Table 6-1.

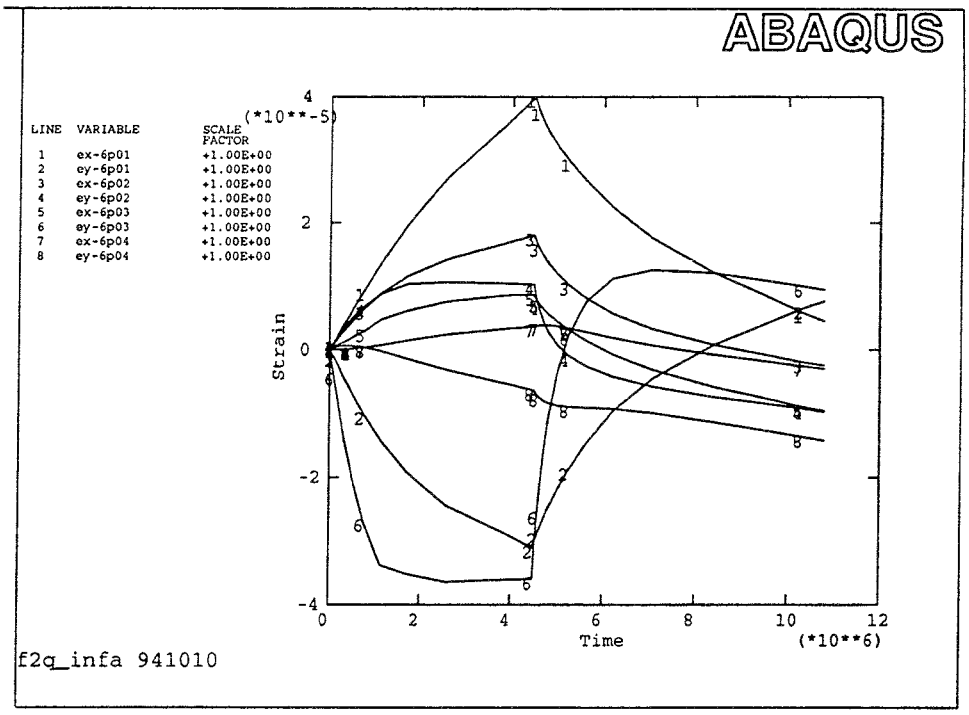

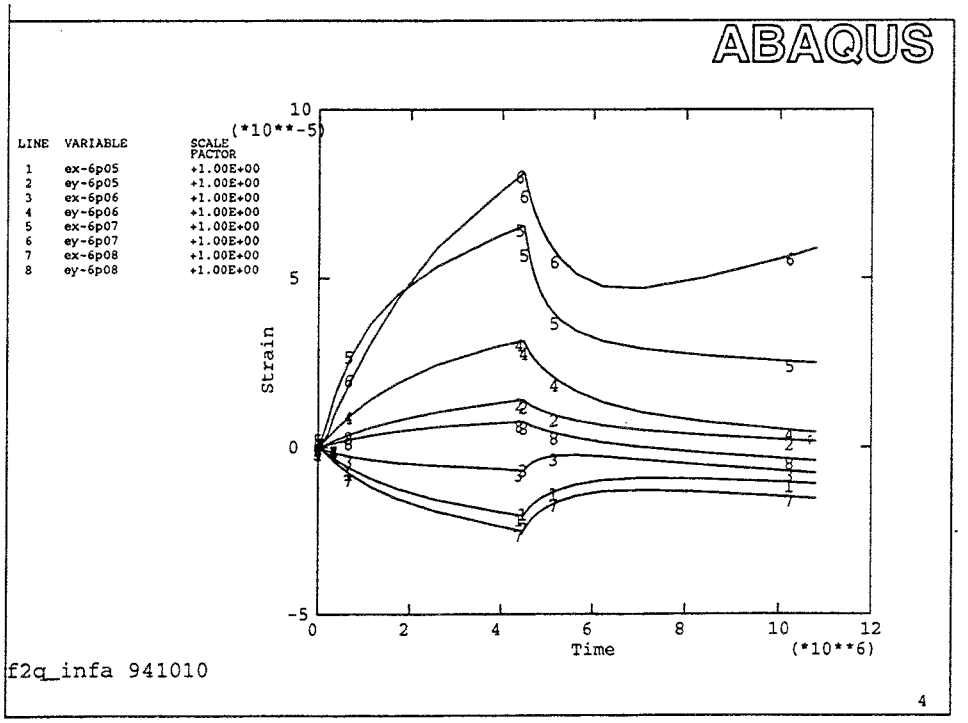

Figure 6-45. *Fracture calculation. Strain in the floor. See Table 6-2.*

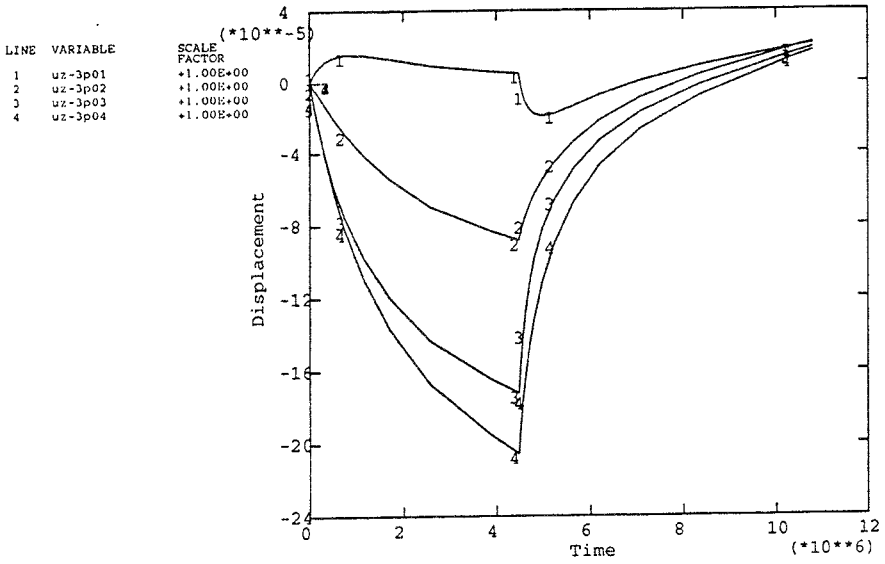

f2q_infa 941114

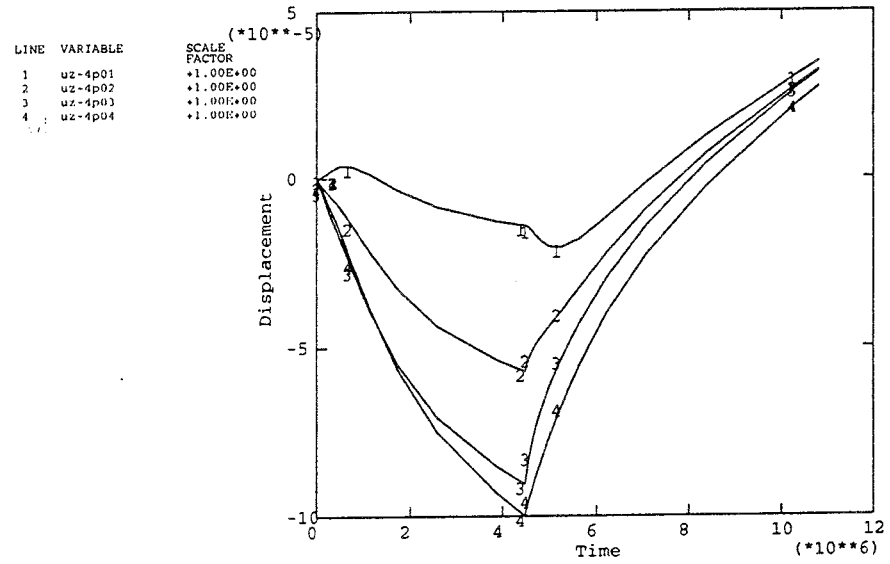

f2q_infa 941114

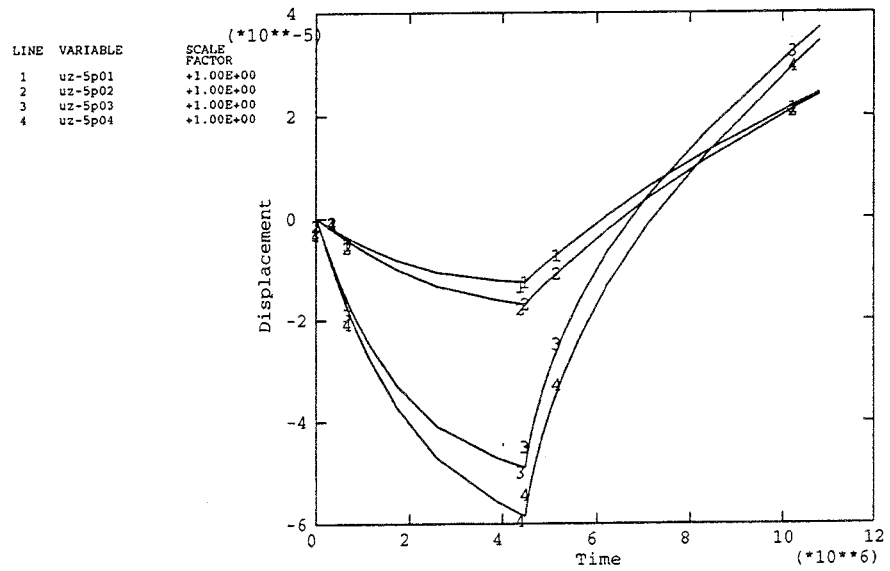

f2q_infa 941114

Figure 6-46. *Fracture calculation. Expansion of the rock. See Table 6-3.*

List of SKB reports

Annual Reports

1977-78
TR 121
KBS Technical Reports 1 – 120
Summaries
Stockholm, May 1979

1979
TR 79-28
The KBS Annual Report 1979
KBS Technical Reports 79-01 – 79-27
Summaries
Stockholm, March 1980

1980
TR 80-26
The KBS Annual Report 1980
KBS Technical Reports 80-01 – 80-25
Summaries
Stockholm, March 1981

1981
TR 81-17
The KBS Annual Report 1981
KBS Technical Reports 81-01 – 81-16
Summaries
Stockholm, April 1982

1982
TR 82-28
The KBS Annual Report 1982
KBS Technical Reports 82-01 – 82-27
Summaries
Stockholm, July 1983

1983
TR 83-77
The KBS Annual Report 1983
KBS Technical Reports 83-01 – 83-76
Summaries
Stockholm, June 1984

1984
TR 85-01
Annual Research and Development Report 1984
Including Summaries of Technical Reports Issued during 1984. (Technical Reports 84-01 – 84-19)
Stockholm, June 1985

1985
TR 85-20
Annual Research and Development Report 1985
Including Summaries of Technical Reports Issued during 1985. (Technical Reports 85-01 – 85-19)
Stockholm, May 1986

1986
TR 86-31
SKB Annual Report 1986
Including Summaries of Technical Reports Issued during 1986
Stockholm, May 1987

1987
TR 87-33
SKB Annual Report 1987
Including Summaries of Technical Reports Issued during 1987
Stockholm, May 1988

1988
TR 88-32
SKB Annual Report 1988
Including Summaries of Technical Reports Issued during 1988
Stockholm, May 1989

1989
TR 89-40
SKB Annual Report 1989
Including Summaries of Technical Reports Issued during 1989
Stockholm, May 1990

1990
TR 90-46
SKB Annual Report 1990
Including Summaries of Technical Reports Issued during 1990
Stockholm, May 1991

1991
TR 91-64
SKB Annual Report 1991
Including Summaries of Technical Reports Issued during 1991
Stockholm, April 1992

1992
TR 92-46
SKB Annual Report 1992
Including Summaries of Technical Reports Issued during 1992
Stockholm, May 1993

1993
TR 93-34
SKB Annual Report 1993
Including Summaries of Technical Reports Issued during 1993
Stockholm, May 1994

1994

TR 94-33

SKB Annual Report 1994

Including Summaries of Technical Reports Issued during 1994.
Stockholm, May 1995

List of SKB Technical Reports 1995

TR 95-01

Biotite and chlorite weathering at 25°C. The dependence of pH and (bi) carbonate on weathering kinetics, dissolution stoichiometry, and solubility; and the relation to redox conditions in granitic aquifers

Maria Malmström[1], Steven Banwart[1], Lara Duro[2], Paul Wersin[3], Jordi Bruno[3]
[1] Royal Institute of Technology, Department of Inorganic Chemistry, Stockholm, Sweden
[2] Universidad Politécnica de Cataluña, Departmento de Inginería Química, Barcelona, Spain
[3] MBT Tecnología Ambiental, Cerdanyola, Spain
January 1995

TR 95-02

Copper canister with cast inner component. Amendment to project on Alternative Systems Study (PASS), SKB TR 93-04

Lars Werme, Joachim Eriksson
Swedish Nuclear Fuel and Waste Management Co, Stockholm, Sweden
March 1995

TR 95-03

Prestudy of final disposal of long-lived low and intermediate level waste

Marie Wiborgh (ed.)
Kemakta Konsult AB, Stockholm, Sweden
January 1995

TR 95-04

Spent nuclear fuel corrosion: The application of ICP-MS to direct actinide analysis

R S Forsyth[1], U-B Eklund[2]
[1] Caledon-Consult AB, Nyköping, Sweden
[2] Studsvik Nuclear AB, Nyköping, Sweden
March 1995

TR 95-06

Palaeohydrological implications in the Baltic area and its relation to the groundwater at Äspö, south-eastern Sweden – A literature study

Bill Wallin
Geokema AB, Lidingö, Sweden
March, 1995

TR 95-07

Äspö Hard Rock Laboratory Annual Report 1994

SKB
April 1995

TR 95-08

Feasibility study for siting of a deep repository within the Storuman municipality

Swedish Nuclear Fuel and Waste Management Co., Stockholm
January 1995

TR 95-09

A thermodynamic data base for Tc to calculate equilibrium solubilities at temperatures up to 300°C

Ignasi Puigdomènech[1], Jordi Bruno[2]
[1] Studsvik AB, Nyköping, Sweden
[2] Intera Information Technologies SL, Cerdanyola, Spain
April 1995

TR 95-10

Investigations of subterranean microorganisms. Their importance for performance assessment of radioactive waste disposal

Karsten Pedersen[1], Fred Karlsson[2]
[1] Göteborg University, General and Marine Microbiology, The Lundberg Institute, Göteborg, Sweden
[2] Swedish Nuclear Fuel and Waste Management Co., Stockholm, Sweden
June 1995

TR 95-11

Solute transport in fractured media – The important mechanisms for performance assessment

Luis Moreno, Björn Gylling, Ivars Neretnieks
Department of Chemical Engineering and Technology, Royal Institute of Technology, Stockholm, Sweden
June 1995

TR 95-12
Literature survey of matrix diffusion theory and of experiments and data including natural analogues
Yvonne Ohlsson, Ivars Neretnieks
Department of Chemical Engineering and Technology, Royal Institute of Technology, Stockholm, Sweden
August 1995

TR 95-13
Interactions of trace elements with fracture filling minerals from the Äspö Hard Rock Laboratory
Ove Landström[1], Eva-Lena Tullborg[2]
[1] Studsvik Eco & Safety AB
[2] Terralogica AB
June 1995

TR 95-14
Consequences of using crushed crystalline rock as ballast in KBS-3 tunnels instead of rounded quartz particles
Roland Pusch
Clay Technology AB
February 1995

TR 95-15
Estimation of effective block conductivities based on discrete network analyses using data from the Äspö site
Paul R La Pointe[1], Peter Wallmann[1], Sven Follin[2]
[1] Golder Associates Inc., Seattle, WA, USA
[2] Golder Associates AB, Lund, Sweden
September 1995

TR 95-16
Temperature conditions in the SKB study sites
Kaj Ahlbom[1], Olle Olsson[1], Stefan Sehlstedt[2]
[1] Conterra AB
[2] MRM Konsult AB
June 1995

TR 95-17
Measurements of colloid concentrations in the fracture zone, Äspö Hard Rock Laboratory, Sweden
Anna Ledin, Anders Düker, Stefan Karlsson, Bert Allard
Department of Water and Environmental Studies,Linköping University, Linköping, Sweden
June 1995

TR 95-18
Thermal evidence of caledonide foreland, molasse sedimentation in Fennoscandia
Eva-Lena Tullborg[1], Sven Åke Larsson[1], Lennart Björklund[1], Lennart Samuelsson[2], Jimmy Stigh[1]
[1] Department of Geology, Earth Sciences Centre, Göteborg University, Göteborg, Sweden
[2] Geological Survey of Sweden, Earth Sciences Centre, Göteborg, Sweden
November 1995

TR 95-19
Compaction of bentonite blocks. Development of technique for industrial production of blocks which are manageable by man
Lars-Erik Johannesson, Lennart Börgesson, Torbjörn Sandén
Clay Technology AB, Lund, Sweden
April 1995

TR 95-20
Modelling of the physical behaviour of water saturated clay barriers. Laboratory tests, material models and finite element application
Lennart Börgesson[1], Lars-Erik Johannesson[1], Torbjörn Sandén[1], Jan Hernelind[2]
[1] Clay Technology AB, Lund, Sweden
[2] FEM-Tech AB, Västerås, Sweden
September 1995

TR 95-21
Conceptual model for concrete long time degradation in a deep nuclear waste repository
Björn Lagerblad, Jan Trägårdh
Swedish Cement and Concrete Research Institute
February 1994

TR 95-22
The use of interaction matrices for identification, structuring and ranking of FEPs in a repository system. Application on the far-field of a deep geological repository for spent fuel
Kristina Skagius[1], Anders Ström[2], Marie Wiborgh[1]
[1] Kemakta, Stockholm, Sweden
[2] Swedish Nuclear Fuel and Waste Management Co, Stockholm, Sweden
November 1995

TR 95-23
Spent nuclear fuel. A review of properties of possible relevance to corrosion processes
Roy Forsyth
Caledon Consult AB
April 1995

TR 95-24

Studies of colloids and their importance for repository performance assessment

Marcus Laaksoharju[1], Claude Degueldre[2], Christina Skårman[1]
[1] GeoPoint AB, Sollentuna, Sweden
[2] University of Geneva, Switzerland
December 1995

TR 95-25

Sulphate reduction in the Äspö HRL tunnel

Marcus Laaksoharju (ed.)
GeoPoint AB, Sollentuna, Sweden
December 1995

TR 95-26

The Äspö redox investigations in block scale. Project summary and implications for repository performance assessment

Steven Banwart (ed.)
Dept. of Civil and Environmental Engineering, University of Bradford, UK
November 1995

TR 95-27

Survival of bacteria in nuclear waste buffer materials. The influence of nutrients, temperature and water activity

Karsten Pedersen[1], Mehrdad Motamedi[1], Ola Karnland[2]
[1] Department of General and Marine Microbiology, the Lundberg Institute, Göteborg University, Göteborg, Sweden
[2] Clay Technology AB, Lund, Sweden
December 1995